AD-757 510

NONDESTRUCTIVE HOLOGRAPHIC TECHNIQUES FOR STRUCTURES INSPECTION

R. K. Erf, et al

United Aircraft Research Laboratories

Prepared for:

Air Force Materials Laboratory

October 1972

DISTRIBUTED BY:

NTIS

National Technical Information Service
U. S. DEPARTMENT OF COMMERCE
5285 Port Royal Road, Springfield Va. 22151

AD757510

AFML-TR-72-204

NONDESTRUCTIVE HOLOGRAPHIC TECHNIQUES FOR STRUCTURES INSPECTION

R. K. ERF

J. P. WATERS

R. M. GAGOSZ

F. MICHAEL

G. WHITNEY

UNITED AIRCRAFT RESEARCH LABORATORIES

TECHNICAL REPORT AFML-TR-72-204

D D C
RECEIVED
MAR 13 1973
B

OCTOBER 1972

Reproduced by
NATIONAL TECHNICAL
INFORMATION SERVICE
U S Department of Commerce
Springfield VA 22151

Approved for public release; distribution unlimited.

AIR FORCE MATERIALS LABORATORY
AIR FORCE SYSTEMS COMMAND
WRIGHT-PATTERSON AIR FORCE BASE, OHIO

NOTICE

When Government drawings, specifications, or other data are used for any purpose other than in connection with a definitely related Government procurement operation, the United States Government thereby incurs no responsibility nor any obligation whatsoever; and the fact that the government may have formulated, furnished, or in any way supplied the said drawings, specifications, or other data, is not to be regarded by implication or otherwise as in any manner licensing the holder or any other person or corporation, or conveying any rights or permission to manufacture, use, or sell any patented invention that may in any way be related thereto.

ACCESSION for

NTIS White Section ☑

DDC Buff Section ☐

UNANNOUNCED ☐

JUSTIFICATION .....

BY .....

DISTRIBUTION/AVAILABILITY CODES

Dist.	AVAIL. and/or SPECIAL	
A		

Copies of this report should not be returned unless return is required by security considerations, contractual obligations, or notice on a specific document.

AIR FORCE/56780/8 February 1973 — 700

NONDESTRUCTIVE HOLOGRAPHIC TECHNIQUES FOR STRUCTURES INSPECTION

R. K. ERF
J. P. WATERS
R. M. GAGOSZ
F. MICHAEL
G. WHITNEY

UNITED AIRCRAFT RESEARCH LABORATORIES

Approved for public release; distribution unlimited.

I

FOREWORD

This report was prepared by R. K. Erf, J. P. Waters, R. M. Gagosz, F. Michael and G. Whitney of the United Aircraft Research Laboratories, United Aircraft Corporation, East Hartford, Connecticut 06108. The work is being supported by the NDI and Mechanics Branch, Metals and Ceramics Division of the Air Force Material Laboratory under Contract F33615-71-C-1874. The Air Force Project Monitor is Captain James W. Bohlen.

This technical report has been reviewed and is approved.

Thomas D. Cooper
Chief, NDT and Mechanics Branch
Metals and Ceramics Division

UNCLASSIFIED
Security Classification

DOCUMENT CONTROL DATA - R&D
(Security classification of title, body of abstract and indexing annotation must be entered when the overall report is classified)

1. ORIGINATING ACTIVITY (Corporate author) United Aircraft Research Laboratories, a Division of United Aircraft Corporation East Hartford, Connecticut 06108	2a. REPORT SECURITY CLASSIFICATION Unclassified 2b. GROUP
3. REPORT TITLE Nondestructive Holographic Techniques for Structures Inspection	
4. DESCRIPTIVE NOTES (Type of report and inclusive dates) Annual Technical Report (1 July, 1971 through 30 April, 1972)	
5. AUTHOR(S) (Last name, first name, initial) Erf, R. K.; Waters, J. P.; Gagosz, R. M.; Michael, F.; Whitney, G.	
6. REPORT DATE October, 1972	7a. TOTAL NO. OF PAGES ~~127~~ 138 / 7b. NO. OF REFS 29
8a. CONTRACT OR GRANT NO. F33615-71-C-1874 b. PROJECT NO. 7351 c. d.	9a. ORIGINATOR'S REPORT NUMBER(S) L991208-12 9b. OTHER REPORT NO(S) (Any other numbers that may be assigned this report) AFML-TR-72-204
10. AVAILABILITY/LIMITATION NOTICES DISTRIBUTION OF THIS DOCUMENT IS UNLIMITED	
11. SUPPLEMENTARY NOTES Details of illustrations in this document may be better studied on microfiche.	12. SPONSORING MILITARY ACTIVITY Air Force Materials Laboratory Wright-Patterson AFB, Ohio 45433

13. ABSTRACT

This program is investigating the feasibility of using holographic interferometry for the inspection of large aircraft structures in a manufacturing or maintenance environment. The ~~first year~~'s work comprised the following: 1 - An investigation of various problems to be encountered in technically difficult physical environments as a result of ambient lighting, vibration and suspended aerosols, and including successful pulsed holographic experiments on composite rotor blades in the Fatigue Test Laboratory at Sikorsky Aircraft; 2 - An evaluation of the effects that various surface finishes have on the holographic construction process, which indicated that surface roughnesses from 4 microinches (very smooth) to 1000 microinches are amenable to the method; 3 - The development of the theory required to relate holographic records to the strain patterns and areas of maximum strain present on large structures, together with experimental studies exhibiting good correlation between the holographically calculated strain and that measured with gages; 4 - Successful application of both continuous-wave (cw) and pulsed laser systems to time-averaged interferometric holography of composite compressor blades subjected to ultrasonic stressing, demonstrating the potential of this combination for the nondestructive inspection of composite structures.

DD FORM 1 JAN 64 1473

UNCLASSIFIED
Security Classification

UNCLASSIFIED
Security Classification

14. KEY WORDS	LINK A ROLE	LINK A WT	LINK B ROLE	LINK B WT	LINK C ROLE	LINK C WT
Holography						
Interferometric Holography						
Hostile Environments						
Aircraft Structures						
Nondestructive Inspection						
Strain Pattern Visualization						
Maximum Strain Points						
Surface Finish Effects						
Composite Fan Blades						
Speckle Reference Beam Holography						

INSTRUCTIONS

1. ORIGINATING ACTIVITY: Enter the name and address of the contractor, subcontractor, grantee, Department of Defense activity or other organization *(corporate author)* issuing the report.

2a. REPORT SECURITY CLASSIFICATION: Enter the overall security classification of the report. Indicate whether "Restricted Data" is included. Marking is to be in accordance with appropriate security regulations.

2b. GROUP: Automatic downgrading is specified in DoD Directive 5200.10 and Armed Forces Industrial Manual. Enter the group number. Also, when applicable, show that optional markings have been used for Group 3 and Group 4 as authorized.

3. REPORT TITLE: Enter the complete report title in all capital letters. Titles in all cases should be unclassified. If a meaningful title cannot be selected without classification, show title classification in all capitals in parenthesis immediately following the title.

4. DESCRIPTIVE NOTES: If appropriate, enter the type of report, e.g., interim, progress, summary, annual, or final. Give the inclusive dates when a specific reporting period is covered.

5. AUTHOR(S): Enter the name(s) of author(s) as shown on or in the report. Enter last name, first name, middle initial. If military, show rank and branch of service. The name of the principal author is an absolute minimum requirement.

6. REPORT DATE: Enter the date of the report as day, month, year; or month, year. If more than one date appears on the report, use date of publication.

7a. TOTAL NUMBER OF PAGES: The total page count should follow normal pagination procedures, i.e., enter the number of pages containing information.

7b. NUMBER OF REFERENCES: Enter the total number of references cited in the report.

8a. CONTRACT OR GRANT NUMBER: If appropriate, enter the applicable number of the contract or grant under which the report was written.

8b, 8c, & 8d. PROJECT NUMBER: Enter the appropriate military department identification, such as project number, subproject number, system numbers, task number, etc.

9a. ORIGINATOR'S REPORT NUMBER(S): Enter the official report number by which the document will be identified and controlled by the originating activity. This number must be unique to this report.

9b. OTHER REPORT NUMBER(S): If the report has been assigned any other report numbers *(either by the originator or by the sponsor)*, also enter this number(s).

10. AVAILABILITY/LIMITATION NOTICES: Enter any limitations on further dissemination of the report, other than those imposed by security classification, using standard statements such as:

(1) "Qualified requesters may obtain copies of this report from DDC."

(2) "Foreign announcement and dissemination of this report by DDC is not authorized."

(3) "U. S. Government agencies may obtain copies of this report directly from DDC. Other qualified DDC users shall request through _____."

(4) "U. S. military agencies may obtain copies of this report directly from DDC. Other qualified users shall request through _____."

(5) "All distribution of this report is controlled. Qualified DDC users shall request through _____."

If the report has been furnished to the Office of Technical Services, Department of Commerce, for sale to the public, indicate this fact and enter the price, if known.

11. SUPPLEMENTARY NOTES: Use for additional explanatory notes.

12. SPONSORING MILITARY ACTIVITY: Enter the name of the departmental project office or laboratory sponsoring *(paying for)* the research and development. Include address.

13. ABSTRACT: Enter an abstract giving a brief and factual summary of the document indicative of the report, even though it may also appear elsewhere in the body of the technical report. If additional space is required, a continuation sheet shall be attached.

It is highly desirable that the abstract of classified reports be unclassified. Each paragraph of the abstract shall end with an indication of the military security classification of the information in the paragraph, represented as *(TS)*, *(S)*, *(C)*, or *(U)*.

There is no limitation on the length of the abstract. However, the suggested length is from 150 to 225 words.

14. KEY WORDS: Key words are technically meaningful terms or short phrases that characterize a report and may be used as index entries for cataloging the report. Key words must be selected so that no security classification is required. Identifiers, such as equipment model designation, trade name, military project code name, geographic location, may be used as key words but will be followed by an indication of technical context. The assignment of links, roles, and weights is optional.

DD FORM 1 JAN 64 1473 (BACK)

UNCLASSIFIED
Security Classification

*U.S.Government Printing Office: 1973 — 759-450/320

III-4

TABLE OF CONTENTS

Section		Page
I	SUMMARY	1
II	INTRODUCTION	4
	HOLOGRAPHIC RECORDING AND THE TECHNIQUES OF HOLOGRAPHIC INTERFEROMETRY	4
	PROGRAM ORGANIZATION	6
III	GENERAL STUDIES - PHYSICAL ENVIRONMENT EFFECTS	9
	INTRODUCTION	9
	PULSED RUBY LASER SYSTEM	10
	PHYSICAL ENVIRONMENT TESTS	12
	Effects of Ambient Illumination	12
	Effects of Vibration	27
	Effects of Suspended Aerosols	29
IV	GENERAL STUDIES - SURFACE FINISH EFFECTS	33
	INTRODUCTION	33
	EXPERIMENTAL INVESTIGATIONS	34
	Simulated Airframe Panel	34
	2' x 2' Panel	36
	4' x 4' Panel	39
	Standard Roughness Specimens	45
V	SPECIFIC PROBLEM INVESTIGATIONS - MAXIMUM STRAIN AND STRAIN PATTERNS	51
	INTRODUCTION	51
	THEORETICAL ANALYSIS	52
	Mathematical Description of Holographic Interferometry	56
	Conversion of Holographic Data to In-Plane Strain Data	61
	EXPERIMENTAL INVESTIGATIONS	66
	Cantilevered Beam	67
	Simulated Airframe Panel	69
	Cylinder	81

TABLE OF CONTENTS (Contd.)

Section		Page
VI	SPECIFIC PROBLEM INVESTIGATIONS - NDT OF COMPOSITE COMPRESSOR BLADES	85
	INTRODUCTION	85
	EXPERIMENTAL PROCEDURE	87
	EXPERIMENTAL RESULTS	89
	Boron and Graphite Polyimide Airfoils	89
	Borsic(R)-Aluminum Fan Blades	93
	Correlation Studies	100
VII	CONCLUSIONS AND RECOMMENDATIONS	103
	PHYSICAL ENVIRONMENT EFFECTS	103
	SURFACE FINISH EFFECTS	104
	MAXIMUM STRAIN & STRAIN PATTERNS	104
	NDT-COMPOSITE COMPRESSOR BLADES	105
REFERENCES		107
APPENDIX A-ABSTRACT - STRAIN ANALYSIS OF LARGE AIRFRAME STRUCTURES		109
APPENDIX B-OBJECT MOTION COMPENSATION BY SPECKLE REFERENCE BEAM HOLOGRAPHY		110
	INTRODUCTION	112
	SPECKLE REFERENCE BEAM HOLOGRAPHY	112
	ELIMINATION OF STRINGENT VIBRATION ISOLATION REQUIREMENTS OF CW HOLOGRAPHY	115
	DETERMINING PHASE OF VIBRATING OBJECTS	122
	ELIMINATION OF RESIDUAL FRINGES IN PULSE INTERFEROGRAMS	125
	REFERENCES	127

LIST OF ILLUSTRATIONS

		Page
Figure 1	Program Organizational Diagram	7
Figure 2	Program Plan Chart	8
Figure 3	Pulse Ruby Laser Schematic	11
Figure 4	UARL Pulsed Ruby Laser	13
Figure 5	Holographic Test Configuration-Sikorsky Aircraft	15
Figure 6	Reconstruction of Composite Helicopter Blade Undergoing Fatigue Cycling.	17
Figure 7	Reconstruction of IRB Blade Section Undergoing Fatigue Cycling	18
Figure 8	Holographic Setup for Ambient Light Effects Test	19
Figure 9	Shutter Assembly-Ambient Light Effects Test.	22
Figure 10	Holographic Construction: Single Pulse-No Ambient Illumination.	23
Figure 11	Effect of Normal Room Lighting on Holographic Construction.	24
Figure 12	Reconstructions of Holograms Under Varying Ambient Light Levels.	25
Figure 13	Reconstruction of Interferometric Hologram Constructed in Fatigue Test Laboratory.	28
Figure 14	Aerosol Chamber.	31
Figure 15	Reconstructions of Pulsed Holograms Made in Smoke Environments.	32
Figure 16	Surface Finish Effect Studies - Simulated Airframe Panel	35
Figure 17	Surface Finish Effect Studies - 2' x 2' Panel.	37

LIST OF ILLUSTRATIONS (Contd.)

		Page
Figure 18	Surface Finish Effect Studies - 2' x 2' Panel	38
Figure 19	Surface Finish Effect Studies - 4' x 4' Panel	40
Figure 20	Surface Finish Effect Studies - Experimental Setup. . .	41
Figure 21	Beam Ratio Studies.	43
Figure 22	Diffuse Illumination Studies.	44
Figure 23	Retro-reflecting Sheeting Studies	46
Figure 24	Standard Roughness Specimens.	47
Figure 25	Holographic Reconstructions - Standard Roughness Specimens.	49
Figure 26	Maximum Strain and Strain Patterns - Analytical Analysis Parameters.	58
Figure 27	Effect of Rigid Body Motion on Holographic Strain Measurements - Reconstructions of Cantilevered Beam.	68
Figure 28	Experimental Data Results for Cantilevered Beam	70
Figure 29	Maximum Strain and Strain Patterns - Stressing Frame and Test Panel	71
Figure 30	Experimental Test Setup	73
Figure 31	Strain Gage Location.	74
Figure 32	Interferograms Used to Obtain In-Plane Strain	77
Figure 33	Interferograms Made Between 800 με and 500 με	80
Figure 34	Holographic Strain Analysis of Asymmetrically Loaded Cylinder.	83
Figure 35	Composite Airfoils.	86
Figure 36	Composite Fan Blade Inspection-Experimental Setup . . .	88

LIST OF ILLUSTRATIONS (Contd.)

		Page
Figure 37	Holographic Indications on Boron Polyimide Blade-B1. . .	90
Figure 38	Ultrasonic Indications on Boron Polyimide Blade-B1 . . .	91
Figure 39	Holographic Indications on Boron Polyimide Blade-B2. . .	92
Figure 40	Ultrasonic Indications on Boron Polyimide Blade-B2 . . .	94
Figure 41	Holographic Indications on Graphite Polyimide Blade-G1 .	95
Figure 42	Ultrasonic Indications on Graphite Polyimide Blade-G1. .	96
Figure 43	Holographic Indications on Boron Polyimide Blade-B3. . .	97
Figure 44	Ultrasonic Indications on Boron Polyimide Blade-B3 . . .	98
Figure 45	Borsic(R)-Aluminum Fan Blades -- General Disbonding . . .	99
Figure 46	Borsic(R)-Aluminum Fan Blade - Pulsed Laser Time-Average Holography.	101
Figure B1	Portable CW Holography in a Materials Testing Laboratory.	111
Figure B2	Speckle Reference Beam Holography.	114
Figure B3	Reconstructed Images - Non-Isolated Object	116
Figure B4	Phase Change Parameters.	118
Figure B5	Speckle Reference Beam Holography - Schematic.	119
Figure B6	Reconstructions of Speckle Reference Beam Holograms. . .	120
Figure B7	Speckle Reference Beam Holocamera.	123
Figure B8	Reconstructions of Holograms Recorded with Tripod-Mounted Holocamera.	124
Figure B9	Vibratory Phase Determination.	126

SECTION I

SUMMARY

Presented herein is a description of the work performed during the first ten months (ending 30 April, 1972) of a 36 month effort under Contract F33615-71-C-1874. The investigation is directed at: determining the feasibility of using holographic interferometry in manufacturing or maintenance environments; establishing strain analysis techniques for aircraft and large aircraft components; and establishing pulsed holographic interferometric techniques for the detection of cracks in actual or simulated aerospace hardware. The program has been organized into seven major areas, and the main body of the present report is divided into four sections, representing those areas in which work was performed during the reporting period.

Section III - Physical Environment Effects
Section IV - Surface Finish Effects
Section V - Maximum Strain and Strain Patterns
Section VI - NDT, Composite Compressor Blades

Section III reviews the problem areas to be considered in conducting holographic studies in likely application environments, and describes the experimental investigations, performed to date, concerned with the effects of ambient illumination, vibration, and suspended aerosols. In addition, the specifications for the UARL-developed pulsed ruby laser system being utilized in the program are presented together with a description of some system development tests conducted in the Fatigue Test Laboratory at Sikorsky Aircraft to gain operating experience in an actual manufacturing type of environment. Study of the deleterious effects of extraneous lighting demonstrated that levels up to 200 foot-candles (reflected to the holographic plate) could easily be tolerated. Further, it was shown that while the reference to object beam intensity ratio should be greater than unity, there is considerable latitude in this number, with ratios between 2:1 and 30:1 producing comparable results. Similarly, it is not necessary to precisely match the two pulse intensities when constructing double-pulse interferometric holograms. The Fatigue Test Laboratory work demonstrated that high vibrational fields, at frequencies up to 1 KHz, should not adversely affect the holographic construction process.

It was concluded from the study of surface finish effects, reported in Section IV, that interferometric holography can be usefully employed on well polished surfaces (roughness of approximately 4 μ in.) and that the degree of surface roughness up to 1000 μ in. does not significantly affect fringe location.

However, the scattered radiation intensity from very smooth surfaces is highly peaked in the specular direction which may set an upper limit on the area coverage. Therefore, the specular point should be centered on the surface area of interest in order to obtain the maximum recorded area. In some associated studies it was found that holographic interferometric quality is independent of the type of object beam expander element (diffuser plate or simple lens) and that retro-reflecting surface preparations may afford an enormous increase in allowable area coverage for a given laser system.

A detailed mathematical description of the required theory, along with a review of the extensive experimental investigations performed on both a simulated airframe skin and a cylindrical surface to study the pertinent parameters associated with holographically visualizing strain patterns and areas of maximum strain concentrations on large structures are the subjects of Section V. The theoretical work established that holographic interferometry is a viable technique for performing such studies with minimal restrictions placed on the experimental setup; the illumination source and holographic plate should be located adjacent to each other at a distance greater than one meter from the object, and the viewing angle limited to $\pm 45^\circ$ to the surface normal. The experimental measurements reported support the theoretical conclusions by showing that good correlation exists between the principal strain fields on thin structures as sampled by conventional strain gages, and as determined by means of holographic interferometry. In addition, a theoretical and experimental study of the effects of surface geometry and rigid body motion on the interferometric fringe data reduction procedures indicated that they will not affect the determination of high strain areas or relative strain magnitudes.

Finally, laboratory investigations of holographic nondestructive testing procedures as applied to composite compressor blades are described in Section VI. The results of this work indicate that the use of ultrasonic stressing, combined with interferometric holographic readout may offer one of the most inclusive test methods for the detection and characterization of bond defects in composite material components. In general, it appears that this approach can define the area of delamination, determine which surface it is nearer to, has the potential to determine the degree of disbonding, and is applicable to complex surface geometries. It is applicable to the inspection of large areas in a single test; and the low frequency range (up to a few hundred kilohertz) employed relative to the megahertz operating frequencies of more conventional ultrasonic NDT methods facilitates transducer coupling and minimizes the effects of grain scattering, acoustic attenuation and surface roughness on resolution capability. The experimental work reported includes a demonstration of pulsed laser time-average holographic interferometry, illustrating one potential method for implementing HNDI in a production or maintenance type of environment.

Before proceeding to a more detailed discussion of the areas summarized above, an introductory section has been included which very briefly reviews the motivation for the current investigations, discusses the holographic process in brief general terms along with a description of interferometric holography (the technique of interest to the present work), and presents the program organization.

Included as Appendices A and B to the present report are: first - an abstract of a paper presented to the Spring 1972 Meeting of the Optical Society of America and entitled "Strain Analysis of Large Airframe Structures"; and second - a paper entitled "Object Motion Compensation by Speckle Reference Beam Holography" which recently appeared in Applied Optics. The former item reported work performed under the current contract, whereas the latter item was part of UARL's Corporate sponsored research program; it is most apropos to the present contract work, however, since it offers a viable technique for applying the continuous wave laser holographic process in a practical environment, and as such, serves to complement the use of pulsed laser holographic techniques in such a situation.

SECTION II

INTRODUCTION

The ever-increasing complexity and sophistication of aerospace structures and components, together with the demand for lighter, stronger and more reliable materials, inherently requires a more detailed knowledge of any design deficiencies or flaws which may be present. New manufacturing processes and fabrication techniques to realize such structures pose two potentially dangerous problems: the nature of the flaws which might be encountered in production or develop in service are not well understood and critical flaw identification is becoming more difficult. Consequently, application of conventional NDI methods to these problems must be re-examined to determine their suitability; and new tests must be developed and demonstrated. Holography is one such tool that has recently become available and well established. Therefore, the present program was undertaken to explore the feasibility of using this technique when seeking solutions to the inspection of advanced aircraft and aerospace hardware.

HOLOGRAPHIC RECORDING AND THE TECHNIQUES OF HOLOGRAPHIC INTERFEROMETRY

With the advent of the laser, the science of holography, as first developed by Gabor (Ref. 1), has enjoyed an active revival. Advances in holography have been especially rapid since Leith and Upatnieks (Ref. 2) developed the reflected light holographic technique. Rather than reviewing the mathematical theory in detail, suffice it to say that holography provides a method of storing three-dimensional information on a two-dimensional recording plane for subsequent viewing of the object in its original three-dimensional form. This radically different concept in photographic optics does not require the use of lenses or other image forming devices; instead, an intensity pattern is recorded which is related to both the amplitude and phase of light waves diffracted around, or reflected from, an object using a one-beam (Gabor) or two-beam (Leith and Upatnieks) interferometric process. The recorded pattern, called a hologram, bears little or no resemblance to the original object, but nevertheless contains all the information about the object that would be contained in an ordinary photograph plus the additional information about the phase which is required for visualization of the third dimension. The creation of an intelligible image from the hologram is known as the reconstruction process. In this process, the hologram is illuminated with monochromatic, coherent light; the hologram diffracts this light into waves, which are essentially indistinguishable from the original waves which had been diffracted around, or reflected from, the object and which will produce all the optical phenomena that characterized the original waves.

Of particular interest to the present contract is the method of interferometric holography (Ref. 3), a technique whereby minute surface deformations (on the order of microinches) induced by various stressing methods, can be detected by comparing each point on the surface with itself before and after stressing. These surface deformations can then be examined in the holographic reconstruction process as a means of interpreting the components' structural integrity.

In applying interferometric holography, a hologram is constructed in a manner similar to conventional holography except that two exposures and, hence, two holograms of the test object, are made on the same photographic plate, the surface of the test object being altered between the two exposures. Upon reconstruction, the two reconstructed images will interfere with each other and produce a set of bright and dark interference fringes (in the reconstructed image) which represent contours of equal displacement along the viewing axis. Each successive fringe represents a displacement of approximately one-half the wavelength of the illuminating source used in the construction process, or in the case of a He-Ne laser (6328 Å), approximately 12 microinches of surface displacement. The surface of the test object can be modified between the two exposures in several ways which include: internal pressurization, mechanical force, thermal heating, and acoustic vibration. The method employed would depend upon the component itself, the type of defect, and the accessibility of the component (i.e., whether the component can be tested by itself or as part of a complex system). Holographic nondestructive inspection (HNDI) is potentially applicable to any problem wherein application of a force manifests itself as a change in the surface shape of the object in a way which is indicative of the anomaly being sought.

Several variations of interferometric holography may be used.

a. Static double-exposure cw (continuous wave laser output) interferometric holography - in which two holographic recordings with the test piece in two states of stress (e.g., before and after application of a static stress), are made on the same film prior to photographic processing.

b. Dynamic time-average cw interferometric holography - in which a single holographic recording is made of a test piece undergoing a cyclic vibratory motion, with interference occurring between the ensemble of images corresponding to the time-average positions of the test piece, and with the positions near zero velocity contributing most strongly to the holographic exposure.

c. Real-time cw interferometric holography - in which a holographic recording is made of the unstressed piece. The film is processed in place, and upon reconstruction, the image, as viewed through the hologram, is formed superimposed upon the actual test piece. Any subsequent stress-produced fringe patterns can be observed as they appear in real-time.

d. Dynamic double-exposure pulsed interferometric holography - in which two holograms are recorded sequentially before photographic processing. This last technique, which makes production floor holography a reality, is applicable in both static and dynamic, whether cyclic or transient, stress situations; and in optically hostile environments where such effects as vibration, ambient light, and particulate matter may be present.

PROGRAM ORGANIZATION

As diagrammed in Fig. 1, the program has been organized into seven major areas which fall under two principal tasks: 1) a general study to develop suitable techniques for performing pulsed holographic interferometry tests in a manufacturing or maintenance environment; and 2) investigations in three specific problem areas. Both of these tasks are planned in two phases: laboratory studies, and actual maintenance environment studies. The bold faced boxes in the figure correspond to the seven major areas of study.

As shown in Fig. 1, three of these areas are organized under Task I: 1) physical environment effects; 2) surface finish effects; and 3) development of the final techniques for an actual maintenance environment. The remaining four are to be considered as part of Task II: 1) maximum strain and strain patterns; 2) fatigue cracks; 3) NDT; and 4) correlation studies. The first three of these last mentioned topics are the problems themselves, for which various holographic solutions have been proposed and are to be studied, while the fourth area calls for correlating the holographic results with previously determined, or known, flaw locations and strain distributions. Presented in Fig. 2 is a program plan chart, which corresponds to the organizational diagram of Fig. 1, and indicates the scheduled dates for initiation and completion of the various items to be studied under the program. As noted in Fig. 2, work has been initiated in five of the major study areas: 1) physical environment effects; 2) surface finish effects; 3) maximum strain and strain patterns; 4) NDT-composite compressor blades; and 5) correlation studies. Items 1 through 4 are the topic headings for the following sections of the present report, while the correlation studies are reviewed within the individual sections to which they are appropriate.

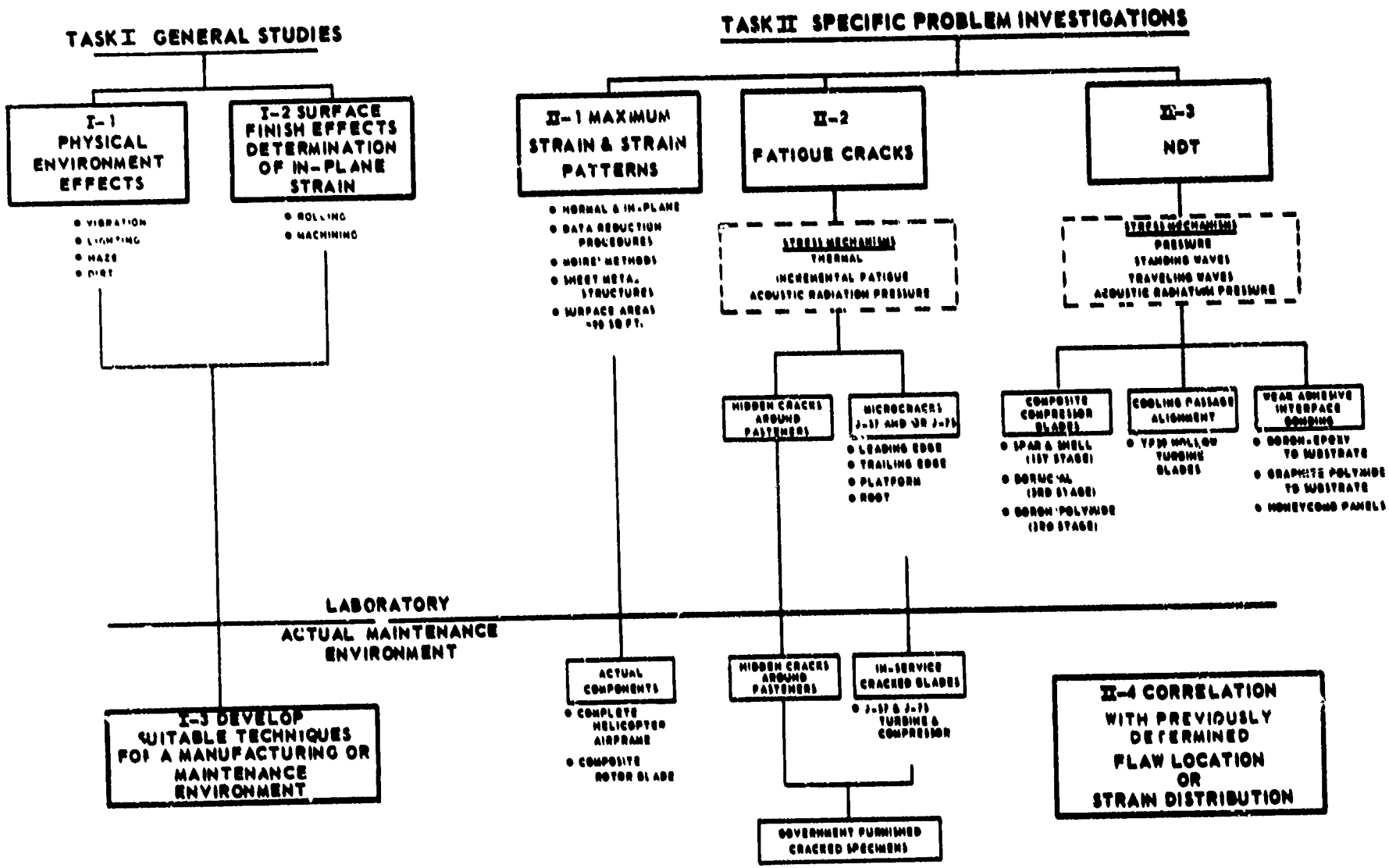

FIGURE 1. PROGRAM ORGANIZATIONAL DIAGRAM

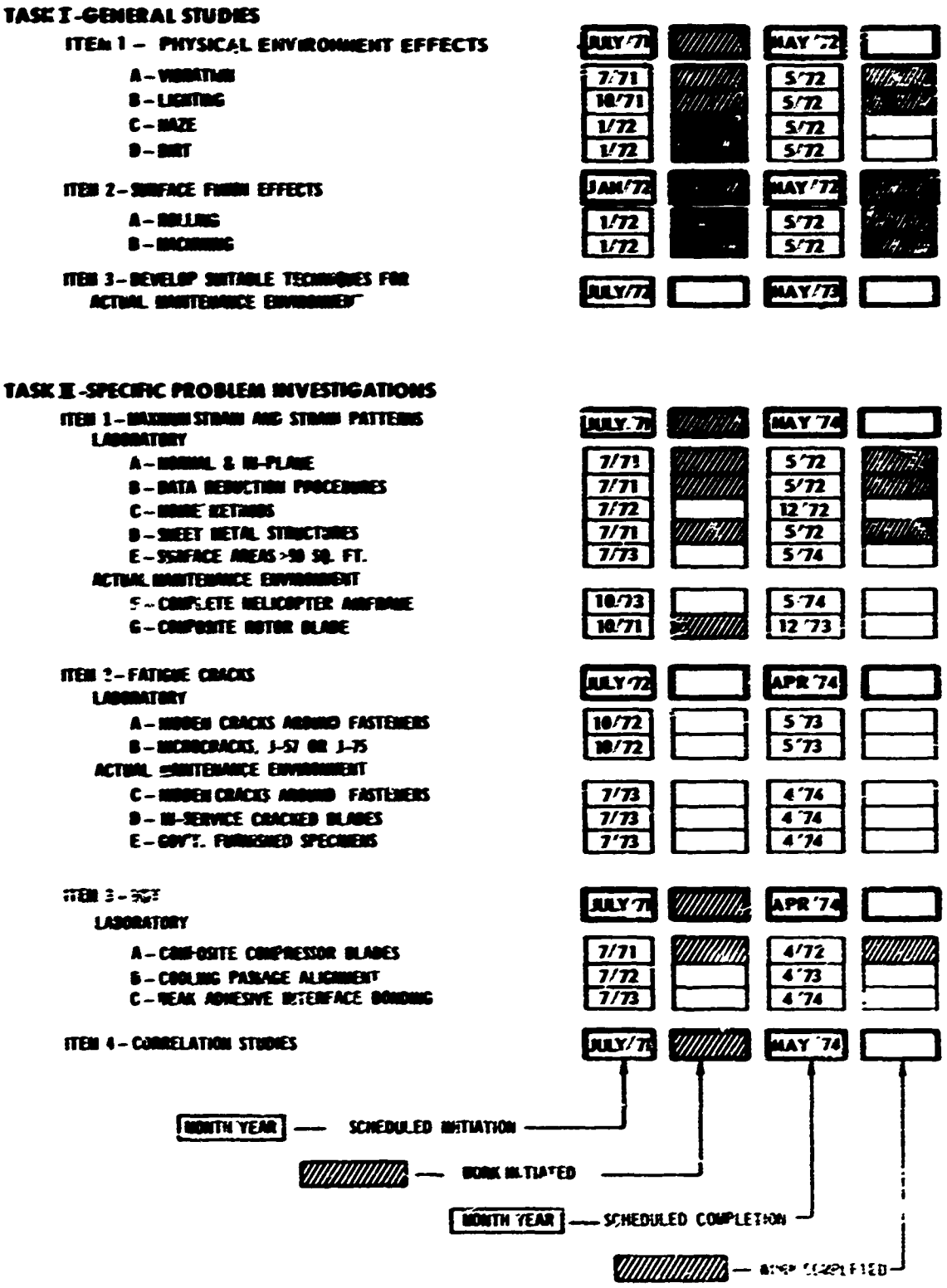

FIGURE 2. PROGRAM PLAN CHART

SECTION III

GENERAL STUDIES
PHYSICAL ENVIRONMENT EFFECTS

INTRODUCTION

Successful application of any holographic nondestructive inspection (HNDI) procedure to aerospace problems in a practical environment will require overcoming the adverse effects of these environments as they relate to the reconstructed image quality. The particular environmental characteristics which can affect the holographic image quality include vibration, ambient illumination, and ambient media perturbations (density variations and the presence of scattering objects). These characteristics prohibit the use of long exposure methods. Random variations of the holographic phase fronts during the exposure time caused by vibration of the optical components will degrade the image quality, the extent of the degradation being dependent upon the magnitude of the phase variations. Fogging of the holographic plate due to ambient illumination during the exposure time will also degrade reconstructed object intensity or, if the extraneous exposure is sufficient, wash out the image completely. Consequently, the more suitable approach for holography in a hostile environment is to utilize pulsed lasers which have the capability of short exposure times, on the order of 20 nanoseconds, to overcome these debilitating environmental characteristics. By employing a portable system, which could be installed at existing test rigs, full scale components could be examined without the need for disassembly of the structure. The use of pulsed lasers in such problem areas minimizes the effects of the environment and allows construction of good quality holograms. However, the laser cavity itself is susceptible to the ambient conditions (in particular the vibration) which may detune the cavity from optimum conditions. In addition, the simple transport of the laser may be sufficient to detune the cavity. Therefore, in order to avoid the unnecessary time required to retune the laser cavity, a suitable laser package must be available to the holographic system which would minimize laser adjustments and allow the user to concern himself primarily with the holographic aspects of HNDI.

Therefore, an experimental program was initiated to examine system parameters which control the quality of interferometric holograms constructed under adverse conditions (non-optical laboratory). In this regard, the program has been conducted to: 1 - examine laser operating characteristics to provide reliable operation; 2 - conduct preliminary investigations in a maintenance or test environment (Fatigue Test Laboratory at Sikorsky Aircraft was utilized) and thereby ascertain potential problem areas for further optical laboratory investigations; and 3 - examine the governing parameters with respect to holographic image quality and develop limits of operation for the problem areas defined in (2).

PULSED RUBY LASER SYSTEM

The pulsed ruby laser system developed at UARL for holographic studies has a coherence length of approximately 1.5 meters and a pulse duration of 20 nanosec. As shown in Fig. 3, the system employs a 6 inch by 1/2 inch diameter, Czochralski grown, ruby rod with Brewster angled end faces for the active medium. The laser cavity consists of a dielectric-coated full reflector with a 10 meter radius of curvature and a Fabry-Perot etalon as a resonant reflector. Since the fluorescent line width of the ruby is sufficiently broad to amplify many of the Fabry-Perot modes of the laser cavity itself, the etalon is used to reduce the number of oscillating modes to one, thereby providing the long coherence length required for holographic purposes. In addition to these components, a Pockels cell for synchronized active Q-switching, and an aperture to control the transverse mode structure are mounted internally to the laser cavity. (The Pockels cell can be replaced with a bleachable dye cell for passive Q-switching.) The Pockels cell is driven by a Lasermetrics high voltage power supply capable of delivering two negative pulses with pulse separations variable from 10 microseconds to 200 microseconds. The jitter in synchronizing to an external event is approximately 0.2 μsec. Most of the experiments to date have been conducted with a pulse separation of approximately 100 microseconds.

As indicated in the Introduction, laser cavity alignment is susceptible to the effects of the environment, especially the vibratory aspects of the environment. These conditions could subject the laser cavity mirrors to misalignment away from optimum. This would not only cause variations in the pulse-to-pulse amplitude, but also cause variations in the transverse mode structure (i.e. a non-uniform intensity distribution normal to the direction of propagation). Because of the very nature of the operation of pulsed lasers, the adjustment for realigning the laser to optimum conditions is time consuming. Therefore, to be effective, the laser system should be free of susceptibility to environmental characteristics. Furthermore, the possibility exists for misalignment due to handling during transit from one facility to another. For most efficient operation, this possibility should be minimized. Both conditions necessitate a rigid structure for the laser system.

Based upon the above considerations, modifications were made to the UARL pulsed ruby laser system. This phase of the work, conducted under Corporate sponsorship, was directed at providing a high degree of reliability and mobility for the tests conducted at Sikorsky Aircraft. The modifications included: 1) more rugged component mounts to insure stability of their position; and 2) a rigid aluminum honeycomb base to provide a stable, distortion-free platform for mounting of the laser components. In addition, a more powerful He:Ne laser (5 mw) was mounted on the pulsed laser system package to provide a better alignment beam for the holographic apparatus at the test site.

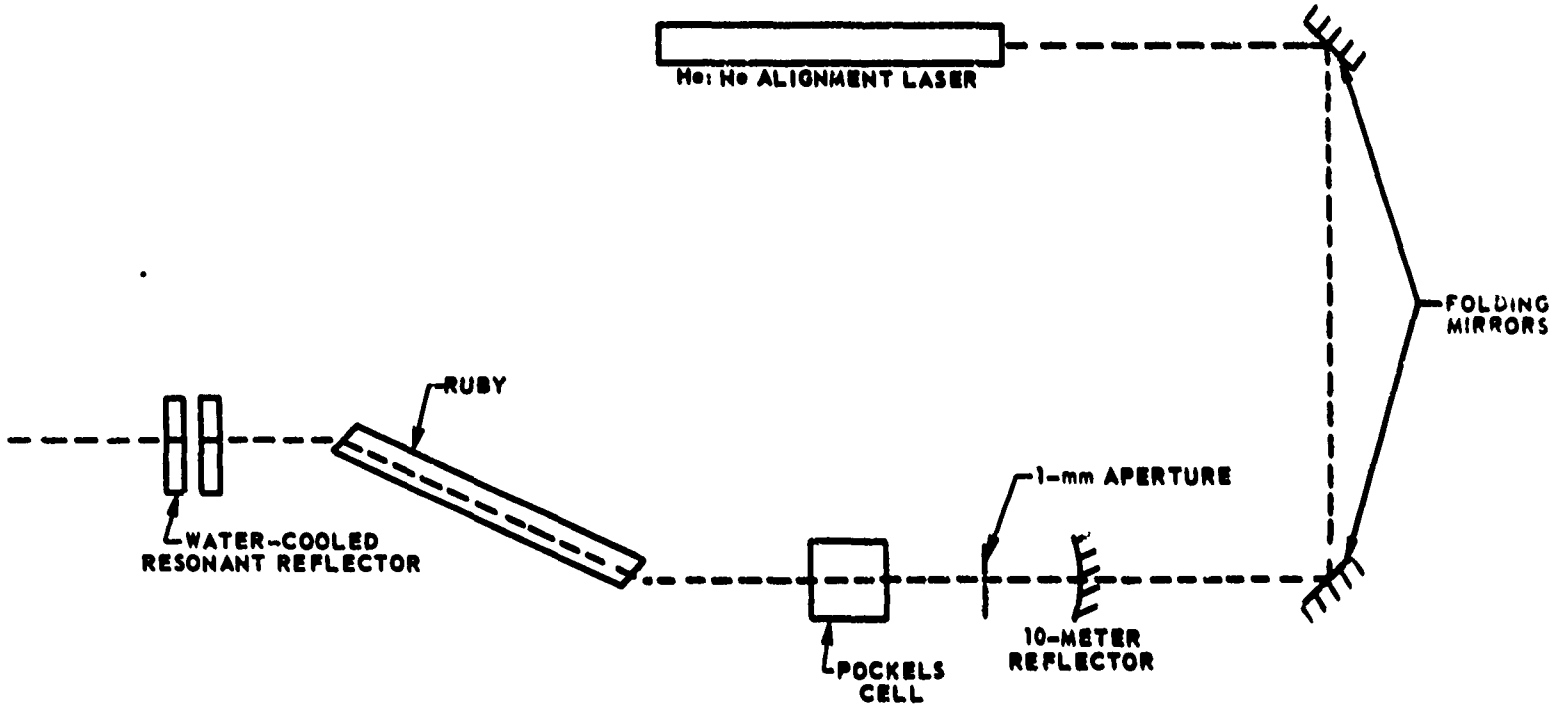

FIGURE 3. PULSE RUBY LASER SCHEMATIC

Satisfactory and reliable operation of the laser system is only achieved when the optical components which comprise the laser are in good condition. Component damage due to high laser power densities within the cavity causes deleterious effects with regard to available output energy and transverse mode structure. These would seriously degrade holographic image quality as well as limit the extent of the area to be examined. Particularly troublesome areas are the dielectric full reflector and the Pockels cell windows. Both of these components have suffered damage which has necessitated adjustments and replacements. Further effort is planned in this area to determine the tolerable operating limits for reliable operation.

Nevertheless, the new UARL laser system package, illustrated in Fig. 4, provided quite satisfactory operation. In day-to-day work, laser retuning has not been required except for minor variations in flashlamp pump voltage, or in the timing of the Pockels cell delay.

PHYSICAL ENVIRONMENT EFFECTS

Experiments were conducted at the Fatigue Test Laboratory of Sikorsky Aircraft and at UARL using the UARL pulsed ruby laser, to holographically examine those environmental characteristics which control holographic image quality. The purpose of the Sikorsky tests was twofold: 1) to study the effect of an optically hostile physical environment on the holographic process; and 2) to examine the surface deformation of composite rotor blades undergoing fatigue testing. With regard to the first item, the objective was to explore and define the specific characteristics of the environment which are critical and determine their effect on the holographic process for subsequent study in controlled laboratory conditions. The primary characteristics of the environment which could affect the holographic process during this series of tests included ambient illumination levels and ambient vibration levels. With regard to the ambient illumination, the photographic density due to the presence of this illumination could cause non-linear recording effects to predominate and thereby reduce image quality. In the second case, if significant motion occurred during the holographic exposure time, then the phase information would be reduced, if not lost, thereby resulting in a degradation of image quality.

Effects of Ambient Illumination

As indicated previously, high ambient light levels may preclude the construction of a hologram due to undue or excessive fogging of the photographic plate by the ambient illumination. That is, the d.c. component due to the non-coherent ambient radiation may saturate the plate so that the phase information of the coherent holographic process (recorded as interference fringes) is not recorded. The use of a pulsed laser to construct the hologram provides the means to alleviate this problem since the photographic plate need only be exposed for a

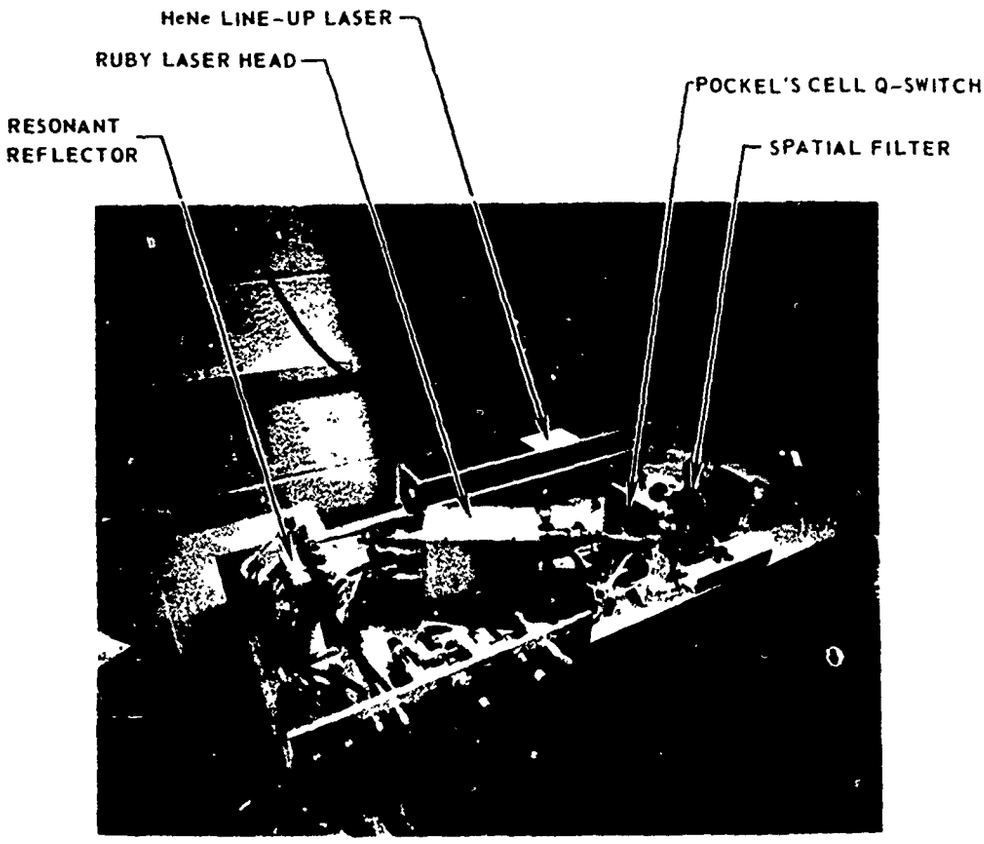

FIGURE 4. UARL PULSED RUBY LASER

short period of time to the ambient illumination. An interference filter tuned to the output radiation can be used to reduce the spectral content of the ambient radiation to further reduce the level of ambient radiation. In general, this is not a satisfactory solution since the bandpass of the filter is dependent upon the angle of incidence to the filter. This characteristic would limit a particular filter to a particular configuration, i.e. limit the angular separation between the reference and object beams. In addition, the interference filter can induce polarization effects in the transmitted beams thereby altering the transmission properties.

Since the use of an interference filter is not desired, a certain amount of ambient light will unnecessarily expose the photographic plate. This will also introduce noise and reduce image contrast since the depth of modulation of the holographic fringes in the recording will be diminished. A method for optimizing the signal-to-noise ratio when reconstructing images from holograms constructed in the presence of an incoherent source (e.g. ambient illumination) is described in Ref. 4 and involves varying the relative intensities of the reference and object beams dependent upon the ambient level.

The amount of ambient illumination which exposes the photographic plate can be minimized by using a shutter immediately in front of the photographic plate and timing the shutter opening to allow the two laser pulses to be recorded during its opening. This solution is an effective one since the shutter need only be open for the duration of the two laser pulses, including the pulse separation time which is generally on the order of 100 microseconds. Large aperture focal plane shutters are not available in this speed range, but with suitable modifications shutter speeds of less than 1/10 second are possible, and should provide for a reduction of the ambient exposure level sufficient to construct holograms.

a. Fatigue Test Laboratory Experiments

As indicated above, the purpose of the Sikorsky tests was twofold: 1) to study the effects of a working environment on the holographic process; and 2) to examine the surface deformation of composite rotor blades undergoing fatigue testing. A typical experimental setup is shown in Fig. 5. During this set of experiments, a hand operated shutter was used. Nominally, 1 to 2 second exposure times were used, but this could not be accurately controlled. A microswitch was installed on the shutter actuating mechanism to fire the laser when the shutter was fully opened. Light meter readings obtained at the test installation indicated an ambient light level of 18 foot-candles.

During the initial phase of these tests, an interference filter was used immediately adjacent to the photographic plate in order to limit the amount of ambient illumination to a tolerable level because shutter durations shorter than 2 seconds were not available. Because of the shift in spectral bandpass with

short period of time to the ambient illumination. An interference filter tuned to the output radiation can be used to reduce the spectral content of the ambient radiation to further reduce the level of ambient radiation. In general, this is not a satisfactory solution since the bandpass of the filter is dependent upon the angle of incidence to the filter. This characteristic would limit a particular filter to a particular configuration, i.e. limit the angular separation between the reference and object beams. In addition, the interference filter can induce polarization effects in the transmitted beams thereby altering the transmission properties.

Since the use of an interference filter is not desired, a certain amount of ambient light will unnecessarily expose the photographic plate. This will also introduce noise and reduce image contrast since the depth of modulation of the holographic fringes in the recording will be diminished. A method for optimizing the signal-to-noise ratio when reconstructing images from holograms constructed in the presence of an incoherent source (e.g. ambient illumination) is described in Ref. 4 and involves varying the relative intensities of the reference and object beams dependent upon the ambient level.

The amount of ambient illumination which exposes the photographic plate can be minimized by using a shutter immediately in front of the photographic plate and timing the shutter opening to allow the two laser pulses to be recorded during its opening. This solution is an effective one since the shutter need only be open for the duration of the two laser pulses, including the pulse separation time which is generally on the order of 100 microseconds. Large aperture focal plane shutters are not available in this speed range, but with suitable modifications shutter speeds of less than 1/10 second are possible, and should provide for a reduction of the ambient exposure level sufficient to construct holograms.

a. Fatigue Test Laboratory Experiments

As indicated above, the purpose of the Sikorsky tests was twofold: 1) to study the effects of a working environment on the holographic process; and 2) to examine the surface deformation of composite rotor blades undergoing fatigue testing. A typical experimental setup is shown in Fig. 5. During this set of experiments, a hand operated shutter was used. Nominally, 1 to 2 second exposure times were used, but this could not be accurately controlled. A microswitch was installed on the shutter actuating mechanism to fire the laser when the shutter was fully opened. Light meter readings obtained at the test installation indicated an ambient light level of 18 foot-candles.

During the initial phase of these tests, an interference filter was used immediately adjacent to the photographic plate in order to limit the amount of ambient illumination to a tolerable level because shutter durations shorter than 2 seconds were not available. Because of the shift in spectral bandpass with

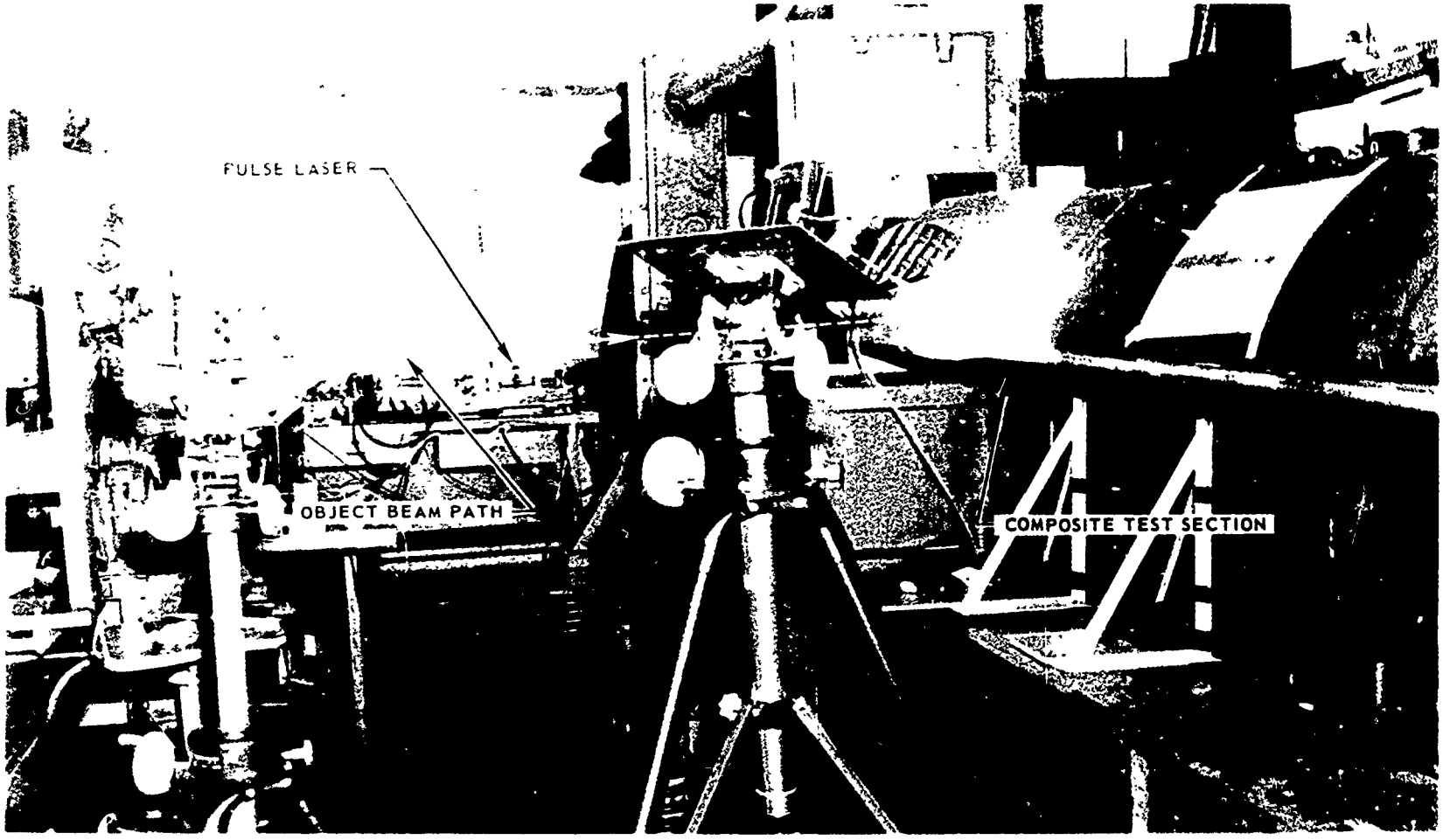

FIGURE 5. HOLOGRAPHIC TEST CONFIGURATION–SIKORSKY AIRCRAFT

respect to the angle of incidence as mentioned earlier, the deviation of the beam must be limited to less than 10 degrees from the normal. In general, because of the constraints imposed upon the holographic process by the object (uniformly illuminated and extended objects), a low spatial offset frequency (small angular separation between the reference and object beams) cannot be used because of the ensuing spectral orders which can overlap producing a noisy or defocused image (Refs. 5 and 6). These effects are especially pronounced in the presence of non-linear recording, i.e., when the combined average intensity of the reference and object beams is not located in the center of the linear portion of the curve representing the film's transmission versus exposure characteristics. In the presence of ambient illumination this (non-linear recording) will be especially true.

Figures 6 and 7 illustrate some typical results obtained from tests conducted in the Fatigue Test Laboratory with a nominal one second exposure and without the use of an interference filter. Figure 6 is a reconstruction of a hologram constructed of an experimental composite blade test section undergoing dynamic fatigue cycle testing. The flexural amplitude was approximately 9 inches at a frequency of 15 Hz. In this case, with the laser pulses 100 microseconds apart, considerable displacement occurred between the two pulses resulting in the high spatial frequency of the interference pattern. However, no anomalies were observed in the fringe pattern. Figure 7 illustrates the results obtained from the examination of an IRB (Improved Rotor Blade) blade section also undergoing flexural fatigue testing. Sections of the blade had been examined prior to the holographic tests and skin delamination, as identified using a coin tap, had occurred in some areas. This area was examined holographically and is, as shown in the figure, easily observed as a change in the background fringe pattern. For this test (IRB blade section) an oscillator-amplifier laser configuration was used in order to increase the total energy available for holographic recording. A Korad pulsed ruby laser was set up, without the cavity mirrors, for use as the amplifier. Approximately 0.3 joules were obtained in this operating mode; gain with the 4" Korad amplifier was approximately 6.

b. Optical Laboratory Experiments

Experimental tests were conducted at UARL to examine, parametrically, the effects of the superposition of the ruby laser illumination and the incoherent ambient illumination. The objective was to determine suitable operating conditions for constructing interferometric holograms in a manufacturing and maintenance environment. Figure 8 illustrates the experimental configuration used for this study. As in a standard holographic configuration, the laser pulse was split into two beams by a beamsplitter for subsequent direction to the holographic plate via beam expander and plane mirror (reference beam) and a ground glass and object (object beam). The beam intensity ratio (relative amount of energy in the respective beams) was varied by the use of attenuation filters in each beam.

SIKORSKY FATIGUE TESTING LAB

FIGURE 6. RECONSTRUCTION OF COMPOSITE HELICOPTER BLADE UNDERGOING FATIGUE CYCLING

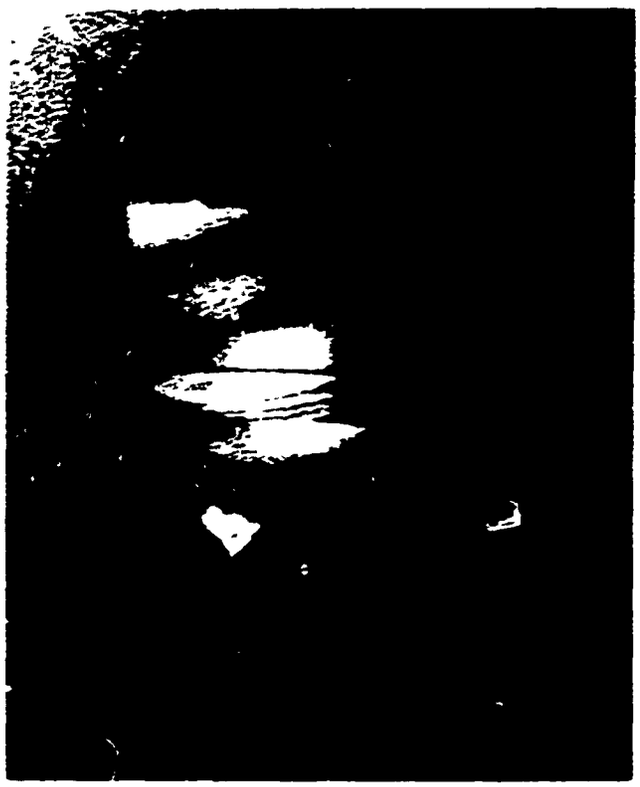

FIGURE 7. RECONSTRUCTION OF IRB BLADE SECTION UNDERGOING FATIGUE CYCLING

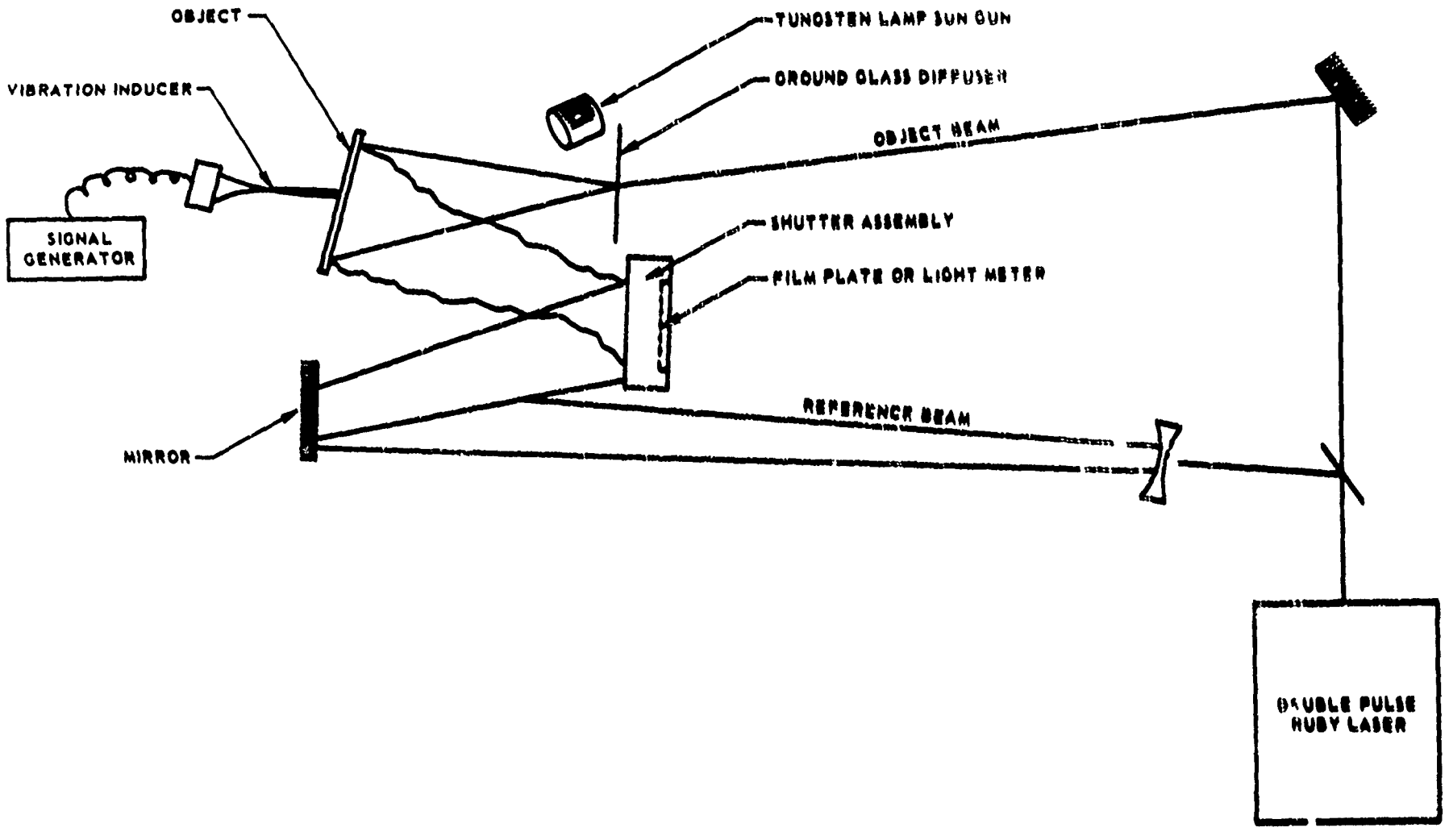

FIGURE 8. HOLOGRAPHIC SETUP FOR AMBIENT LIGHT EFFECTS TEST

Intensity ratios (reference beam to object beam) examined ranged from 40:1 to 1:20. The laser output was monitored using a variety of methods. A small fraction of the output power was directed to a high speed (nanosecond response time) diode and its output observed on a high speed oscilloscope, Tektronix 519, to examine the axial mode structure of the output beam. The diode output was also fed through an integrating circuit to determine the energy content of the individual laser pulses. Thus, the interference fringe contrast, as related to the relative strengths of the two pulses could be examined. Relative energy in the reference and object beam at the photographic plate was determined by a pair of PIN diodes and associated integrating circuitry. These measurements are made after a particular configuration has been established and prior to the holographic construction.

A 12" x 12" aluminum plate was used as the object for these studies. The interference pattern is obtained by stressing the plate acoustically between the two pulses. A transducer and exponential horn were used to generate guided waves along the surface of the plate at approximately 61 KHz. Pulsed ultrasonic excitation was utilized to minimize the effect of reflections from the edges of the plate. The ultrasonic pulse is initiated between the two laser pulses so that the interference fringes recorded on the doubly-exposed hologram represent the surface deformation of the aluminum plate between the unstressed and stressed conditions. An NBS resolution chart has been affixed to the surface of the plate so that, in addition to examining the fringe contrast, the resolution obtained under various conditions could also be examined.

A Weston Electrical Corporation Model 614 foot-candle meter was used to determine the light level of the ambient illumination. For these measurements, the meter was inserted into the shutter assembly into approximately the same position as the photographic plate. As such, it recorded the incident light primarily from the object, but included the background as well. Several light sources and light levels were used because of the significantly different spectral output of the sources and the spectral response of the photographic plate. The fluorescent lights common to most laboratories emit a line spectrum which is predominantly blue and green. In this region the film plates used are less responsive and higher levels of exposure can be tolerated. A Sylvania No. 8 Sun Gun (i.e. a DVY 650 watt tungsten-halogen lamp) was used to simulate worst case conditions. By diffusing the light source and varying its position relative to the object and photographic plate, light levels of up to 200 foot-candles (incident on the photographic plate as reflected off the object) could be obtained. This particular level, as described by the Health and Safety Code, is hazardous, irritating and non-conducive to a good overall working environment.

In order to evaluate the effects of ambient light on the holographic recording process, a curtain-type 4" x 5" focal plane shutter was modified to provide a repeatable 75 millisecond exposure duration. The ruby laser was set up

to fire the double pulse when the shutter was fully open. The 100 microsecond pulse separation of the two 20 nanosecond pulses was easily enclosed within the 75 millisecond shutter time. In addition, a 1.25" diameter aperture was installed in the shutter assembly between the curtain and the photographic plate (Fig. 9a) in order to permit the recording of several holograms on the same plate. Similarly, the plateholder could be installed (Fig. 9b) behind the aperture in any of nine different positions by a magnetic assembly. This permitted the recording of nine different holograms on the same photographic plate while maintaining the relative geometry of the holographic components. Aside from the economical advantages of this assembly, the respective recording of holograms with differing beam intensity ratios could now be assured of identical processing, handling and reconstructing setups.

Initially, double pulse holograms were constructed with no ambient light and the ratio of reference beam energy to object beam energy was varied from 40:1 to 1:20 in nine intervals. Because of the absorbing and reflecting nature of the filters used to alter the respective beam energies, the total energy incident on the photographic plate could not be held constant. That is, to reduce the energy in the reference beam, a gelatin type neutral density filter was inserted into its path. The reduction in energy was not transferred to the object beam to maintain the total energy on the photographic plate, but was instead absorbed in the filter. The consideration of constant total incident energy is germane because of density vs. exposure characteristics of the photographic emulsions. For example, in the situation where the reference beam was 40 times as strong as the object beam, the total energy was high enough to significantly darken the photographic plate. However, when the ratio was altered so that the object beam was 20 times the reference beam's energy, the plate was barely exposed. In this regard the greatest degradation in image quality was a stronger function of the total energy on the plate than of the actual beam ratios.

Figures 10 through 12 illustrate some typical results of the tests conducted using the apparatus described above. As indicated previously, holographic tests were conducted over a range of ambient light levels (from zero foot-candles to 200 foot-candles) with the reference-to-object beam ratio varied in 9 incremental steps from 40:1 to 1:20. The initial tests were conducted to examine the effects on image quality directly and did not include two pulse interferometric holograms for evaluation of fringe contrast effects.

Figure 10 illustrates the results obtained at zero foot-candles (total darkness) and the effect of varying the reference-to-object beam intensity ratio. Three ratios are illustrated 10:1, 2:1 and 1:20. No discernible difference is indicated between 10:1 and 2:1, but image degradation does occur at the 1:20 ratio (Fig. 10c). In Fig. 11 a comparison of the effect of varying the ambient illumination level, with the same reference-to-object beam intensity ratios (5:1), is presented. The ambient level was varied from total darkness to 30 foot-candles

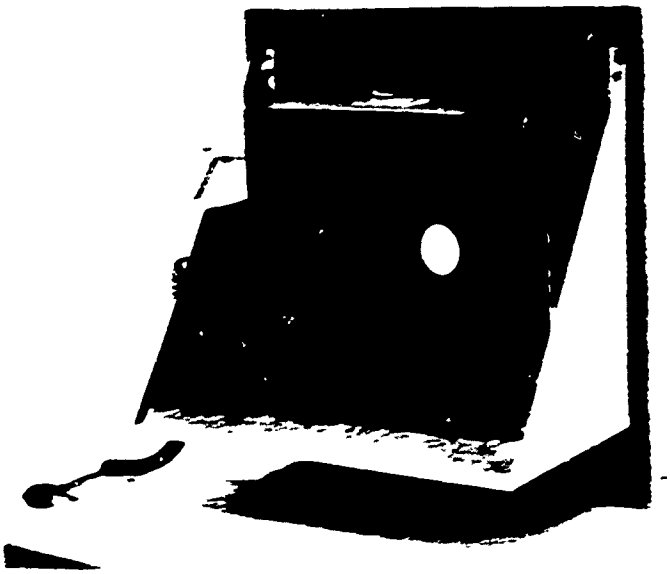

(a)

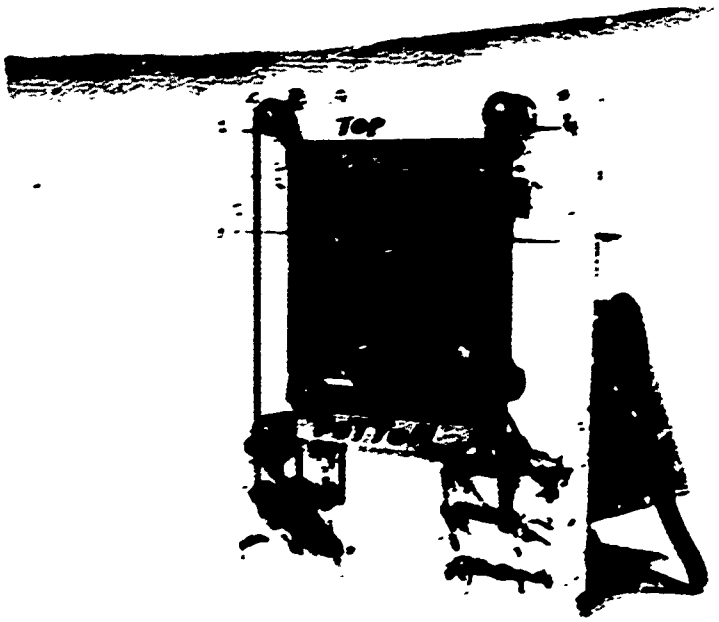

(b)

FIGURE 9. SHUTTER ASSEMBLY

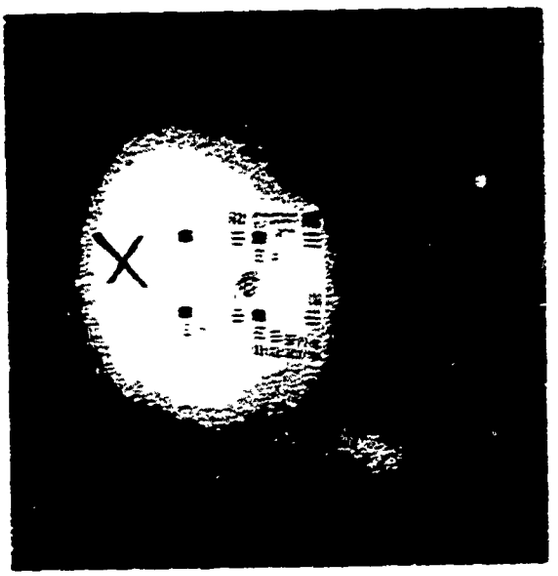

a) R:0 10:1

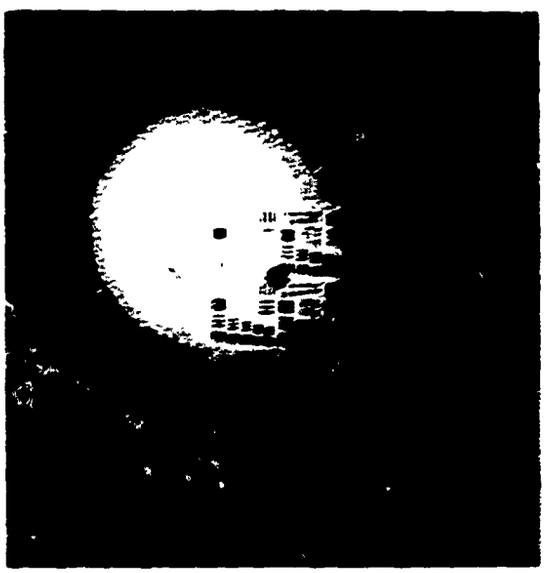

b) R:0 2:1

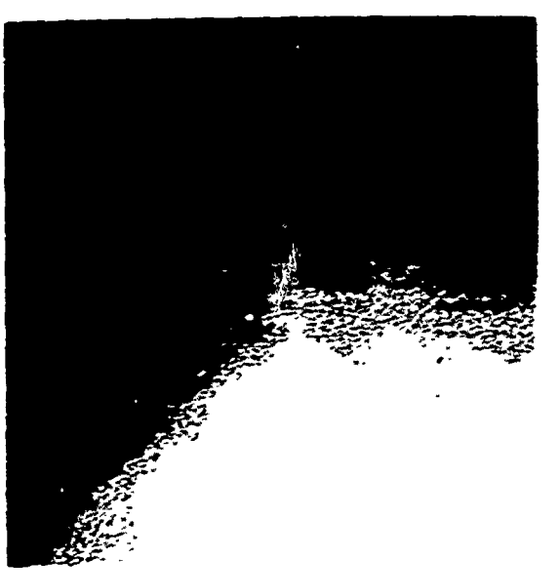

c) R: 0 1:20

FIGURE 10. HOLOGRAPHIC CONSTRUCTION : SINGLE PULSE

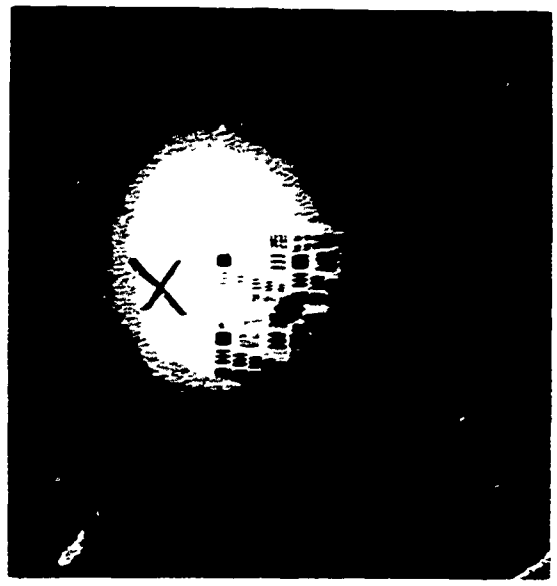

a) R: 0 5:1 0 FT – CDLS

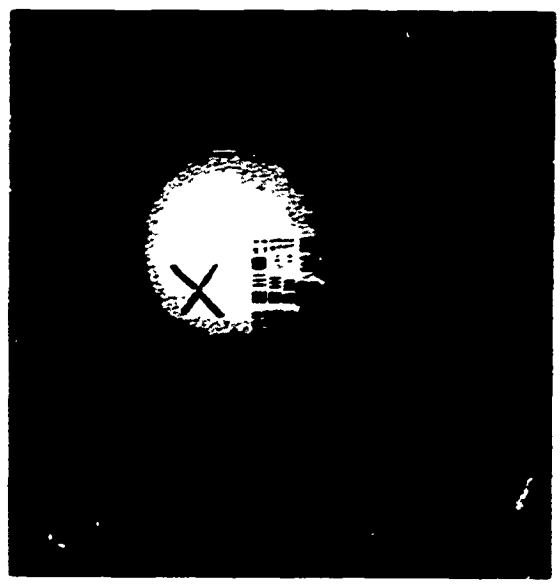

b) R: 0 - 5:1 30 FT – CDLS

FIGURE 11. EFFECT OF NORMAL ROOM LIGHTING ON HOLOGRAPHIC CONSTRUCTION

150 FOOT-CDLS

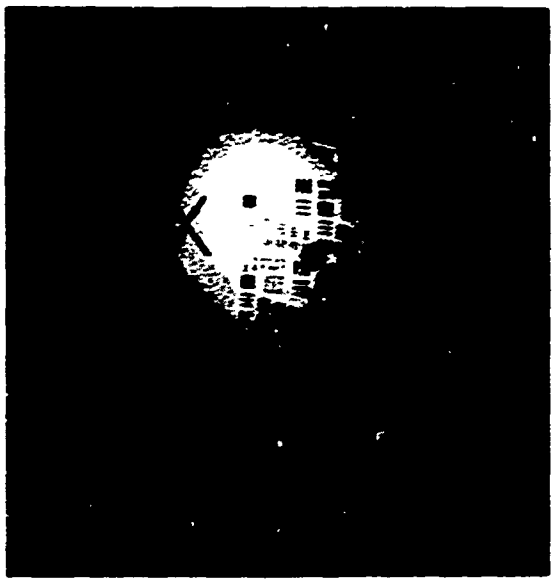

a) R: 0 9:1

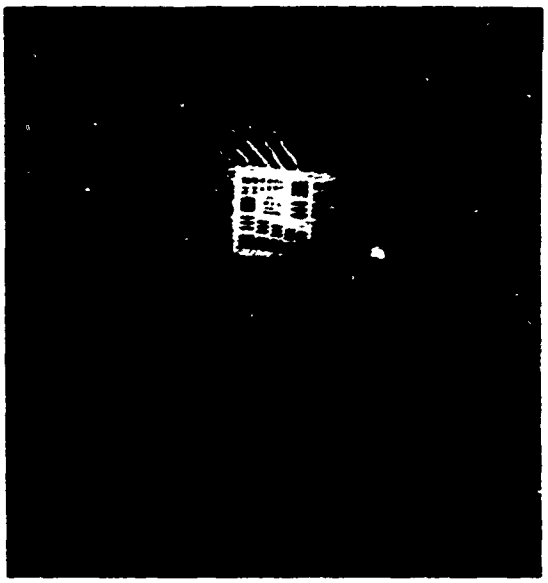

b) R:0 30:1; P_1:P_2 1:8

200 FOOT-CDLS

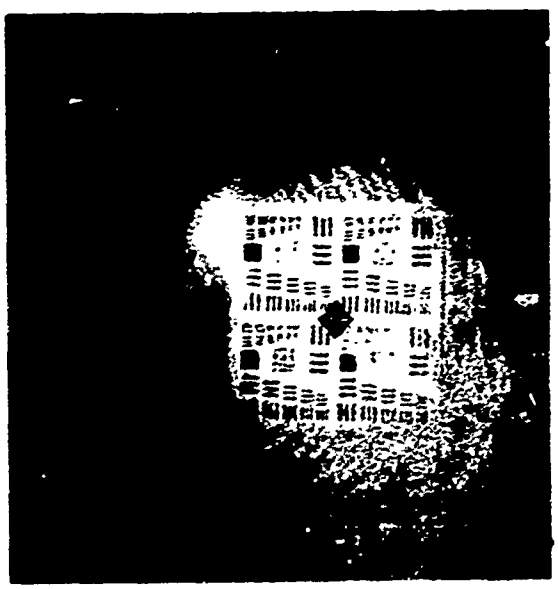

c) R:0 9:1; P_1 : P_2 - 3:1

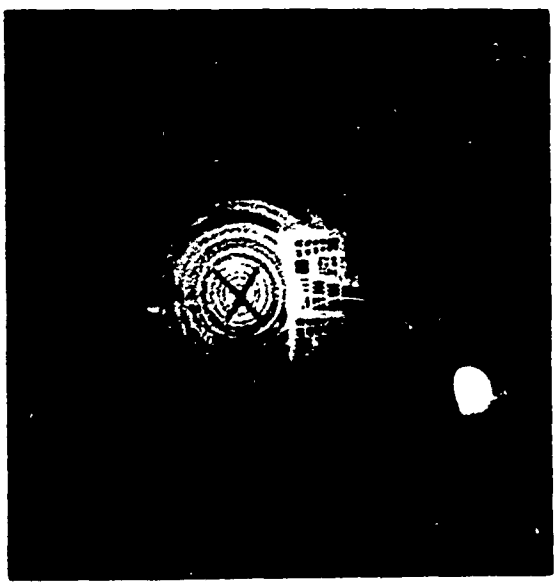

d) R:0 2:1; P_1 : P_2 1:1

FIGURE 12. RECONSTRUCTIONS OF HOLOGRAMS UNDER VARYING AMBIENT LIGHT LEVELS

which represents the normal light level in the optical laboratory. It should be reiterated that the light level is measured in the plane of the photographic plate. Again no discernible difference is noted. Further comparison of Figs. 11a and b with Figs. 10a and b illustrates again that there is little significant difference in image quality when varying the reference-to-object intensity ratio from 10:1 to 2:1.

Typical results of tests conducted at higher levels of ambient illumination (150 to 200 foot-candles) are illustrated in Fig. 12. Several observations can be made by comparing these reconstructions. Comparing Fig. 12a with Fig. 10a (both are single pulses with nearly the same reference-to-object beam intensity ratio; 9:1 for Fig. 12a and 10:1 for Fig. 10a), indicates that little, if any, resolution is lost when constructing holograms with large levels of ambient illumination. The remaining photographs in Fig. 12 depict some of the typical results related to the effects of ambient illumination upon the interferometric fringe contrast. As indicated in the figure, the reference-to-object beam intensity ratios were 30:1, 9:1 and 2:1 for Figs. 12b, c, d respectively. Relative pulse amplitudes (P_1 & P_2) for these same figures were 1:8, 3:1 and 1:1 respectively. The fringe contrast is comparable in the reconstructions although it may appear to be slightly enhanced in Fig. 12b. As a result of the direct comparison of the holograms, it is felt that this apparent difference is more a function of the reconstruction exposure than it is of the construction parameters. (It should be indicated at this point that the interference fringes are not observed on the resolution chart since it was simply taped to the aluminum plate and, hence, was suitably decoupled from the acoustic deformation induced in the plate.)

c. Conclusions

Based upon these results, it appears that good quality interferometric holograms can be constructed in areas which contain high levels of ambient illumination, without filtering, provided that the exposure time can be controlled. For example, the tests conducted with 200 foot-candles measured at the photographic plate indicate this to be the limit for a 75 millisec exposure. However, extrapolation suggests that holographic exposures can be constructed with the object in direct sunlight (average subject produces 600 foot-candles on reflection) by reducing the exposure time to approximately 25 milliseconds. This duration of exposure time is possible with the present shutter assembly by reducing the length of the curtain opening. The results further indicate that there is considerable latitude in the construction parameters within which the quality of the reconstructed objects does not degrade. For example, it is desirable to maintain the reference-to-object beam intensity ratio greater than unity, but the results appear comparable for ratios which range from 30:1 to 2:1. In addition, it is evident that in constructing double-pulse interferometric holograms, it is not necessary that the two pulse amplitudes be precisely matched to optimize the reconstructed fringe contrast.

Effects of Vibration

The short pulse duration (approximately 20 nanosec) of the pulsed ruby laser provides an exposure time which is short enough to eliminate the effects of all mechanical vibration in the construction of a singly exposed hologram. However, as discussed in Ref. 3 the application of double pulsed holographic interferometry still requires stability of the position of the reflecting object (test piece) and the optical components to prevent the formation of secondary fringes which may obscure the desired results. If the relative motion is large, the fringe spacing may be so small as to preclude their resolution and detection. Therefore, the separation of the two pulses used to construct the interferometric hologram must be short enough in time, so that between the two exposures the components have remained essentially motionless, except of course for the deformation introduced intentionally by the deformation generating mechanism.

Fatigue Test Laboratory test pieces studied (composite rotor blade sections) were placed under flexural and torsional loads. Consequently, there were two factors to be considered in the construction of interferometric holograms in this particular facility. The first was the random motion of the optical components relative to the test piece caused by ambient vibration, and the second was the periodic motion of the test piece undergoing fatigue testing.

If considerable motion occurred between the holographic components, a set of interference fringes would be produced (related to their relative line-of-sight displacement) which would not be related to the surface deformation of interest. In the present case, pulse separations of 100 μsec were employed to construct the interferometric holograms. Therefore, only those frequencies above approximately 1 KHz should affect the holographic construction apparatus, if they exist with sufficient amplitude to cause relative displacements greater than 0.347 microns. To test the ability of the laser and holographic apparatus to construct interferometric holograms in this environment, several holograms of a test object in a static unloaded case were constructed. Shown in Fig. 13 is a representative reconstruction of one of these holograms. No interference fringes are visible indicating that vibrational motion above approximately 1 KHz did not have sufficient amplitude to cause relative motion between any of the components during the 100 μsec pulse separation.

The results previously depicted in Figs. 6 and 7 further substantiate that vibrational effects will not interfere with the construction of interferometric holograms in high vibration fields. In these cases the total optical path lengths approached 60 feet which would have exaggerated the beam displacement if the vibration levels were too high. Vibration measurements using a Kistler Model 303B13 accelerometer were taken at various positions in the Fatigue Test Lab which corroborated this conclusion. For example, with the accelerometer mounted on the shakeframe, or on the optical table, the 1 KHz component was determined to

SAMPLE : 6 IN. ALUMINUM PLATE
PULSE SEPARATION 100 SECONDS
AMBIENT LIGHT LEVEL 20 FOOT CANDLES

FIGURE 13. RECONSTRUCTION OF INTERFEROMETRIC HOLOGRAM CONSTRUCTED IN FATIGUE TEST LABORATORY

have an amplitude of less than 2×10^{-4} micron. This would cause a displacement of approximately 2×10^{-5} microns between the two laser pulses which should be insufficient to cause degradation in the holographic image. Vibration tests were also made with two 100,000 pound test machines, which are located in the laboratory, in operation. The displacements calculated were approximately 1,100 microns directly on the machine shake frame and approximately 33μ on the optical table at the resonant driving frequency for the machines of 15 Hz. At 1 KHz the displacements were calculated to be 0.25 microns directly on the shakeframe and approximately 7.5×10^{-3} microns on the optical table or floor.

The results obtained in the Fatigue Test Laboratory indicate that holograms could be constructed in such an environment with pulse separations as long as 100 microseconds. For this case, the displacements which occur at 1 KHz were not large enough to cause image degradation. The displacements at 1 KHz would have to approach approximately 0.04 microns before subsidiary fringes related to optical component shift would be detected.

With regard to motion of the object itself due to the stressing mechanism, the composite blades are generally driven at 500 rpm. In the case of pure flexural motion, the maximum amplitude is approximately 3". Assuming a pulse separation of 100 μsec, the normal line-of-sight displacement would be approximately 120 microns. During the individual 20 nanosecond pulse duration, the test object would move approximately 0.02 microns and should not cause any particular difficulty.

Assuming a maximum allowable motion of approximately 1/8 wavelength along the optic axis in order to maintain a high holographic quality gives a displacement of 0.087 microns during a 20 nanosecond exposure. This leads to a maximum displacement velocity along the line of sight of approximately 430 cm/sec for the object itself before image quality would degrade due to object motion.

Effects of Suspended Aerosols

Another important consideration in the utilization of holographic techniques in an industrial environment is the state of the atmosphere through which the laser beams must propagate to construct the hologram. Of particular importance are the presence of scatterers in the air such as dust, smoke, etc. An obvious solution to this problem is the encasement of the holographic recording system to provide a uniform, non-scattering environment. Although this would not require as massive a structure as that required for vibration isolation, such a structure would reduce the portability of the system and also reduce the versatility.

The size of the aerosol will determine the particular effect it may have upon the holographic image quality. If the aerosol is less than 1 micron in diameter, scattering of the transmitted radiation will predominate. The effect

should be to reduce the total transmission of laser energy to the photographic plate thereby possibly causing image degradation because of insufficient exposure. On the other hand, if the aerosols are of sufficient size (larger than 1 micron diameter) the particle will be resolved in the reconstruction, in addition to causing a loss of transmitted energy. Upon reconstruction, therefore, the particles will be seen causing an obstruction of the observed target.

In order to examine the effects of airborne aerosols upon the holographic image quality, a chamber was fabricated to house the holographic optical components and to contain the aerosols. Figure 14 illustrates the components and the chamber. Aerosol distributions can be inserted and circulated to remove the effects of settling by a small Muffin type fan at one end of the chamber. Since the eventual use of holographic nondestructive inspection methods will require the exposure of all the holographic components to the ambient atmosphere, it was felt that these tests should be conducted in the same manner, i.e. to examine the effects of aerosol concentrations in both the reference and object beams.

The American Conference of Governmental Industrial Hygienists has established a threshold limit value on particulate concentrations in industrial environments. For example, an upper limit of 5 milligrams/cubic meter is given for the concentration of oil vapors. These would generally be limited to particle sizes less than 10μ in diameter.

Preliminary investigations have been carried out to examine the effects of small $<1\mu$ particles (smaller than typical oil droplet sizes of 10μ) upon holographic image quality. These tests have incorporated the use of cigar smoke, with a range of particle sizes approximating 0.01 to 1 microns. No quantitative analysis has been conducted to date, but the results depicted in Fig. 15 are illustrative of the effects of dense smoke on image quality. Even with smoke concentrations far in excess of the threshold limit value for oil vapors, holograms could be constructed, although there was a noticeable loss in both resolution and contrast.

Figure 15b shows considerable image degradation in the resolution chart although the fringes themselves are quite sharp. The standing wave character of this fringe pattern is indicative of improper triggering of the driving transducer in advance, so that the two laser pulses occurred with the plate vibrating, leading to this anamolous fringe pattern. This also may have provided some motion to the resolution chart resulting in the apparent loss in resolution. Additional work in this area is planned for the coming months.

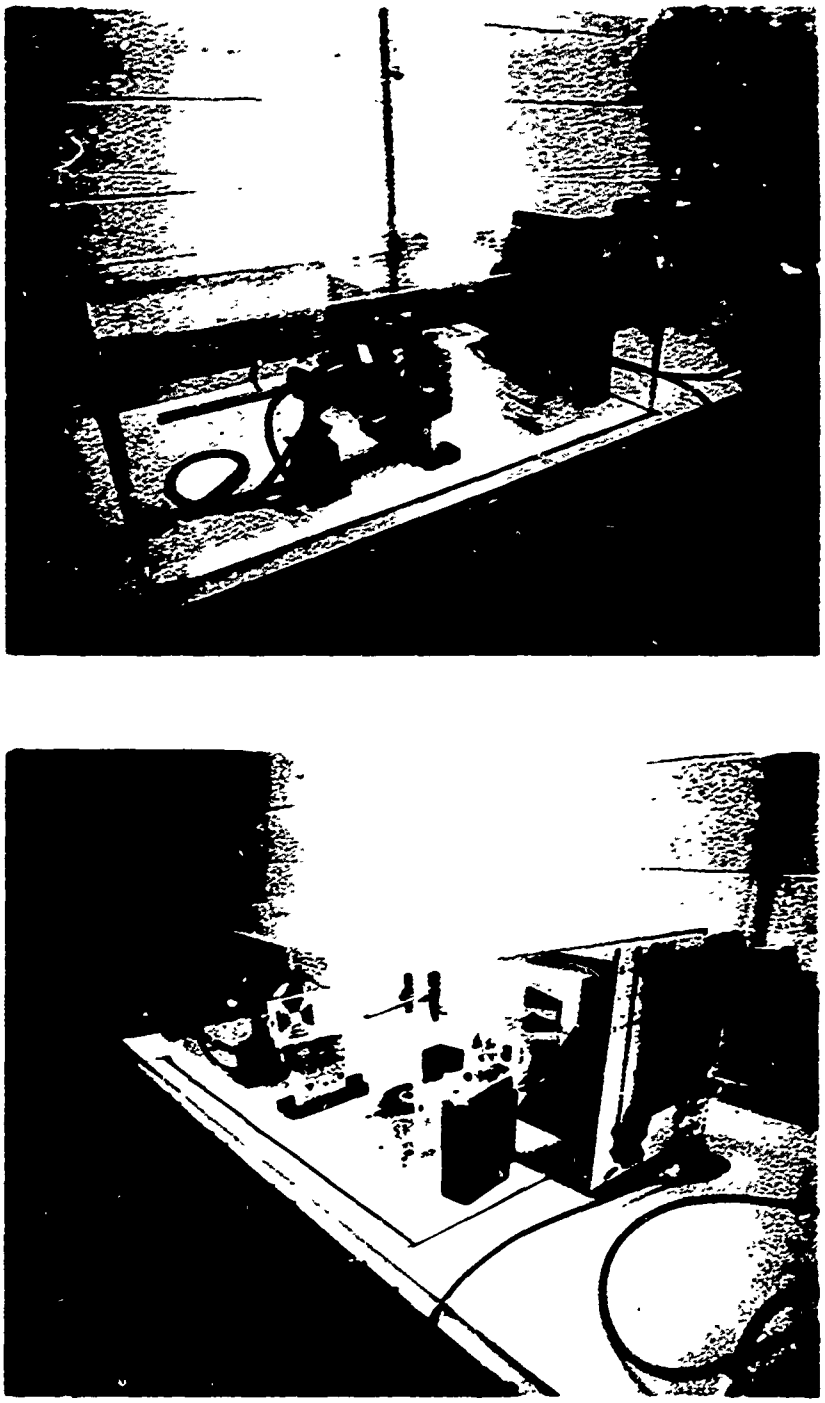

FIGURE 14. AEROSOL CHAMBER

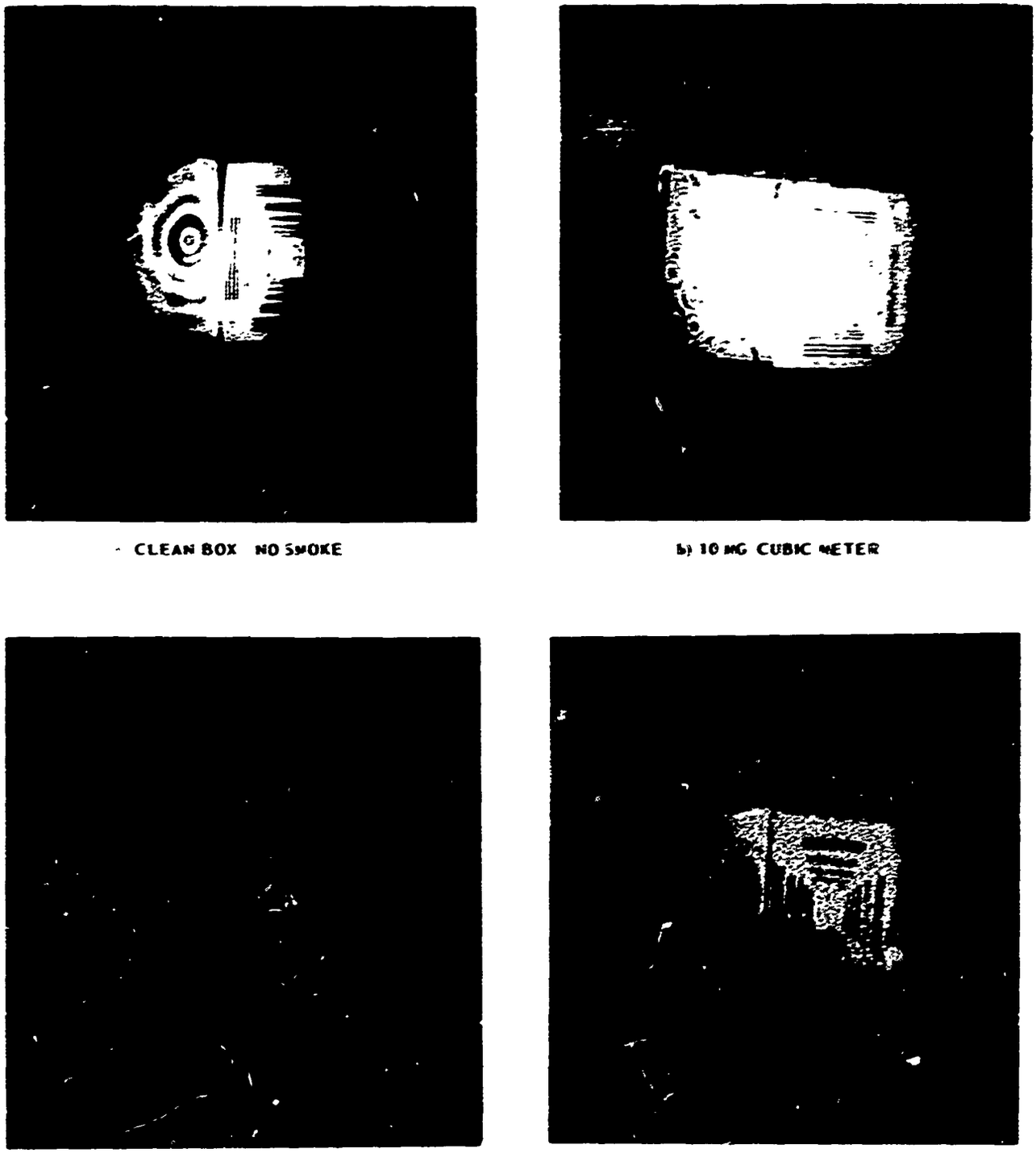

a) CLEAN BOX NO SMOKE

b) 10 MG CUBIC METER

c) 100 MG CUBIC METER

d) 350 MG CUBIC METER

FIGURE 15. RECONSTRUCTIONS OF PULSED HOLOGRAMS MADE IN SMOKE ENVIRONMENTS

SECTION IV

GENERAL STUDIES
SURFACE FINISH EFFECTS

INTRODUCTION

A study was conducted to determine the effects of component surface finish when recording interferometric holograms. The surfaces studied were fabricated by rolling, machining and grinding operations and had average surface roughnesses varying between 4 μ in and 2,000 μ in. The major portion of the experimental effort was directed toward the smoother types of surface finish; those with a measured value under 32 μ in. It is this type of surface which will have the greatest effect on the interferometric fringe quality because of the increased specular content of the scattered light. Since specularly scattered light obeys the mirror reflection law, this portion of the light will have a greater intensity than the diffusely scattered light and could therefore effect the interferometric fringe contrast. It is also possible that the location of a fringe in a specular region could be affected. In addition, the reflectivity of the object surface will determine the amount of energy directed to the holographic plate. All of these considerations will then affect object orientation and maximum object size.

The laser employed in these studies was a pulsed Korad ruby laser operating in an open lase mode. By not Q-switching the laser, an effective pulse length on the order of milliseconds is obtained. (The actual pulse is composed of several microsecond pulses for a duration of a millisecond.) This type of pulse duration has several advantages. First, the pulse duration would be short enough to effectively isolate objects moving due to environmental vibrations, i.e., vibratory frequencies less than 100 Hz. Second, cyclic vibrations higher than 1000 Hz would be time-averaged. This would allow the use of the pulsed laser for time-average holographic interferometry and could be done without the use of vibration isolation systems which are necessary in cw holography. (An example of pulsed time-average holographic interferometry is presented in the section on NDT of Composite Compressor Blades.) Third, the total energy in the laser pulse is increased by about a factor of ten over a Q-switched pulse for the same flash lamp power. This allows larger surfaces to be illuminated which is advantageous for the laboratory studies of rolling and machining effects. Fourth, the power density is considerably decreased and thus conventional expander, spatial filter optics can be employed with a much lower susceptibility to air breakdown effects. The two main disadvantages are: 1) transient events cannot be studied with the laser operating in this fashion, and 2) the temporal coherence length is relatively short, 20 cm. (This latter disadvantage, however, was not found to be a limitation for surface areas as large as 16 sq ft.)

In the following section, results are presented from experiments performed on the 2" x 2" simulated airframe test panel which was also used in the studies for determining areas of maximum strain and strain patterns. In addition, test results are examined from two aluminum panels, one 2" x 2" and the other 4" x 4", each having a different surface finish. Finally, test results are given for ten standard surface roughness specimens. Also included in these studies were experiments performed using the 4" x 4" panel to: 1) determine optimum beam ratios for recording large surfaces exclusive of ambient light effects; 2) investigate differences between diffuse illumination and specular illumination; and 3) evaluate the use of retro-reflecting sheeting for increasing the reflected energy.

EXPERIMENTAL INVESTIGATIONS

Simulated Airframe Panel

The experiments with the simulated airframe panel, which had a machine rolled finish (average surface roughness of 8 μ in), were conducted using double-exposure holographic interferometry with static stress applied to the panel between the pulsed laser exposures. The applied stress was identical to that to be described in the section on Maximum Strain and Strain Patterns (an initial load of 100 με on the center bolt, two outside bolts tightened, and then an additional 700 με applied to the center bolt). The surface of the panel had been preconditioned with dulling spray in order to eliminate all specular reflections during the strain analysis work. It was therefore left in this condition for these experiments because of the difficulty in its removal without damaging the delicate strain gages.

The experimental results obtained with this type of finish showed that the scattered radiation was highly peaked in the specular direction and that the holographic reconstructed image had an appearance of being unevenly illuminated. (This same effect had been observed previously, during the course of the cw holographic work, but was not as pronounced and more easily corrected since a variable exposure time was available.) The panel was therefore tilted so that its center was scattering the maximum amount of radiation in the direction of the hologram (i.e. the center was the apex of the specular angle), thereby providing maximum holographic coverage with pulsed techniques.

Photographs of reconstructed holograms showing this effect are presented in Fig. 16. Figure 16a shows the light distribution when the apex of the specular angle (incident angle of illumination equals recording angle) is located about one-third of the way up the panel; in 16b the apex is centered on the panel; and in 16c the apex is located two-thirds of the way up the panel. In addition, it should be noted that the results of this investigation, using pulsed holographic techniques, confirmed the strain measurements made on this panel using cw holographic interferometry to be reported in a subsequent section of the present report.

(a)

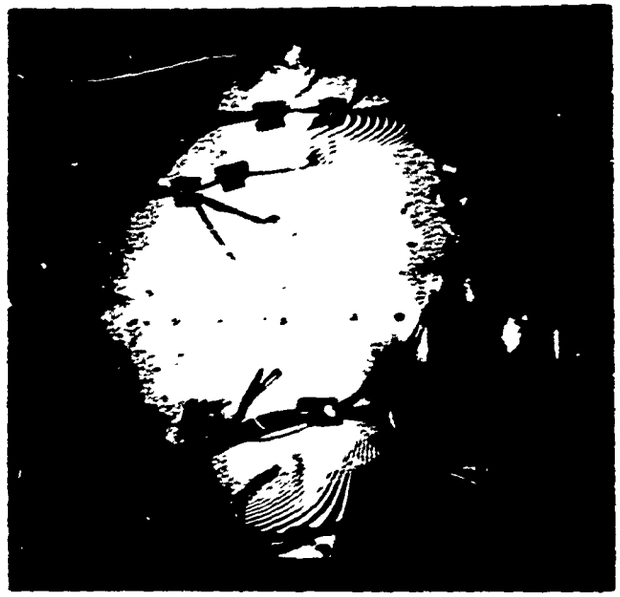

(b)

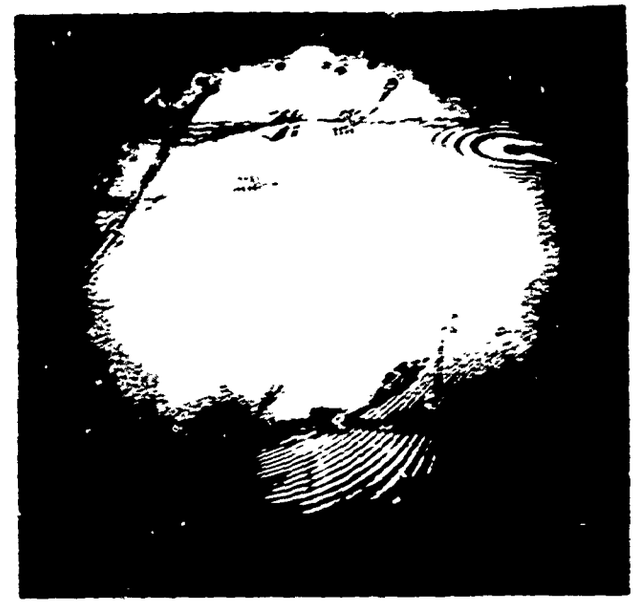

(c)

FIGURE 16. SURFACE FINISH EFFECT STUDIES

In all of the results presented below, the various panels and test specimens were arranged so that the point of specular reflection was centered, thereby providing maximum surface coverage.

2" x 2" Panel

The 2" x 2" panel was machined rolled aluminum 1/32" thick. One surface had an average roughness of 32 μ in while the other was mirror-like, 4 μ in. Upon reflection from this latter surface, images of objects could be recognized, but the surface did have a very fine grain structure in the rolling direction. Photographs of both sides of the panel are presented in Fig. 17. As can be seen, the panel was marked off in both directions in 10 cm increments and the rolling direction indicated by arrows. The panel was affixed to a 10" wide by 1/2" thick plate extending along the vertical center-line. The plate and panel were then clamped in a conventional machine vise. The panel was not damped in any fashion except for the support plate up the center of the panel. By supporting the panel in this fashion, and simply setting it on a table, environmental influences produced movement of the panel between pulsed holographic exposures which resulted in interferometric fringes in the reconstruction. (The supporting plate was necessary to limit the number of fringes so that resolvable fringes could be obtained over the entire surface.) The effect of surface finish on these fringes could then be evaluated.

For the results presented and discussed below, it should be noted that the panel to hologram distance was increased over that utilized in the simulated airframe panel experiments. Thus, although the panel under discussion is the same size, its image appears smaller (it is farther back of the hologram) and has a more even photographic exposure density (the extent of the reconstructed image does not exceed the camera's angular field of view) since the same photographic reconstruction setup was employed. It is for a similar reason that the reconstructions of the simulated airframe panel described previously (Fig. 16) are not as asthetically pleasing as those presented later (Figs. 32-34) in the section on Maximum Strain and Strain Patterns.

Two double-exposure pulsed holographic interferograms were recorded of each side of the panel. One recording was made with the rolling direction vertical to the table and the other with it in the horizontal direction. The results of these tests are shown in Fig. 18. Figures 18a and 18b are the smoother surface finish, while 18c and 18d illustrate the results obtained with the rougher surface.

Interferometric fringes on the smoother surface are clearly visible well beyond the center of the panel (point of specular reflection). The intensity does, however, fall off quite rapidly and as a result the edges of the panel are not visible. The fringes near the specular point are still quite well resolved,

2 FT × 2 FT PANEL

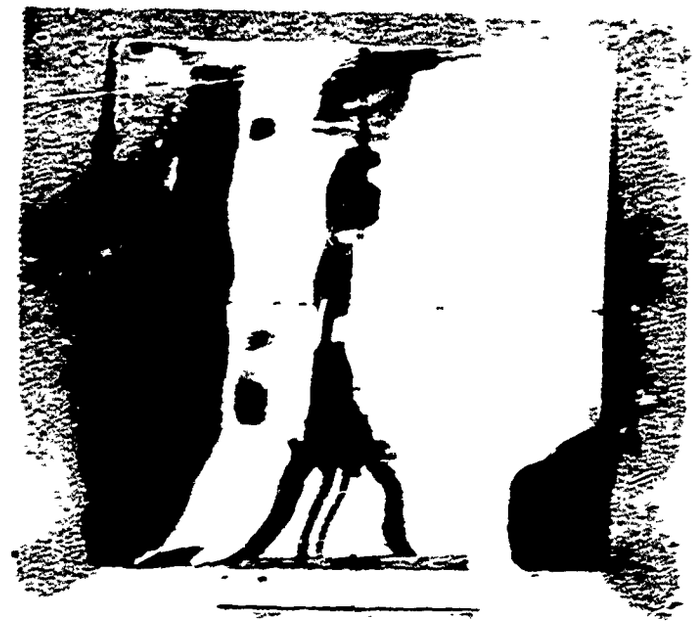

(a) SURFACE ROUGHNESS ~ 4 μ IN

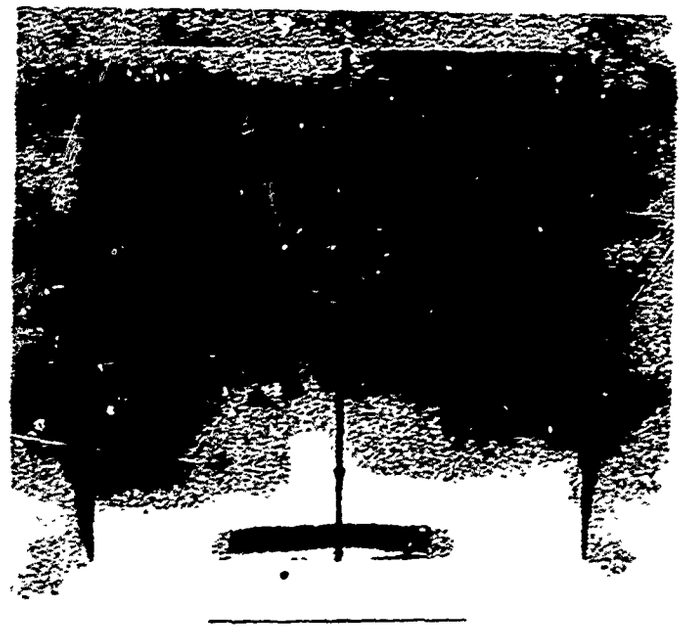

(b) SURFACE ROUGHNESS ~ 32 μ IN

FIGURE 17. SURFACE FINISH EFFECT STUDIES

2 FT x 2 FT PANEL

(R.D. - ROLLING DIRECTION)

(a) R.D. - VERTICAL

(b) R.D. - HORIZONTAL

SURFACE ROUGHNESS~4 μIN

(c) R.D. - VERTICAL

(d) R.D. - HORIZONTAL

SURFACE ROUGHNESS~32 μIN

FIGURE 18. SURFACE FINISH EFFECT STUDIES

but right at the specular point all interferometric information is lost. Also seen in the photograph of the reconstructions is a streak of intense light running through the center of the panel perpendicular to the rolling direction and is a result of the surface structure (fine scratches in the rolling direction). These scratches tend to specularly reflect light perpendicular to themselves. Interferometric fringes passing through this region are unaffected except for a slight narrowing.

Results from the rougher surface (Figs. 18c and d) show that the intense specular point is no longer evident; the overall intensity distribution varies much less across the panel (edges of the panel are visible); and the streak of light perpendicular to the rolling direction is still present with the attendent fringe narrowing at these points.

4' x 4' Panel

In order to assess the surface finish effects of larger surface areas, a 4' x 4' machine rolled aluminum panel 1/16" thick was studied. One surface of the panel was painted with a flat white paint and the other left natural (average roughness approximately 8μ in). Each surface was marked off in 10 cm increments and arrows placed on the natural surface to indicate the rolling direction. Photographs of the panel are presented in Fig. 19. The panel was supported in a manner similar to the smaller panel, in that a 4" wide by 1" thick bar extending along the vertical centerline of the panel was used for support. The bar and panel were then clamped in a machine vise and set on a table. A photograph showing the experimental arrangement with this panel mounted in position is presented in Fig. 20. Also shown in the figure is the pulse laser, optical components and a ray trace of the optical paths. The holographic plate and illumination beam were elevated to the center line of the panel so that the specular point could also be located along this line.

The problem of uneven exposure density and inability to photograph the entire image in the reconstruction process is especially evident in the results presented below (Figs. 21-23). The distance between the 4" x 5" hologram and the 4' x 4' panel was approximately 6'. Thus, while the reconstructed image of the entire panel is easily observed visually, a lens with the proper combination of focal length and angular field-of-view was not available to photograph it.

a. Beam Ratio Studies

The first series of experiments was conducted using the flat white surface of the panel in order to optimize the geometrical parameters. (These tests can then be compared with the results obtained from the unpainted surface.) When double pulsed holograms were made of the white surface, it was found that the light was again scattered primarily in the specular direction. Even though the

4 FT × 4 FT PANEL

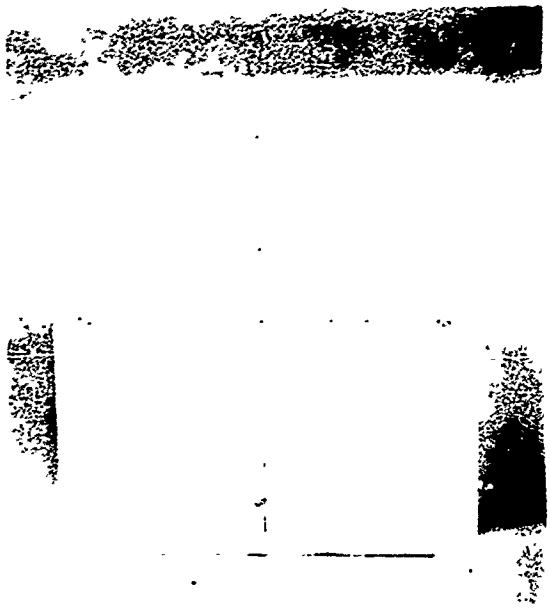

(a) FLAT WHITE

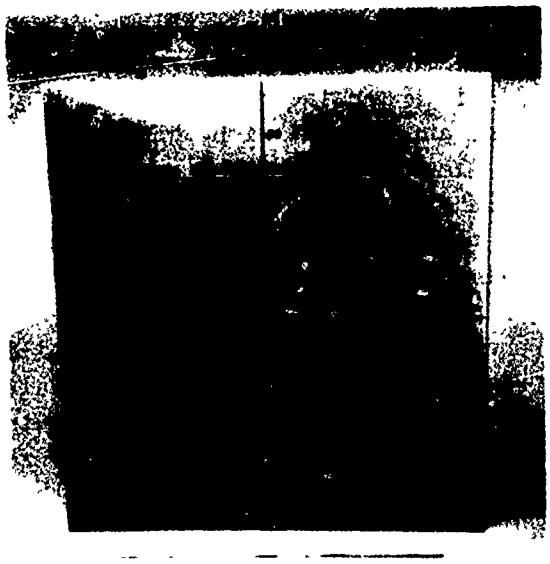

(b) NATURAL ROLLED FINISH
(ROUGHNESS 8 μ IN.)

FIGURE 19. SURFACE FINISH EFFECT STUDIES

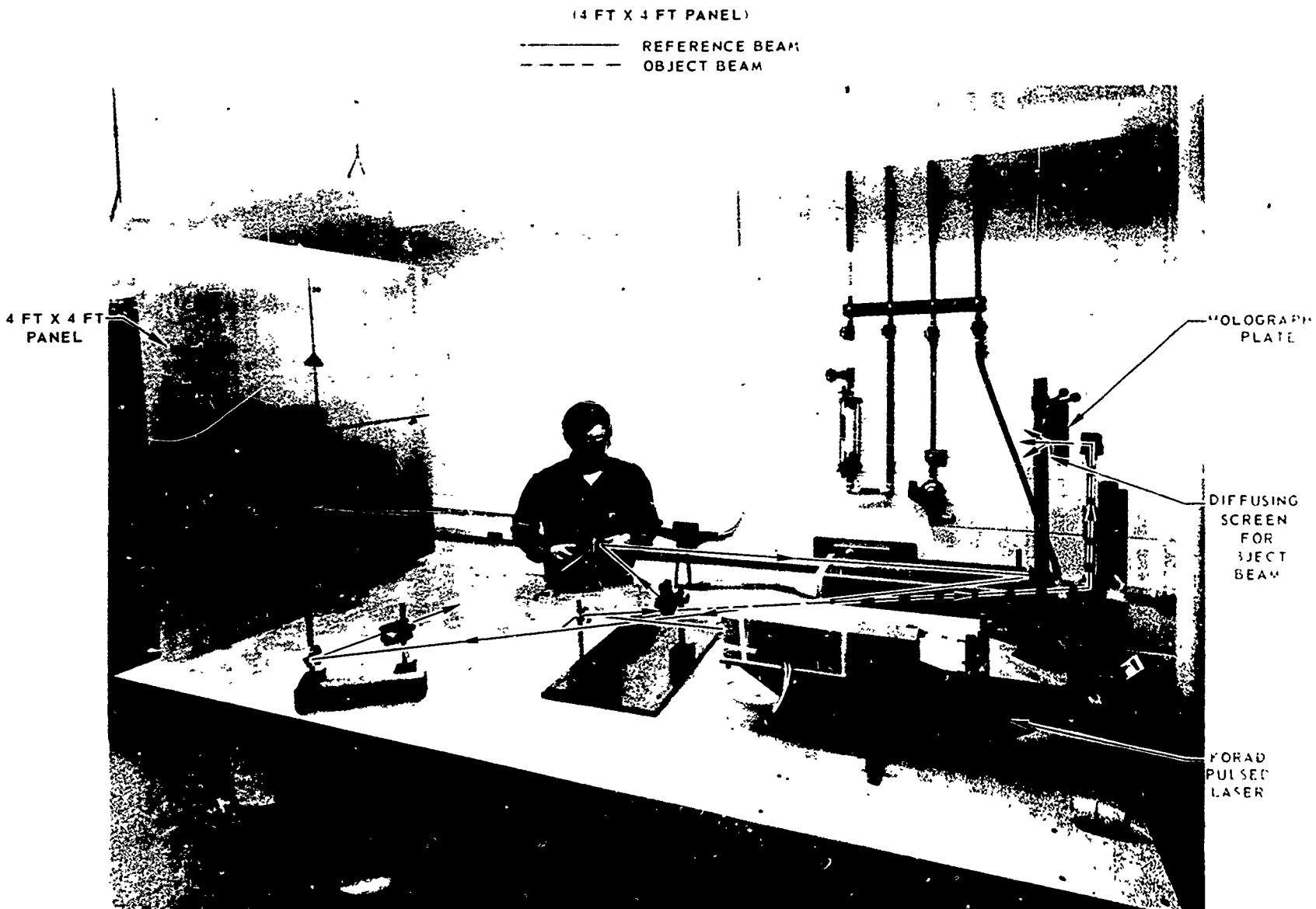

FIGURE 20. SURFACE FINISH EFFECT STUDIES

panel, hologram, and illumination source were aligned so that its center was scattering the maximum amount of light in the direction of the hologram, only the center portion of the panel could be recorded. It was found, however, that by increasing the intensity of the light energy in the reference beam when making the holographic exposures, it was possible to record the entire panel; and, just as significantly, improve the fringe contrast. Three photographs of double pulsed holographic reconstructions are presented in Fig. 21 demonstrating the latter effect. Figure 21a was taken from a hologram which used a 40X objective in the reference leg of the optical system. This provided approximately equal intensities in the object and reference beam, and resulted in a hologram having a silver density equivalent to a neutral density (N.D.) filter of approximately 0.3. As seen in the figure only the center portion of the panel is visible. Figures 21b and c were taken from holograms recorded in a manner identical to that in Fig. 21a except for the power of the beam expander in the reference leg which was decreased to increase the reference beam intensity level. Figure 21b was recorded with a 20X microscope objective, and Fig. 21c with a 10X microscope objective. The resulting holograms had N.D.'s of approximately 0.6 and 1.2 respectively. Both holograms recorded the entire panel, although the reconstruction from the denser hologram (Fig. 21c) was not as bright as the other.

It appears that once the point has been reached where the exposure from the reference beam produces an adequate silver density (N.D. of 0.6) on the holographic plate, further increases in the intensity provide no additional benefits. It is suppositioned that due to the non-linearity of the photographic film, as described in the Physical Environment Effects section, the intense reference beam causes the film to reach the more sensitive portion of the characteristic exposure-density curve. This then allows the lower light level from the outlying regions of the panel to be recorded.

The interferometric fringes recorded in the hologram having a N.D. of 0.6 were of excellent quality towards the center of the panel, with the contrast degrading slightly in regions near the edges. This is a result of the lower recorded intensity in these regions.

b. Diffuse Illumination Studies

In addition to using a simple lens system for expansion of the laser beam to illuminate the 4 foot square panel, a ground glass diffuser plate was also employed as the beam expansion element. These tests were made in order to ascertain the effectiveness of this type of device for recording holographic interferometric fringes. Figure 22 shows the results of these tests. The photograph in Fig. 22a was taken from a hologram recorded using a lens as the expansion element while the reconstruction in Fig. 22b was recorded with a ground glass diffusing plate mounted in the same location as the lens. As seen, there are no significant differences between the two holographic reconstructions in either

BEAM RATIO STUDIES

4 FT X 4 FT PANEL – PAINTED FLAT WHITE SURFACE

(a) 40X

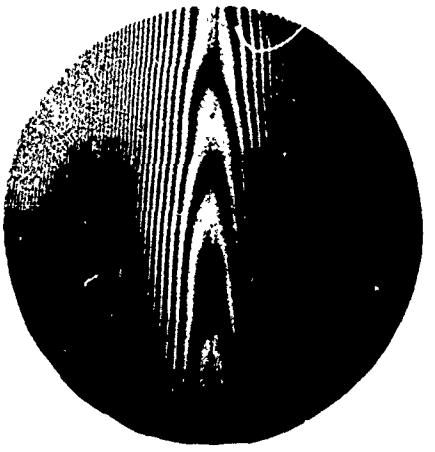

(b) 20X

(c) 10X

FIGURE 21. SURFACE FINISH EFFECT STUDIES

DIFFUSE ILLUMINATION STUDIES

4 FT X 4 FT PANEL - PAINTED FLAT WHITE SURFACE

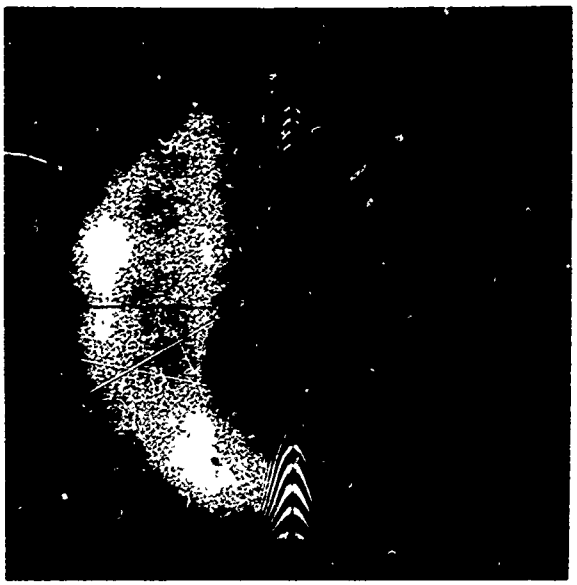

(a) BEAM EXPANSION WITH LENS

(b) BEAM EXPANSION WITH DIFFUSER PLATE

FIGURE 22. SURFACE FINISH EFFECT STUDIES

fringe quality or area coverage. In subsequent tests, however, one advantage of using a diffuser plate became most evident. Regardless of the intensity distribution across the raw (unexpanded) laser beam, the object illumination beam could be rendered quite uniform with a diffuser plate as the expansion element. This is not true with a lens expander which essentially maintains the intensity distribution in the beam passing through it.

The panel was next turned around and the effects of a large unpainted machine rolled surface were holographically examined with the rolling direction both vertical and horizontal to the plane of the support table. Two representative holographic reconstructions are presented in Figs. 23a and b. As shown in these photographs, the intensity of the reconstructed image falls off far more rapidly than in the case of the flat white surface. In addition, a streak of light perpendicular to the rolling direction is evident as was found for the case of the smaller panel. The interferometric fringes are of excellent quality near the center, but again fall off in contrast nearer the edges.

c. Retro-reflecting Sheeting Studies

In order to demonstrate that the intensity drop-off near the edges of the panel is a result of surface finish and its attendant effects on reflected laser illumination, rather than being due to a lack of coherence length, an 8" x 6" piece of retro-reflecting sheeting was placed in the upper righthand corner of the panel. (The retro-reflecting sheeting was supplied to UARL by W. F. Fagan of Paisley College of Technology, Scotland. A spray paint having similar optical properties is currently under development by Fagan in conjunction with the 3M Company and could provide an effective means for recording large surface areas with low energy output lasers.) A photograph of the reconstruction, illustrating the enormous increase in reconstructed intensity in the area of the retro-reflecting sheeting is presented in Fig. 23c. In addition, the fringe contrast is improved but is difficult to compare with those on the panel because of the two radically different types of surfaces. (The increased fringe density on the sheeting is a result of only the corners being fastened to the panel. This allowed the center to move freely as a result of the environmental influences.)

Standard Roughness Specimens

The 2" x 2.5" standard surface roughness specimens (manufactured by General Electric) used in these studies consisted of ten surfaces of graded roughness. The surfaces, which are made of steel, were manufactured using typical fabrication methods (grinding, lapping, milling, etc.) and represent average surface roughnesses between 4 microinches and 2000 microinches. Figure 24 shows a photograph of the specimens with the average surface roughness labeled beneath each specimen. Seven of the specimens were fabricated by several different machining processes, all yielding the same surface roughness (surface roughness > 16 microinches).

(a.) R. D. – VERTICAL

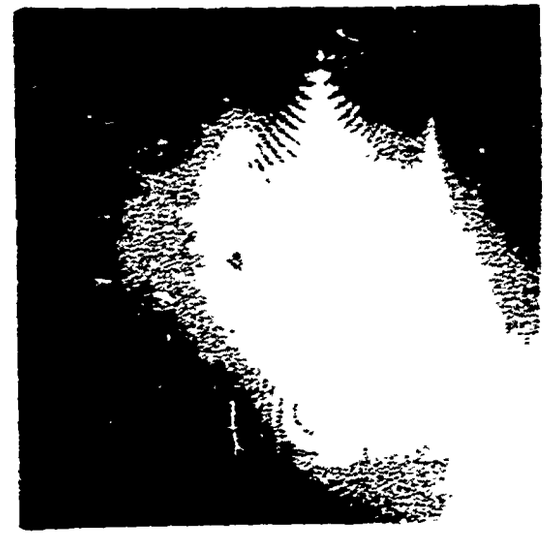

(b.) R.D. – HORIZONTAL

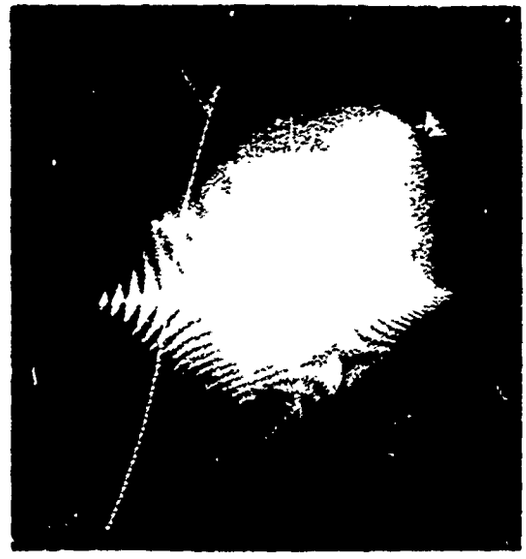

(c.) RETRO-REFLECTING SHEET
R.D. VERTICAL

FIGURE 23. SURFACE FINISH EFFECT STUDIES

STANDARD ROUGHNESS SPECIMENS

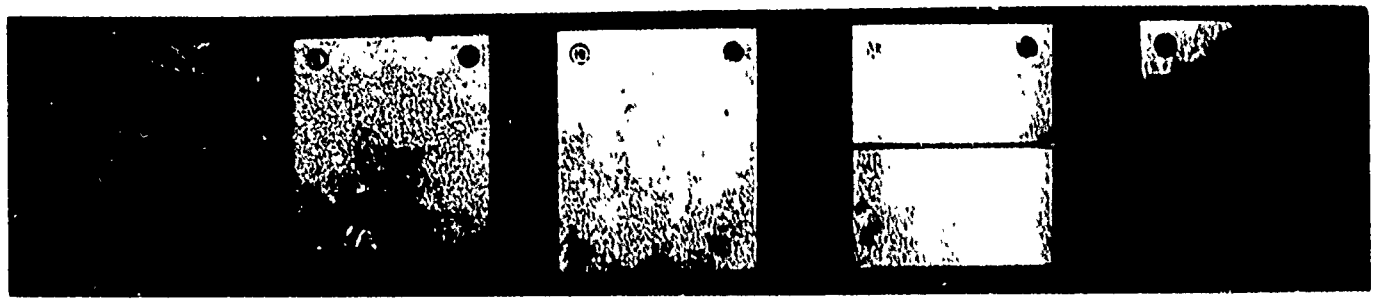

4 μ IN. 8 μ IN. 16 μ IN. 32 μ IN. 63 μ IN.

125 μ IN. 250 μ IN. 500 μ IN. 2000 μ IN. 1000 μ IN.

FIGURE 24. SURFACE FINISH EFFECT STUDIES

Reproduced from best available copy.

The specimens were mounted, as shown in Fig. 24, on a thin aluminum panel having gray paper as the background. This was then attached to a thicker mounting plate (1/2" thick by 10" wide), clamped in a machine vise and set on the holographic table. Double pulse holographic interferograms were then recorded of the panel, and movement between exposures to produce interferometric fringes was provided by environmental influences. Double pulse recordings were made in this fashion with the surface finish direction both vertical and horizontal to the plane of the table.

The results of these experiments are presented in Fig. 25. High contrast interferometric fringes are present on all of the specimens. In addition, fringe location on even the roughest specimens, as well as the others, is relatively unaffected by the large variation in surface finish. (It can be seen that there is some slight deviation in the fringes on the 2000 μ in specimens.)

On the basis of the experimental results, discussed in the preceding paragraphs, which illustrate the effects of various surface finishes (4 μ in to 2000 μ in) and sizes (up to 16 sq ft), the following statements can be made:

1. Interferometric holograms of surfaces with a roughness of less than 4 μ in (a very high polish) have been easily recorded.

2. The intensity of the radiation scattered from a surface is highly peaked in the specular direction. This will tend to limit the area coverage on smooth surfaces. The present tests have demonstrated the capability of recording a 4 foot square object, with a surface roughness of 8 μ with an 8 foot separation between object and hologram.

3. Specular reflections are enhanced perpendicular to the surface finish direction. Thus, interferometric fringe information may be lost or degraded (a slight narrowing of the fringes) in areas of very intense specular reflection (usually a single narrow line).

4. Interferometric fringe contrast decreases as the recorded intensity decreases.

5. Holographic interferometric quality is independent of the laser beam expansion element (simple lens system or diffuser plate), except in cases where the raw laser beam has an uneven intensity distribution; in this event diffuser plates are preferred.

6. To obtain the maximum recorded area in a holographic interferogram, the specular point should be centered about the surface area of interest and in the case of no ambient illumination, the reference beam adjusted to yield a hologram with a N.D. of approximately 0.6.

(a) MACHINE MARKS VERTICAL

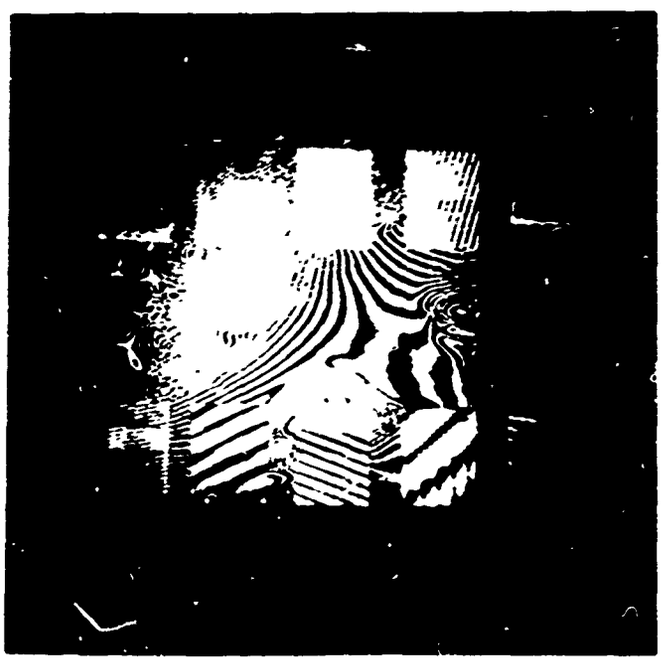

(b) MACHINE MARKS HORIZONTAL

FIGURE 25. SURFACE FINISH EFFECT STUDIES

7. The degree of surface roughness up to 1000 μ in does not significantly affect interferometric fringe location.

8. Retro-reflective surface preparations may afford an enormous increase in allowable area coverage for a given laser system.

SECTION V

SPECIFIC PROBLEM INVESTIGATIONS
MAXIMUM STRAIN AND STRAIN PATTERNS

INTRODUCTION

A study was conducted to anticipate and resolve the problems expected in performing pulsed-laser holographic strain analysis on large aircraft structures in realistic environments. This study involved extremes in both the analytical and experimental conditions.

Analytically, an unambiguous determination of the strain field is required, taking as data the interferometric fringe field from double-exposure holograms of large structures. Possible sources of error in the holographically-recorded interference patterns which had to be considered were: absence of a zero-motion reference point; variations in the illumination and recording angles; effects of translation and rotation; and the curvature and aspect angle of the object. In addition, the size and lack of symmetry in the structural surfaces studied made it necessary to perform a full three-dimensional analysis of the displacement field rather than rely on the conventional two-dimensional interferometric theory.

Experimentally, the extreme viewing angles (up to 45°), large subject surface areas, sensitivity of large unsupported surfaces to extraneous environmental influences even under isolated conditions, and difficulties in data reduction all had to be considered. In addition, the typically extreme sensitivity of holographic interferometry to displacement made it difficult to compare the holographic data with conventional strain gage data for the purpose of verifying data reduction procedures.

The following two major parts of this section provide a comprehensive review of the first year's effort directed toward applying interferometric holography to the determination of maximum-strain concentration points and strain-pattern visualization on large aircraft structures. The first part pertains to the theoretical analysis. It contains discussion of: holographic interferometric theory as applied to large three-dimensional structures; holographic layout geometry; simple translational and rotational rigid body motions which may produce spurious strain data; the effect of object orientation and curvature; and a procedure for data reduction and computation of spatially-resolved strain fields. The second part reviews the experimental phase of the study. It contains a description of the test equipment used in the experiments; procedures to obtain the holographic data; and a comparison of holographic strain measurements with conventional strain gage data recorded on large structural surfaces.

THEORETICAL ANALYSIS

The measurement of surface strain has been achieved by means of various methods employing holographic interferometry. In every case, the methods have had inherent limitations which preclude their application to the measurement of surface strain on large three-dimensional structures in a realistic environment. The following is a survey which reviews the principal holographic approaches implemented in the past and discusses the limitations of each. Following this, a theoretical basis for a method which circumvents or minimizes these limitations is developed.

Haines and Hildebrand (Ref. 7) first analyzed the interferometric fringe field obtained from the superposition of an object surface in two states, recorded in a single hologram. The object motion is expressed as a function of a displacement vector for each point on the surface and the Euler rotation angles of the normal to the surface. The motion field may be solved by measuring fringe frequency about the object point along two orthogonal directions transverse to the line of sight. In order to obtain the full three-dimensional displacement field, however, two different viewing directions of the same scene are required along with a knowledge of the distance from the object to the position of localization of the fringes; the latter generally being a difficult parameter to measure.

A considerably simpler formulation was derived by J. E. Sollid (Ref. 8) and later extended by K. Shibayama and H. Uchiyama (Ref. 9). In this formulation the general motion can be solved completely, but the absolute fringe order as measured from a zero-motion point must be known. Additionally, three holographic viewpoints are required, which for a large object implies three holograms separated by appreciable viewing angles. Both of these requirements are impractical in the application of pulsed holography to large, moving objects.

A method proposed by Alexandrov and Bonch-Bruevich (Ref. 10) describes the surface motion point by point. The Euler angles, the position of localization of the fringe pattern, and absolute fringe order are not necessary if the fringes are viewed in the same plane as the image. A method for data reduction, involving just one hologram, is proposed which works in principle but is severely limited in practice by the solid angle which the object subtends at the hologram.

A feature shared by all of the above methods is that they make a direct measurement of the surface deformation in the direction of strain while recording the holograms at near normal incidence. However, in many cases, the amount of surface deformation in the direction of strain is small even by holographic-interferometric standards. (100 $\mu\varepsilon$ on a two-and-a-half centimeter sample would only result in an observation of a 5×10^{-4} part of a fringe.) A. E. Ennos

(Ref. 11) demonstrated direct measurement of in-plane strain which maximizes the holographic sensitivity to the in-plane motion. The procedure requires that the holographic recording be made at grazing incidence to the surface being measured. There are, however, a number of disadvantages to this procedure, one being that unless the surface is flat, the field-of-view is severely limited. (Even with a flat surface, the reconstructed image is distorted due to the skewed viewing angle.) Another disadvantage lies in the fact that if the surface has an out-of-plane displacement component introduced by the stressing force, two different holographic views of the surface must be recorded, and the strain data obtained by subtracting one set of interferometric fringe contours from the other. This would add a considerable amount of time to the data reduction procedure. A further limitation is that the extent of the surface which can be analyzed is only as long as the coherence length of the laser. (The surface area which can be recorded holographically when the illumination is normal can always be increased by moving the hologram further away.) Because of the above disadvantages, the direct measurement of in-plane strain on large complicated surfaces, recorded at grazing incidence, must be ruled out. Direct measurement at near normal incidence must also be ruled out because of the extremely low sensitivity of holographic interferometry to this type of movement.

Another technique for measuring in-plane strain directly (Ref. 12 and 13) utilizes the speckle effect from a coherent light source. Although this technique cannot be strictly interpreted as being holographic, it does have the advantage of measuring surface strain directly with interferometric type accuracy. The principle of operation is to compare the speckle pattern, produced when a coherent light source illuminates a diffusively reflecting surface, with itself after a stress has been applied. This is done by photographically recording an image of the speckle pattern on the surface of the object caused by illuminating the surface simultaneously from two different directions with a laser light source. This photograph is then placed in the image plane and acts as a "shadow filter" to monitor changes in the speckle pattern due to an applied stress. These changes result in bright and dark fringes covering the image plane. The process is similar to a Moiré technique except that, instead of comparing two grid patterns, two random speckle patterns are compared.

Disadvantages of the technique are that the fringe contrast is generally poor, and it has a limited dynamic range. Another disadvantage would be that the in-plane displacement is usually not as great as the normal displacement in simple bending modes; thus, the technique would not be as effective in this case as the holographic technique. If large in-plane forces are involved, and in-plane displacements must be studied as opposed to normal displacements, the technique would be attractive from the standpoint of visual interpretation of the resulting patterns for qualitative measurements; quantitative results could be achieved by data reduction.

However, in general, the holographic strain measurement must rely on the indirect approach of first determining the out-of-plane surface displacement caused by a stressing force and relating this to the actual in-plane strain. The relationship between the principal in-plane strains and the out-of-plane displacement can be seen by first considering the relationship between the strains in any two orthogonal directions with the strains along the principal axis (Ref. 14):

$$\varepsilon_{\substack{max\\min}} = \frac{\varepsilon_x + \varepsilon_y}{2} \pm \frac{\sqrt{(\varepsilon_x - \varepsilon_y)^2 + \varepsilon_{xy}^2}}{2} \qquad (1)$$

where ε_{max} and ε_{min} are the principal strains, ε_x and ε_y strains in any two orthogonal directions, and ε_{xy} the shear strain. Associated with each strain direction is a surface curvature term (Ref. 15).

$$\varepsilon_y = -c\,\frac{\partial^2(\Delta Z)}{\partial x^2} = -c\;\chi_x$$

$$\varepsilon_y = -c\,\frac{\partial^2(\Delta Z)}{\partial y^2} = -c\;\chi_y$$

$$\varepsilon_{xy} = -2c\,\frac{\partial^2(\Delta Z)}{\partial x\;\partial y} = -2c\;\chi_{xy}$$

where c is the distance of the surface from the neutral surface of the object; $\partial^2(\Delta Z)/\partial x^2$ and $\partial^2(\Delta Z)/\partial y^2$ is the second derivative of the flexure displacement ΔZ with respect to the transverse surface coordinates (surface curvature) which is represented by χ_x and χ_y; $\partial^2(\Delta Z)/\partial x\;\partial y$ is the derivative of the flexure displacement with respect to both orthogonal coordinates (twisting curvature) which is represented by χ_{xy}. Substitution of these above relationships into Eq. 1 yields:

$$\varepsilon_{\substack{max\\min}} = -c\left[\frac{\chi_x + \chi_y}{2} \pm \frac{\sqrt{(\chi_x - \chi_y)^2 + 4\,\chi_{xy}}}{2}\right] = -c\;\chi_{\substack{max\\min}} \qquad (2)$$

where χ_{max} and χ_{min} are the maximum and minimum surface curvature of the surface. This is then the desired relationship: the principle strains are directly proportional to the maximum and minimum surface curvature.

Although this relationship between the strain and the flexure assumes that the object has a constant cross section, it has been shown (Ref. 16) that the

equation is valid for complex surfaces provided that the cross sectional variation is not too extreme. In addition it is also assumed that the applied stress does result in flexural strain of the structure, rather than pure in-plane strain. This is generally the case with large complex structures such as aircraft or aircraft components.

The latter assumption can be justified by considering the simple case of a rectangular cantilevered beam, tip-loaded with a tangential force F_s and a normal force F_n. The strain ε_s induced by F_s is given simply by Hooke's law:

$$\varepsilon_s(x) = \frac{F_s}{2\ cw\ E}$$

where x is the coordinate parallel to the long axis of the beam, w is the width of the beam, and E is Young's modulus. The surface strain due to the normal force ε_n is given (Ref. 17) as:

$$\varepsilon_n(x) = \frac{F_n c}{2\ IE}\ (X-x)$$

where I is the moment of inertia of the beam cross-section, and X is the length of the beam. By ratioing the above two expressions and making the proper substitution for the moment of inertia the following expression is obtained:

$$\frac{\varepsilon_n}{\varepsilon_s} = \frac{F_n}{F_s}\ (\frac{3}{2}\ \frac{X-x}{c}).$$

For thin structures, X-x >> c; hence, the quantity in parentheses is very large except near the point of the applied load, where X-x ≈ c. Thus, even if the two forces are comparable, the strain induced by the normal force dominates the strain contribution from the tangential force at distances greater than c from the point of applied force.

In the following discussion a method will be put forth which eliminates the need for more than one hologram, knowing the zero displacement point, and reduces the data reduction procedure to a simple equation which can reduce the fringe information to strain information directly. The method computes the second derivative of displacement from the fringe data, eliminating the need to first obtain displacement data and then to compute the second derivative. The effects of extraneous (rigid body) motion, object curvature, and fringe curvature are taken into account; and a simple data-reduction formula is obtained. It also provides a system for determining the maximum strain areas by visual inspection of the reconstruction. The method developed meets the demands for strain measurement

by pulsed holographic interferometry of large, three-dimensional objects in a dynamic environment. Prior to this discussion, a brief introductory analysis of basic three-dimensional holographic interferometry will be presented. Then, upon this foundation, the theory for a strain-data reduction procedure will be developed.

Mathematical Description of Holographic Interferometry

The following theoretical description details the necessary mathematics required before an interpretation of strain fields can be made from holographic data. This analysis is concerned with double-exposure holographic interferometry and will be equally applicable to cw systems as well as pulsed systems.

Consider first the recording of two object wavefronts, $\vec{A}_{01}$ and $\vec{A}_{02}$, in the same emulsion along with a reference wavefront, $\vec{A}_{R1}$. The intensity distribution recorded in the hologram plane is then:

$$I = 2|\vec{A}_{R1}|^2 + |\vec{A}_{01}|^2 + |\vec{A}_{02}|^2 + \vec{A}^*_{R1}(\vec{A}_{01} + \vec{A}_{02}) + \vec{A}_{R1}(\vec{A}^*_{01} + \vec{A}^*_{02})$$

where the asterisk indicates the complex conjugate of the function. If the hologram is then processed and illuminated with a wavefront, $\vec{A}_{R2}$, the emerging diffracted wave field will have a term proportional to

$$\vec{A}_{R2}\vec{A}^*_{R1}(\vec{A}_{01} + \vec{A}_{02}).$$

The factor $\vec{A}_{R2}\,\vec{A}^*_{R1}$ can be set equal to one (the special case when the reconstruction wavefront is equal to the original reference wavefront) without any loss in generality since at best it will only introduce a magnification factor effecting both reconstructed wavefronts equally. The reconstructed image then is just the vector summation of the two object wavefronts which were recorded sequentially in time.

It is now assumed that the object is a diffuse scatterer and as such, only identical surface points interfere with each other. This assumption is based on the fact that the surface roughness is greater than the optical wavelength and therefore, each point on the surface will have its own phase signature which is different from every other point in a random fashion. If interference between points of different phase signature takes place, then the result would be a randomly distributed fringe field; this is clearly not the case. (It should be noted from the previous section that even for very smooth surfaces, on the order of optical wavelengths, there are sufficient phase variations to produce a well ordered fringe system. However, in the bright specular regions that were produced as a result of machining direction, this does not seem to be the case.)

As a result of the above assumption, each surface point can be considered separately, greatly simplifying the mathematics. The object wavefield can now be represented as:

$$A_{01} = A_0 \, e^{i\phi_1}$$

$$A_{02} = A_0 \, e^{i\phi_2}$$

where A_0 is the amplitude of the object point, and ϕ_1 and ϕ_2 are the phases of the same point during the first and second holographic exposures. The intensity distribution, I_i, in the reconstructed image is then:

$$I_i = 4|A_0|^2 \cos^2 \left[\frac{\phi_2 - \phi_1}{2}\right] \quad .$$

The intensity distribution in the reconstructed image is a function of the intensity of the object points, $|A_0|^2$, modulated by the cosine factor which is a function of the phase change resulting from the point displacement. The task for the remaining portion of this section, therefore, is to relate this phase change to the point displacement for the general three-dimensional case.

Referring now to Fig. 26a, an object point O is illuminated with a monochromatic coherent point-source, S, a vector distance $\vec{r}_o$ away. If the light scattered from O is detected by means of a photographic emulsion at the point H, a vector distance $\vec{r}$ away, then the phase of the ray SOH is:

$$\phi_1 = k(r + r_o) = 2\pi m$$

where m is the fringe order and $k = 2\pi/\lambda$.

It can be seen then that the locus of all points having constant phase is an ellipsoid of revolution with foci at S, H and a major axis equal to $r + r_o$ which is equal to $m\lambda$. This describes the phase field on the object recorded by the first exposure of a double-exposure hologram.

Now it is assumed that after the first exposure is made, the point O is displaced a distance $\Delta\vec{r}$ to the new point O' so that $\Delta\vec{r}$ is not a chord of the ellipsoid of constant phase. (If this displacement were allowed then no interferometric fringes would be recorded by the hologram since the phase change observed at the point H would be zero.) The phase for the new optical path is:

ANALYTICAL ANALYSIS PARAMETERS

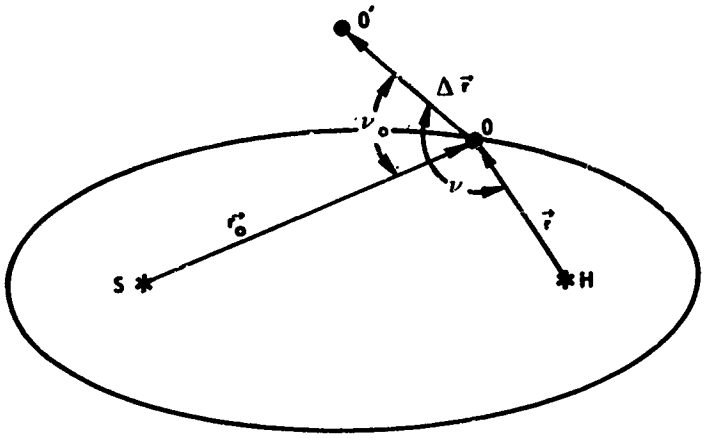

a.

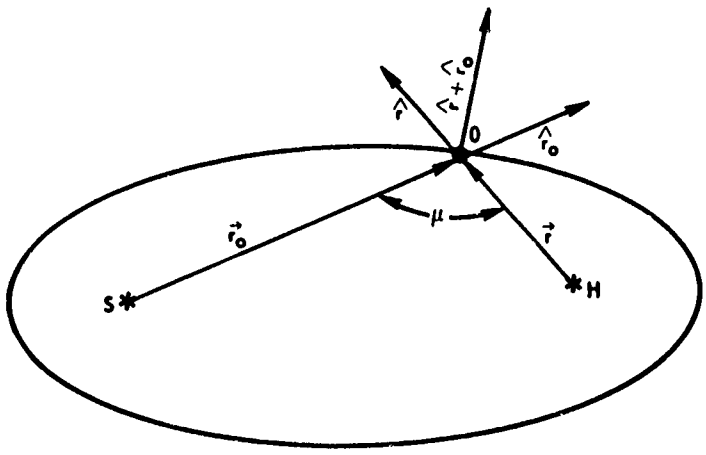

b.

FIGURE 26. MAXIMUM STRAIN AND STRAIN PATTERN

$$\phi_2 = k[|\vec{r} + \Delta\vec{r}| + |\vec{r}_o + \Delta\vec{r}|] = 2\pi(m + \Delta m)$$

which is the equation of a new ellipsoid through O' with foci S, H and major axis equal to $(m + \Delta m)\lambda$.

The second exposure is now made. The phase change describing the object point displacement is then:

$$\phi_2 - \phi_1 = k[|\vec{r} + \Delta\vec{r}| + |\vec{r}_o + \Delta\vec{r}| - (r + r_o)] = 2\pi\Delta m.$$

In order to determine the displacement field from the above, a simplified expression relating the system parameters is required. Considering half of the expression involving r, it will be noted that:

$$|\vec{r} + \Delta\vec{r}| - r = r[(1 + \frac{\Delta r^2}{r^2} + 2\frac{\vec{r}\cdot\Delta\vec{r}}{r^2})^{1/2}] - r \quad . \qquad (3)$$

If now the square root term is expanded in a binomial series and terms smaller than $1/r^2$ are dropped, we have:

$$|\vec{r} - \Delta\vec{r}| - r \approx \frac{\Delta r^2}{2r}\sin^2\nu + \Delta\vec{r}\cdot\hat{r}$$

where ν is the angle between the vector $\vec{r}$ and $\Delta\vec{r}$ and $\hat{r}$ is the unit vector in the direction of $\vec{r}$. A similar result is obtained from the other half of Eq. 3 involving r_o. The final result then is:

$$\phi_2 - \phi_1 = k[\Delta\vec{r}\cdot(\hat{r} + \hat{r}_o) + \frac{\Delta r^2}{2}(\frac{\sin^2\nu}{r} + \frac{\sin^2\nu_o}{r_o})] \quad . \qquad (4)$$

A physical interpretation of this result can be obtained by noting $\hat{r} + \hat{r}_o$ is a vector which bisects the angle, μ, between $\vec{r}$ and $\vec{r}_o$ (see Fig. 26b), and is normal to the surface of the constant-phase ellipsoid. The latter statement can be verified by noting that the ray SOH abeys the reflection laws and as such, the bisector of the angle between $\vec{r}$ and $\vec{r}_o$ must be perpendicular to the surface. It therefore can be concluded that the first term in the brackets is just the projection of the displacement vector $\Delta\vec{r}$ onto the normal of the ellipse, multiplied by the summation of the unit vectors, $2\cos\mu/2$. The second term in

the brackets is harder to interpret except in the limiting case when H and S are identical. For this special case the ellipsoid becomes a sphere and $\Delta r \sin \nu$ is the projection of $\Delta\vec{r}$ onto the tangent of the circle (the first term, for this limiting case, still has the same interpretation as above). Therefore, the second term is just the square of this value divided by the distance r. The relative magnitude of this term compared to the first can now be estimated. If the displacement vector makes an angle of 80° or less to the surface normal, and it is assumed that the distance from the source-hologram combination to the object is greater than 10 cm and the displacement is on the order of wavelengths, then the first term is approximately 3 orders of magnitude greater than the second. For the case when the source point and hologram point are separated, the interpretation is no longer simple, but the relative importance of the second term to that of the first remains unchanged. The only case in which the second term does become significant is for a surface movement nearly tangential to the constant-phase ellipsoid. Therefore, it can be stated that the phase change is:

$$\phi_2 - \phi_1 = 2\pi\Delta m \approx k[\Delta\vec{r}\cdot(\hat{r} + \hat{r}_o)] \tag{5a}$$

or

$$\Delta m \approx [2\ \Delta r \cos\ (\mu/2)\ \cos\ \alpha]/\lambda \tag{5b}$$

where α is the angle between the displacement vector and the surface normal of the constant phase ellipsoid. This is consistent with intuitive reasoning in that a component of displacement normal to the constant phase ellipsoid must contribute more to the phase change than a component of displacement tangential to this surface: the tangential component lies almost on the surface of the ellipsoid and as such the phase change is approximately zero.

Although Eq. 5 is simple in form, there are many difficulties involved with making actual displacement measurements. The first and primary task is to establish from the interferometric fringe data the phase change $\phi_2 - \phi_1$. The determination can be made relatively easy if there is a no-displacement reference point in the reconstructed holographic scene, as is demonstrated by Sollid et al. (Refs. 8, 9, and 11). These techniques require two different holographic viewpoints of the same object scene for the two-dimensional case and three viewpoints for the three-dimensional case. This imposes practical difficulties in making the holograms with a pulsed laser system.

If the no-displacement point does not exist, then the technique of Haines and Hildebrand (Ref. 7) or Alexandrov and Bonch-Bruevich (Ref. 10) could be used. A third alternative is to observe the fringe formation using real-time holographic interferometry and count the fringes passing through the surface point. This, however, is impossible when employing a pulsed laser system.

In the following section, a method will be derived using Eq. 5 which will eliminate the above difficulties and at the same time improve the data reduction procedure necessary to obtain strain data from the displacement field.

Conversion of Holographic Data to In-Plane Strain Data

Since one main program goal is to use the holographic interferometric data to determine in-plane strain on the surface of large aircraft or aircraft structures, certain assumptions relative to the surface displacement have been made. The basic assumption is that, when a stressing force is applied to the structure, one result will be an out-of-plane displacement (bend) and that this out-of-plane displacement will be at least twice as large as any of the tangential components. This is a reasonable assumption in view of the fact that most of any aircraft is hollow thin-walled structure. Thus, commonly used simulated loading conditions impose large bending components. If this basic assumption is met, then there will be no more than a ten percent error introduced if it is further assumed that the entire displacement is perpendicular to the surface. This assumption is made so that a value for the angle α can be obtained. It was demonstrated earlier that holography is insensitive to the component perpendicular to the line of sight and therefore will see the surface displacement as being just that of the component parallel to the line of sight if only one hologram view is recorded. Such an assumption, therefore, eliminates the need for recording two more views of the same scene. If the out-of-plane displacement is at least twice the in-plane displacement and its displacement direction is known, the true value for α may be used thereby reducing the error. (These above assumptions are also consistent with the classical small-deflection theory of plates developed by Lagrange, Ref. 15).

The determination of displacement data from Eq. 5 will be further simplified if the illumination source is placed near the holographic recording plane ($\mu = 0$). This requirement in no way hinders the flexibility or ease of recording the holograms, and is somewhat desirable in that it eliminates shadows on the surface which could obscure points of interest.

Using the above assumptions, Eq. 5a can be written:

$$\Delta m = 2(\Delta\vec{r}\cdot\hat{r})/\lambda \quad .$$

The displacement vector, $\Delta\vec{r}$, can be expressed as:

$$\Delta\vec{r} \approx \hat{n}\ \Delta Z(\vec{r})$$

where $\hat{n}$ is a unit vector normal to the object surface. These two equations can now be combined to yield:

$$\Delta m = \frac{2\Delta Z}{\lambda}\ (\hat{n}\cdot\hat{r}) \quad .$$

Since the displacement ΔZ is in the direction of the surface normal $\hat{n}$, the angle between the source-hologram direction $\hat{r}$ and $\hat{n}$ is just the previously defined angle α. Therefore, the above equation becomes:

$$\Delta m = \frac{2\Delta Z}{\lambda} \cos \alpha \quad . \tag{6}$$

This equation could now be solved for the displacement magnitude, ΔZ, provided the phase change as measured by Δm is determinable. However, it is actually the second derivative of the absolute displacement with respect to the direction of maximum surface change which is the desired quantity for computing in-plane strain. (This is fortunate since the direct calculation of absolute displacement is most difficult.) Consequently, to obtain the desired information from the fringe data, the second derivative is taken on both sides of Eq. 6 with respect to the coordinate axis of maximum surface change, η. (At first it would seem reasonable to use the Laplacian operator which takes the second derivative of a function along the direction of maximum change. For the case where there is no rigid motion this would indeed be applicable. In the presence of rigid motions, however, the direction of maximum change may be different from the direction of maximum surface change.)

$$\frac{\partial^2(\Delta m)}{\partial \eta^2} = \frac{2}{\lambda} \cos \alpha \frac{\partial^2(\Delta Z)}{\partial \eta^2} + \frac{4}{\lambda} \frac{\partial(\Delta Z)}{\partial \eta} \frac{\partial(\cos \alpha)}{\partial \eta} + \frac{2\,\Delta Z}{\lambda} \frac{\partial^2}{\partial \eta^2} (\cos \alpha). \tag{7}$$

The first term on the right in the above equation is the desired quantity, the second derivative of displacement along the direction of maximum surface change. (The actual determination of this direction is discussed later in this section.) The remaining two terms relate to the first derivative of displacement and to the actual displacement. In order to show that these last two terms can in general be neglected if the distance from the source-hologram point, r, is made large enough, it is first assumed that the object is a flat structure with the perpendicular distance from the source-hologram point equal to Z. The elimination of the latter two terms will first be made for this special case which can be orientated in any fashion with respect to the holographic film plane; it will then be extended to show how these results may be applied to several planes at different orientations, and structures having continuously curved surfaces. It is now possible to write the above expression in Cartesian coordinates and take the indicated derivatives where possible:

$$\frac{\partial^2 \Delta m}{\partial \eta^2} = \frac{2Z}{r\lambda} \frac{\partial^2 \Delta Z}{\partial \eta^2} - \frac{4\,\eta Z}{\lambda r^3} \frac{\partial(\Delta Z)}{\partial \eta} - \frac{2\,\Delta Z}{\lambda} \frac{2Z}{r^3} \quad .$$

If it is now assumed that the maximum viewing direction through the hologram will be approximately $\pm 45°$, this then sets the maximum values of the coordinates on the surface of the plane, $\eta = Z = \frac{r}{\sqrt{2}}$. Inserting these values into the above equation:

$$\frac{\partial^2 \Delta m}{\partial \eta^2} = [\sqrt{2}\,\frac{\partial^2(\Delta Z)}{\partial \eta^2} - \frac{2}{r}\frac{\partial \Delta Z}{\partial \eta} - \frac{2\sqrt{2}\,\Delta Z}{r^2}]/\lambda \,. \tag{8}$$

It now only remains necessary to approximate the order of magnitude for a typical displacement and a first and second derivative of displacement. The last term in the above equation will introduce an error (pseudo-strain) into the observed strain patterns from displacement of the object. This displacement can be the result of either a stressing force or a simple out-of-plane translation (a motion in which no stress is induced into the structure). The displacements which are normally measured with double-exposure holographic interferometry have a magnitude of about 10^{-4} cm. The second term will introduce a pseudo-strain by virtue of a change in the displacement. This again can be a result of a stressing force or an out-of-plane rotation (rotation about an axis parallel to the surface). If the total displacement measured is about 10^{-4} cm then a typical change in displacement would be of magnitude 10^{-5} cm/cm. The first term is the strain term and can only be the result of a stressing force applied to the structure (no other rigid motion of the object will result in a value for the second derivative of displacement). The values for typical strain measurements made using holographic interferometry are on the order of microstrain (Ref. 16) or values for the second derivative of 10^{-6} cm/cm^2. If r is at least a meter, then it can be seen that the magnitude of the first term in Eq. 8 is 10 times that of the second and one hundred times that of the third. The distance requirement, $r > 1$ meter, imposes no special complications on the actual experimental setup because when analyzing large structures, the distance from the source-hologram point to the object is expected to be on the order of several meters.

There is one additional case which may introduce a pseudo-strain in the observed strain field and that is the case of a rigid rotation about an axis perpendicular to the object. In this case, however, the displacements are all tangential to the line of sight and therefore have a negligible effect because of the relative insensitivity of holography for recording this motion compared to motion along the line of sight.

It now can be stated that for a flat specimen where the holographic recordings are made at least a meter away, Eq. 7 can be written:

$$\frac{\partial^2 \Delta m}{\partial \eta^2} = \frac{2Z}{\lambda r}\frac{\partial^2 \Delta Z}{\partial \eta^2} \,. \tag{9}$$

This is now in a form where the second derivative of displacement is directly relatable to the change in the fringe spacing. The actual fringe order is no longer necessary and thereby, the complicated data reduction procedure associated with it is eliminated.

Since Eq. 9 was derived for a single plane of arbitrary orientation, its extension to several planes is straightforward. It only has to be remembered that the distance Z is measured from the plane of interest and when more than one plane is present in the holographic reconstruction, the value of Z will be different for each plane. Therefore, in order to calculate $\partial^2 \Delta Z/\partial\eta^2$ for the various planes of different orientations the factor r/Z or cos α (angle between the surface normal and the source hologram point) must be taken into account. The equation is also applicable to curved surfaces since an arbitrary surface can be broken up into infinitesimal plane surfaces.

It now remains to be shown how the quantity $\partial^2(\Delta m)/\partial\eta^2$ can be extracted from the holographic data. The change in Δm is simply the reciprocal of the fringe spacing in the direction η or $\partial\Delta m/\partial\eta = 1/\Lambda$ where Λ is the distance between any two adjacent fringes in the direction η. Therefore, by measuring the spacing between two successive fringes the second derivative is obtained:

$$\frac{\partial^2 \Delta m}{\partial \eta^2} = \left[\frac{1/\Lambda_1 - 1/\Lambda_2}{\Lambda_1 + \Lambda_2} \right]$$

or using Eqs. 2 and 9:

$$\varepsilon_{max} = -c\ \chi_{max} = \frac{-c\lambda}{2 \cos \alpha} \left[\frac{\Lambda_2 - \Lambda_1}{\Lambda_2 \Lambda_1 (\Lambda_2 + \Lambda_1)} \right] \quad . \qquad (10)$$

It can be seen from Eq. 2 that if the measurement of the fringe spacing is made in an arbitrary direction other than the maximum surface change, η, then three quantities have to be measured, χ_x, χ_y, and χ_{xy}. In many cases the measurement of these quantities is hampered by small curvature changes in one of the chosen directions. (Small curvature changes result in large fringe spacing and measurements often have to be made at some distance from the data point of interest, thus introducing errors into the measurement.) It therefore would be desirable to make the measurement along the direction of maximum surface change. This would not only reduce the number of measured quantities to one, χ_{max}, but would also increase the accuracy of the measurement. For the case of straight or nearly straight fringes the direction of maximum change is unique and is perpendicular to the fringes. For the case in which fringe curvature does exist

a few trial claculations, using the bracketed term in Eq. 10, will establish the proper direction. The direction of maximum surface change is that direction for which this term is maximum. This will also be the direction of maximum principal strain.

This result provides an extremely easy and convenient method for determining the second derivative of displacement. Once this value is obtained, multiplication by the distance from the neutral axis to the surface then yields the value of in-plane strain. To obtain relative values of in-plane strain over the surface, only the term in the brackets of Eq. 10 need be calculated, provided the structural thickness remains fairly constant. Further, location of maximum strain areas by direct observation of the reconstructed hologram is now possible. These areas are characterized as being located at the points where the fringe spacing changes most rapidly in the shortest distance.

The equation is applicable to curved surfaces and therefore comparison between points on such a surface would have to include the cos α term. Alternatively, it will be noted that the cos α factor changes very slowly for large r (the conditions required in order to obtain Eq. 10). Therefore changes in the surface normal of up to 20° will not substantially effect the in-plane strain value ($<10\%$). Surfaces which have variations larger than these can be divided up into regions where the variations are within these limits and the cos α factor computed for each region so that a comparison of in-plane strain values can be made between regions.

The one limiting case for which Eq. 10 is not applicable is when the angle between the viewing direction and surface normal exceeds ±45°. It is this angular limitation which has allowed the elimination of the second and third terms of Eq. 7. For relatively flat objects this would allow a viewing cone with an f/number of .5 and would not be a restriction for this type of surface. However, care must be exercised for highly curved surfaces. The surface curvature will limit the viewing cone over which credible data can be obtained from the holographic interferogram. The angular limitation does eliminate, however, effects caused by the motion tangential to the surface of the object since these only become substantial at viewing angles greater than 80°.

The direction of principal strain for a given surface point can also be determined from the holographic data. This direction is the same direction as the maximum surface change (perpendicular to the interferometric fringes) if a rotation of the entire object has not occurred between holographic exposures. If rotation about an in-plane axis has taken place, the result will be a rotation of the fringes and the principal strain direction will not, in general, be along the direction perpendicular to the fringes. (Simple translations or small rotation about an axis normal to the plane will not significantly effect the orientation of the fringes.) In fact, if rotation has taken place in a direction

other than the direction of displacement which was caused by the stressing force, then the fringes will become slightly curved. If not, only additional straight fringes will be added to the fringe field. In the latter case (constantly changing straight fringes), the strain direction is still perpendicular to the fringes and easily determined. For the former case (slightly curving fringes) which might be a result of a rotation or a stressing force, the direction of maximum strain will be in the direction of maximum curvature. Determination of this direction is found by obtaining the direction in which the bracketed term of Eq. 10 is maximum. This technique for finding the direction of principle strain is not difficult if large variations in the fringe field exist (high strain areas), but in areas where small variations are present (low strain areas) the direction of maximum strain can vary considerably.

Future work includes investigation of various Moiré techniques for the acquisition of the holographic strain data. One promising technique, reported by Stetson (Ref. 18), superimposes two identical fringe patterns rotated 180° with respect to each other. At the location where superposition of an identical point occurs, a Moiré beat pattern exists which is a function of the strain-induced fringes. Additionally, the effect of rigid motion is not a factor in the technique. It is claimed that an accuracy of ±20% is achieved with this technique.

In conclusion, a viable technique for reducing holographic interferometric data has been derived which is applicable to both plane and curved surfaces. The restrictions which have been placed on the experimental setup are minimal; viewing angles less than ±45° to the surface normal are required; the object illumination source should be placed next to the holographic plate; and the hologram to object distance should be greater than one meter. These in no way should affect the holographic recording of large structural surfaces. In addition, the effects of simple object rotation and translation on the strain field should amount to less than 10% for the most extreme cases. The determination of principal strain direction in the presence of rigid rotations can also be acquired.

EXPERIMENTAL INVESTIGATIONS

Three experimental investigations were conducted to verify the analytically derived technique for reducing holographic data to in-plane strain data, and to anticipate and resolve the problems expected in applying this technique to large aircraft structures in realistic environments. The first experiment involved a tip-loaded cantilevered beam from which comparisons were made between theoretical and holographically-derived values of principal strain. In addition, rigid body motions were superimposed on the flexural motion of the beam, and the holographic strain value again was compared with the theoretical values. In the second experiment a relatively flat simulated aircraft panel was stressed in such a manner

that the applied tangential forces were large compared to the forces applied normal to the surface. In this case the holographic values of strain were correlated with values measured from strain gages located on the panel. In the third experiment, the role of object curvature was explored by axially loading a cylindrical shell and computing the resulting strain from the holographic fringe pattern. These data were subsequently compared with strain gage values.

Cantilevered Beam

Experimental verification of the analytical expression derived in the previous section (Eq. 10) was performed for the relatively simple case of a cantilevered beam. By using the cantilevered beam, the strain values could be calculated theoretically (Ref. 17) and a direct comparison then made with the absolute values of strain obtained holographically. (The use of theoretical values avoids the problem of matching the sensitivity of holographically derived strain with mechanical strain gages.) Additionally, tests were performed with the cantilevered beam to determine whether rigid body motions (motions of the object which introduced no strain) had an effect on the holographically derived strain data.

The experiments were conducted on a rectangular steel plate having the dimensions: 15.75 cm (length) x 5.08 cm (width) x .476 cm thickness. The plate was clamped at one end and loaded at the other in a direction perpendicular to its surface using a weight of 103 gf. The displacement caused by the stressing force was recorded using double exposure holographic interferometry. This type of displacement was also recorded in combination with a rigid rotation about the long axis of the plate and a rigid tilting about an axis parallel to the width of the plate at the base of the clamp. All motions were first observed by means of real-time holographic interferometry, and then conventional double-exposure holograms were recorded. In this way, the magnitude and direction of the rigid body motion (as well as the flexure) was controlled. Photographs of the holographic reconstructions obtained of these motions separately and in combination are presented in Fig. 27.

Figures 27a, b and c present holographic reconstructions obtained when the beam was placed in flexure (stressing force only applied), tilt (rigid rotational motion only) and flexure plus tilt (combination of an applied stress and a rigid body rotation). The results clearly show that by applying this combination of motions to the beam, the effect is to increase the fringe density. Orientation of the fringes is not effected and therefore the direction of principal strain is perpendicular to the fringes, the expected direction. Figures 27d, e and f are photographs of reconstructions of the beam placed in flexure, rotation (rigid rotational motion only), and flexure plus rotation. The reconstruction (Fig. 27f) of the latter type of motion showed a strong turning of the fringe field in the direction parallel to the long axis of the beam, and a much greater fringe density next to the clamped end of the centilevered beam. By making a few simple

RECONSTRUCTIONS OF CANTILEVERED BEAM

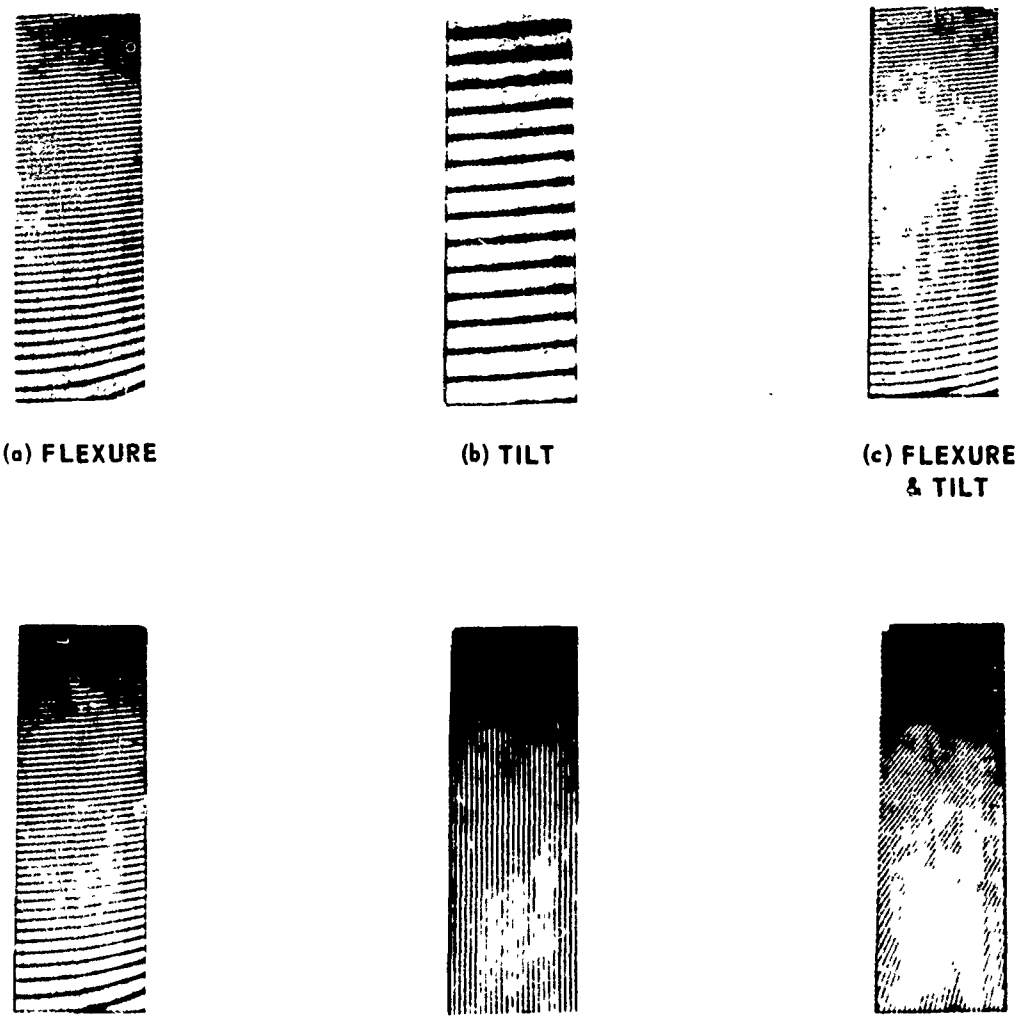

(a) FLEXURE (b) TILT (c) FLEXURE & TILT

(d) FLEXURE (e) ROTATION (f) FLEXURE & ROTATION

FIGURE 27. EFFECT RIGID BODY MOTION ON HOLOGRAPHIC STRAIN MEASUREMENTS

calculations it can be shown that the principal strain direction has not changed due to the induced rigid rotation.

Calculations made from these reconstructions are shown in Fig. 28. For the case of a pure applied stress (flexure), the absolute values of maximum strain obtained from the holographic data and the values obtained theoretically are presented in Fig. 28. The absolute values of maximum strain obtained from the holographic fringe data agree to within 10% of the theoretically calculated strain down to the 3 $\mu\varepsilon$ level. Below this level (not shown in the figure) deviation increases due to inaccuracies in the data readout.

In agreement with the theoretical results obtained in the last section, Fig. 28b demonstrates that a rigid rotation of the plate about the axis parallel to its width (tilt) had negligible effect on the measured strain values. This held true in spite of the increase in the number of interferometric fringes on the plate. This latter result may provide a way of improving the holographic calculation of strain in areas of low fringe density, since in these areas, it would no longer be necessary to average the data over large distances. For example, the cantilevered beam has a maximum strain near the clamped end, which is also the region of minimum fringe density; by introducing rigid motion to the beam, the fringe density is increased and therefore data averaging will be minimized, which increases the accuracy.

The data from the double exposure hologram made of the cantilevered beam which had undergone flexure plus a rigid rotation about an axis parallel to the long axis of the beam is presented in Fig. 28c. The data demonstrates that absolute values of strain are again within 10% of the theoretically calculated strain distribution along the beam down to the 3 $\mu\varepsilon$ level.

The close agreement between the holographic and theoretical values of maximum strain for the case of the cantilevered beam confirms the validity of the local data analysis of holographic-interferometric fringe fields. Further, these experiments verify that at least for this simple case, pseudo-strain errors introduced by rigid body motions, rotation about in-plane axes, are negligible.

Simulated Airframe Panel

In an effort to simulate, in the laboratory, the more complex forces and geometries associated with large aircraft components, a loading frame was fabricated in order to place combinations of bending, torsional and tensile forces on a 2' x 2' test panel. The test panel, which simulates an airframe skin structure, consisted of an aluminum sheet, 50 mils thick, with two, 2' lengths of steel reinforcement ribs (one located at the middle of the panel and the other at the top) affixed to the back of the panel with bolts placed at 2" intervals. Two photographs are presented in Fig. 29 showing both a front and back view of the

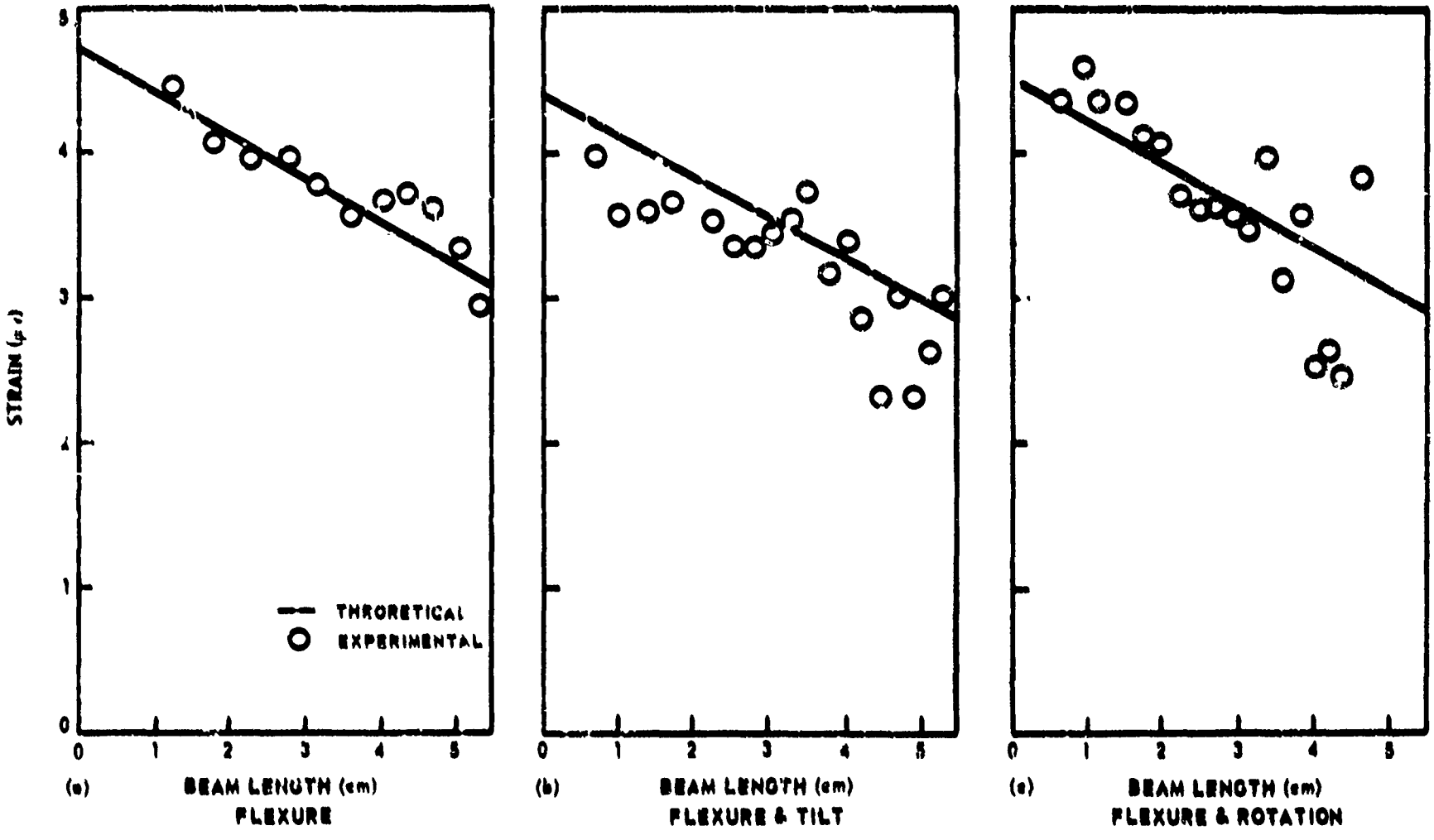

FIGURE 28. EFFECT OF RIGID BODY MOTION ON HOLOGRAPHIC STRAIN MEASUREMENTS

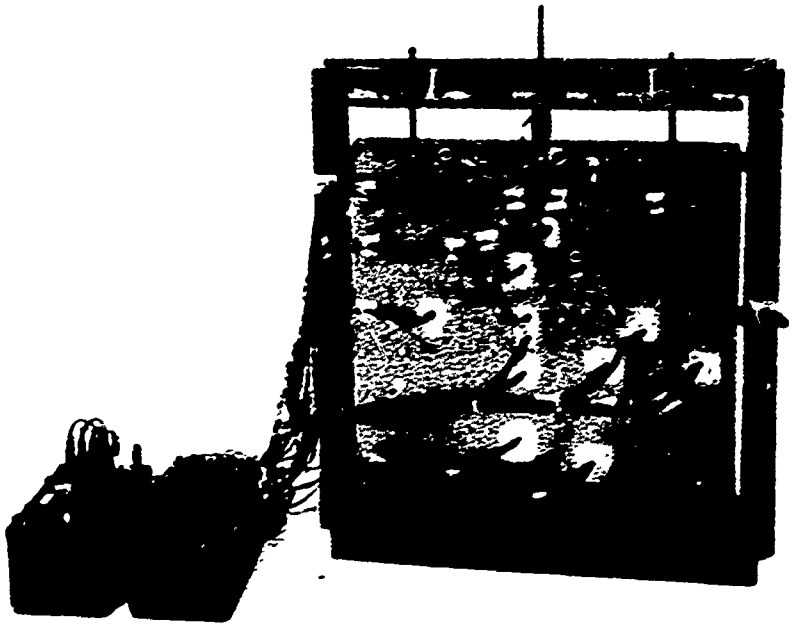

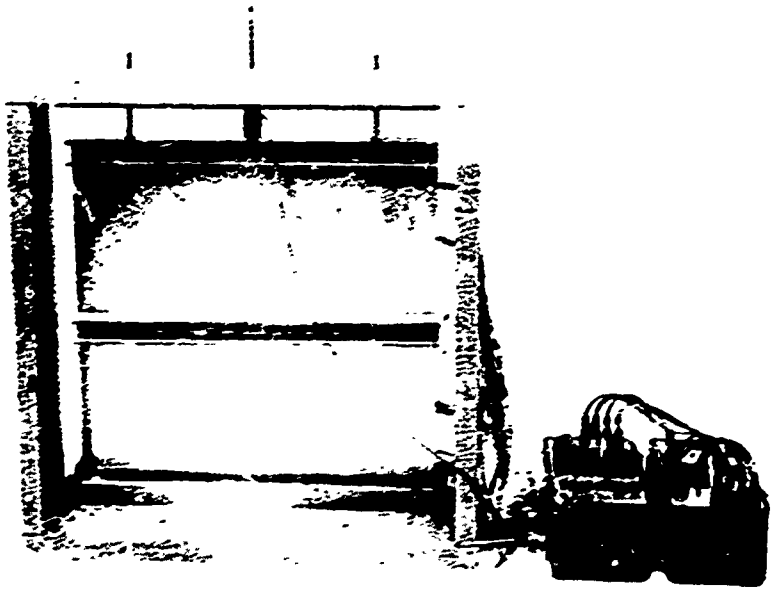

STRESSING FRAME AND TEST PANEL

FIGURE 29. MAXIMUM STRAIN AND STRAIN PATTERNS

test panel positioned in the loading frame. As seen in the figure, the panel was clamped along its bottom edge, and its upper edge was fastened to a loading frame by three bolts which were attached to the upper reinforcement rib. A load cell, used to monitor the stresses applied to the panel, was attached between the panel and the frame on the center bolt. The bolts were used to produce a complicated stress field in the panel which was subsequently analyzed with both holography and strain gages. Pictured in addition to the panel and frame is the equipment used to monitor the strain gages shown cemented on the front side of the panel.

The holographic setup pictured in Fig. 30 was used to obtain the holographic interferometric data on the panel. As shown, the panel and stressing frame are at the far left, one end of the holographic table; the object illumination source is next to the holographic plate holder and both are located a distance of 165 cm (r) from the front of the panel; the expanding and beam steering optics for the reference beam are located on the left side of the panel; and the laser beam (50 mw He-Ne cw laser) enters from the extreme right. The laser beam is split into two beams by the beamsplitter located near the holographic plate holder; one beam illuminates the object, and the other serves as the reference.

Locating the strain gages on the test panel was done by making preliminary, double-exposure holograms of the test panel under stress. Using the results of these tests, fifteen strategic locations (positions of changing fringe density) on the surface of the panel were selected, and overlapping, rectangular rosette strain gages (1/8" in length) were cemented to the panel at each position. A close-up view of the panel showing the gage location is presented in Fig. 31. Also pictured in the figure is a photograph of a reconstruction made from a double exposure hologram of the panel after the gages were mounted. This latter photograph shows that the gages are located both in suspected high strain areas, positions of rapidly changing fringe separation, and in suspected low strain areas, positions of nearly constant fringe separations.

In the course of making the preliminary double-exposure holographic interferograms, it was found that such a structure, consisting of relatively large unsupported spans, tends to vibrate due to environmental influences (air currents, acoustic pickup, etc.) even though the tests were conducted on a vibration isolation table. Effects of this type are observed in the reconstruction, Fig. 31, as a darkening near the upper righthand corner of the reconstructed image. The significance of this result lies in the fact that when actual tests are conducted on full scale pieces, and the loading constraints necessitate a relatively long delay between recording pulses (e.g. under static incremental loading), environmental vibrations can introduce an error into the holographically observed strain patterns since they may be of the same order of magnitude as the incremental strain which is being measured. Total movement of the part (translation or rotation) will not influence these readings because this type of motion does not

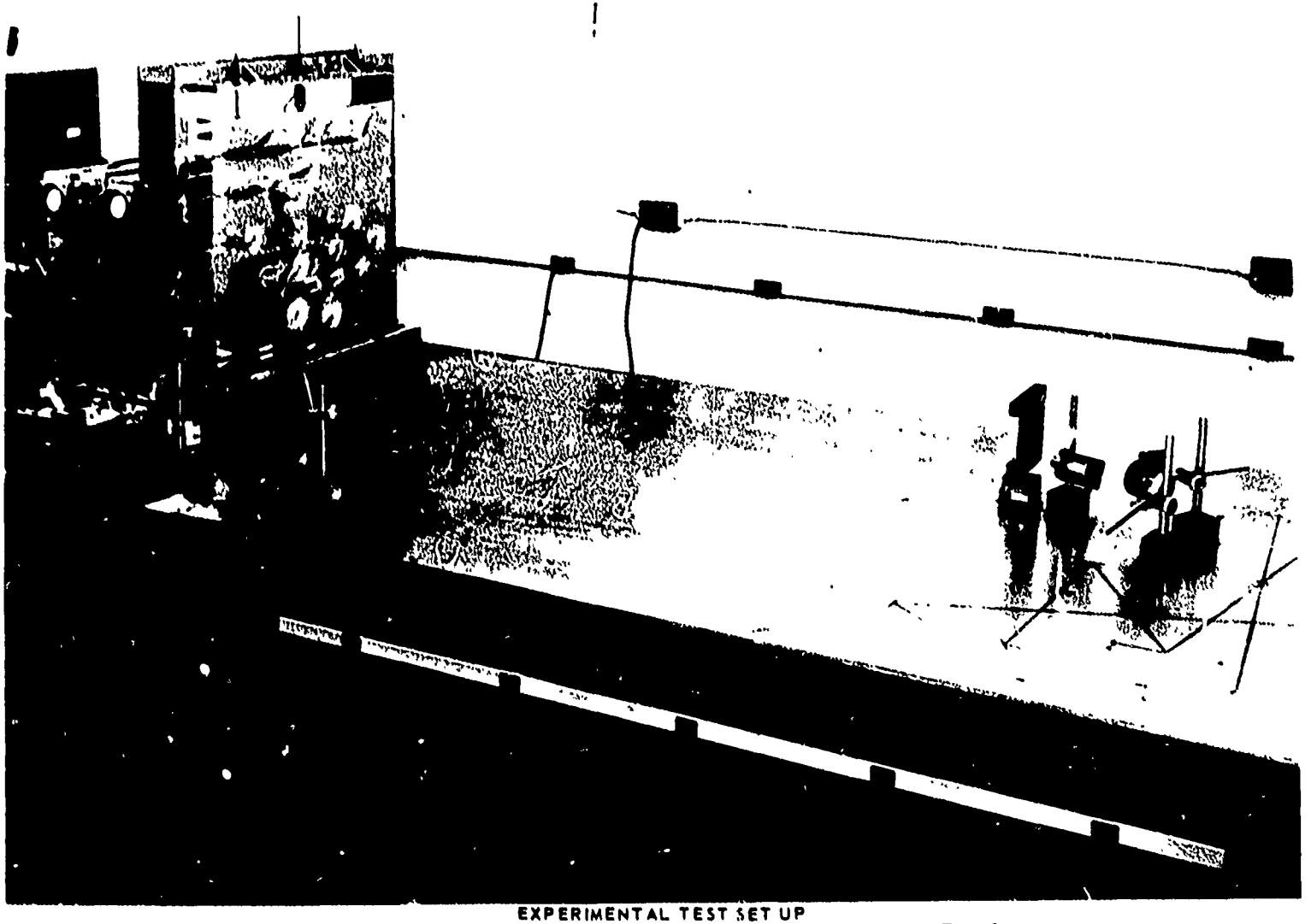

EXPERIMENTAL TEST SET UP

FIGURE 30. MAXIMUM STRAIN AND STRAIN PATTERNS

STRAIN GAGE LOCATIONS

CLOSE-UP OF TEST PANEL

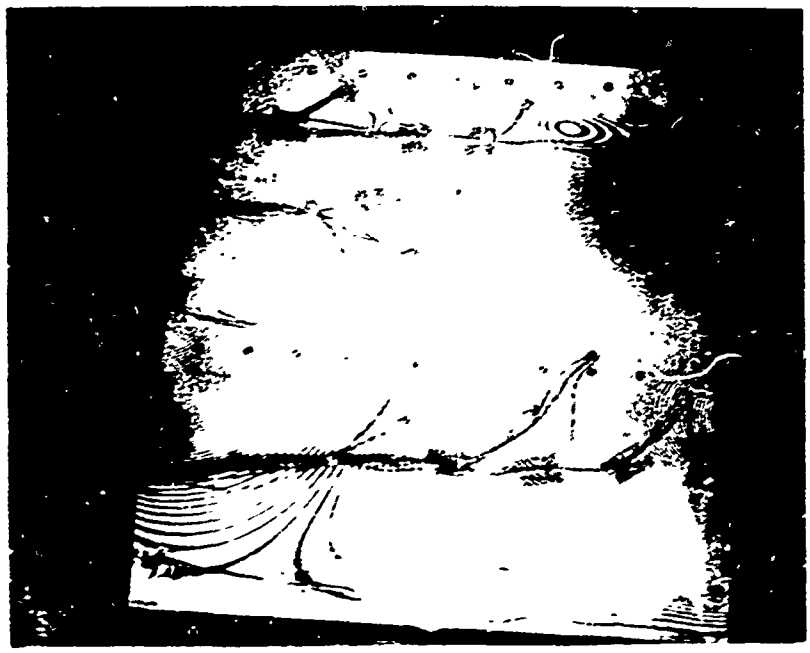

TYPICAL DOUBLE-EXPOSURE INTERFEROGRAM

FIGURE 31. MAXIMUM STRAIN AND STRAIN PATTERNS

introduce a change between adjacent fringes. However, the vibratory motion does introduce a significant change; therefore, it must be taken into account if it is of substantial amplitude compared to the displacement which results from the incremental stress load. The amplitude of these vibrations and thus the expected error can be estimated before the actual tests are made by recording preliminary double-exposure, pulsed holograms; these holograms being made without applying a stressing force between exposures. Another method for eliminating this effect may be to record large stress-induced displacement increments, as is done with Moiré holographic techniques for obtaining surface deformation.

a. Experimental Procedure for Obtaining Holographic Strain Data

The procedure used for obtaining the experimental data was first to place a complicated stress field in the panel. This was accomplished by tightening the center bolt which attaches the panel to the top of the loading frame so that a total of 100 με, as read by the load cell, was obtained. The two outside bolts were then hand tightened so that they applied a slight force in a direction opposite to that of the center bolt. The center bolt was then tightened further until a total of 800 με was obtained.

At this point the first holographic exposure was made. The stress load on the panel was then reduced by a factor of 10 με, and the second exposure made. The applied stress was then changed over a large increment (500 με) and a second double-exposure hologram made at this lower stress level with a 10 με increment between holographic exposures. The differential strain gage readings were taken at the two extreme points of the applied stress.

This procedure of making the holographic exposures over a relatively small increment of the total induced strain recorded by the gages was adopted for two reasons. First, it was done to overcome the relatively low sensitivity of the strain gages as compared to the extreme sensitivity of interferometric holography. (It permitted strain levels high enough to be recorded by the gages and still allowed double-exposure holograms to be made which indicated relative strain levels between gages.) Secondly, performing the experiment in this manner will closely simulate the technique which will be used when conducting tests on an actual aircraft structure, thus gaining insight into potential problems which may arise during such tests.

However, it is necessary in applying this technique to try to ensure that the small strain increment, over which the hologram is recorded, is accurately proportional to the total strain which is recorded by the gages. Thus, two double-exposure holograms, each depicting the effect of a small incremental stress, were recorded; one before and one after the large stress recorded by the gages was applied. Then, if both resulting holograms have the same fringe distribution and slope, the strain can be assumed to be a linear function of the applied

forces, and each hologram will be an accurate representation of the much larger incremental strain recorded by the gages.

Presented in Fig. 32 are photographic reconstructions obtained from the holograms made in the above fashion. The two holographic fringe distributions are similar in that the distribution near the top and middle of the panel are generally the same except for the fringe density. Near the base and edges of the panel, however, the fringe distribution seems to have shifted between the initial and final recording. This demonstrated to a fair approximation, that the flexure at each point on the panel was a linear function of the applied forces (this is particularly true of the points near the center of the panel). Thus it is now possible to obtain data from one of the holograms for the in-plane strain measurements, which then can be compared with the strain measurements recorded by the gages. Because of the fashion in which the data were taken, only relative, not absolute values can be compared.

The interferometric data from the initial double-exposure hologram (800 $\mu\varepsilon$ level) was sampled and reduced at the gage locations to find the principal strain, ε_H (Eq. 10), and principal strain angle, ϕ_H. This was done using a simple 20X lens. The data obtained from the gage rosettes were also reduced to find the principal strain, ε_G, and principal strain angle, ϕ_G. In the course of these measurements, the mean and standard deviation of the gage reading at gage position 16 (the gage positions are presented in Fig. 31) was calculated from seven separate measurements and found to be 170.8 $\mu\varepsilon$ and 5.64 $\mu\varepsilon$ respectively.

b. Correlation Studies

In order to make a relative comparison of the two sets of strain data, the holographically obtained values were adjusted so that the mean value of the ratios between gage and holographic data was unity. The results are presented in Table I and are listed in descending strain magnitude as determined by the gage readings. In addition, the calculated ratios between the holographic and gage values appear on the far right of the table. As can be seen in the table, the two sets of values are in general agreement, particularly at the higher strain levels.

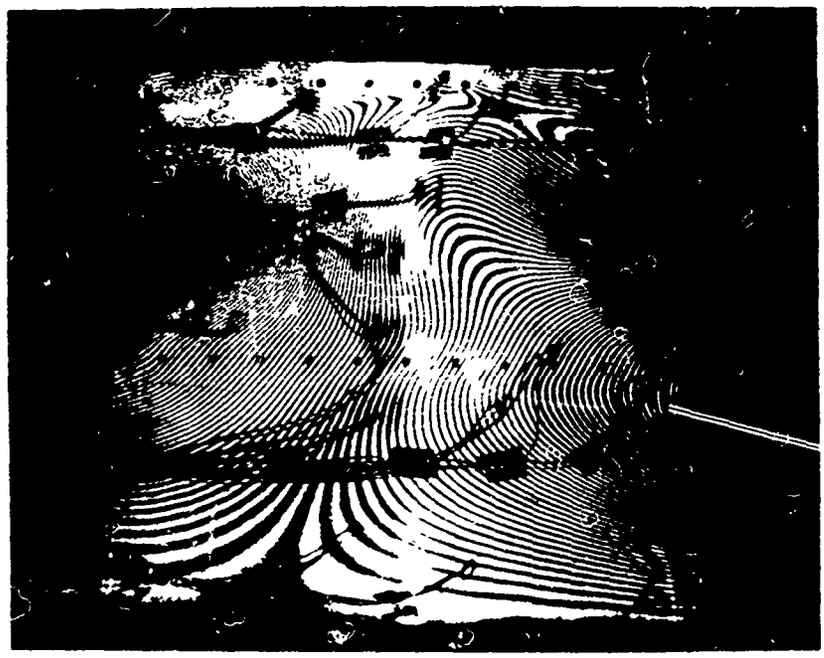

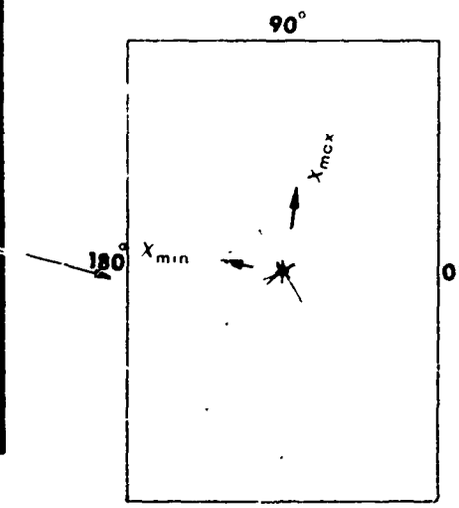

INITIAL (790$\mu\epsilon$ – 800$\mu\epsilon$)

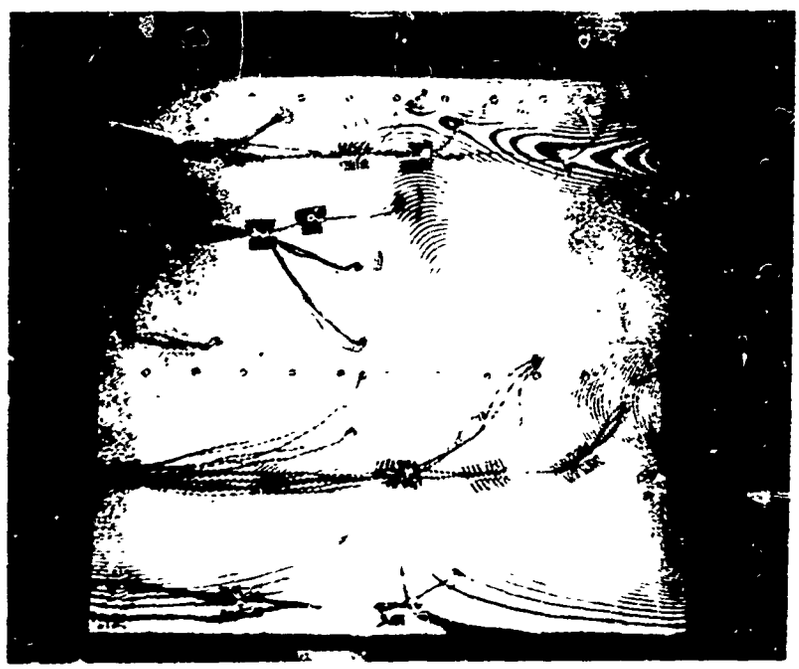

FINAL (500$\mu\epsilon$ – 510$\mu\epsilon$)

FIGURE 32. MAXIMUM STRAIN AND STRAIN PATTERNS

INTERFEROGRAMS USED TO OBTAIN IN-PLANE STRAIN

TABLE I

Comparison of Strain Gage and
Holographic Interferometry Measurements
(Simulated Aircraft Panel)

Gage Position	Strain Gage Measurements		Holographic-Interferometry Measurements		Ratio $\varepsilon_G/\varepsilon_H$
	Principal Strain $\lvert\varepsilon_G\rvert$ ($\mu\varepsilon$)	Principal Strain Angle ϕ_G(°)	Principal Strain $\lvert\varepsilon_H\rvert$ ($\mu\varepsilon$)	Principal Strain Angle ϕ_H(°)	
16	170.8	89.1	101.9	80	.60
2	142.0	91.3	126.2	92	.89
15	104.9	101.0	49.0	120	.47
4	58.0	104.6	22.3	90	.38
6	44.3	86.2	42.7	80	.96
8	28.2	107.5	34.0	110	1.20
11	18.0	92.2	21.8	50	1.21
10	16.3	51.1	17.0	115	1.04
13	14.6	64.1	22.3	12	1.53
1	14.5	67.5	29.1	40	2.01
14	14.2	123.1	7.3	120	.51
9	12.8	106.8	14.6	140	1.14
5	10.8	67.5	10.2	140	.94
7	10.1	50.7	11.2	60	1.11

The correlation between the gage and holographic data is in fair agreement and, with few exceptions, the order of descending strain values is preserved. It should be noted that the holographic data obtained at position 6 is now in good agreement with the gage values. Previously there was considerable disagreement. (This was reported on in the First Interim Technical Report.) This error was a direct result of taking the fringe data perpendicular to the fringes, but because of the fringe curvature, this direction was not the maximum curvature direction. The actual determination of the maximum surface curvature showed that the data should have been taken almost tangent to the fringes. Included in Fig. 32 is a plot which shows the surface curvature as a function of angle. From this plot it can be clearly seen that the maximum surface curvature is 80° from the horizontal. It should also be noted that the minimum surface curvature is at right angles to this direction, as would be expected from strain considerations. (This plot of curvature parallels that obtained when a strain analysis is performed.) Actually, for the case of gage 6 the minimum curvature is opposite in sign. (The curve

passes through zero at 30° and again at 130°.) If they were of the same sign the second lobe would not exist at right angles to the maximum. A minimum or zero would exist at this point. The standard deviation determined from the above data was calculated to be 0.44. This was an improvement over the value found previously (0.61) when all of the data was taken perpendicular to the fringes.

Differences between the two sets of strain values are expected because of the manner in which the experiment was conducted (holographically recording only a small increment of total strain). The total deflection field is expected to be a linear function of the forces, provided the forces act normally to the surface of the structure. However, if tangential forces exist, the deflection may no longer be a linear function of the forces (Ref. 17). In the case of the simulated aircraft panel, there is a substantial tangential force because of the manner in which the panel is loaded and therefore the linearity may be affected.

In order to ascertain the degree of linearity between different increments of the larger total strain, successive holograms were made over the entire increment. Representative results are presented in Fig. 33. These holograms were made at 20 με intervals in order to cover the entire increment with a reasonable number of holograms and, for this reason, the fringe density in many cases is quite large. However, it can be seen that there are larger variations in the fringe pattern near the edges of the panel as compared with the center of the panel. The variations in the fringe pattern are a result of slightly different stress conditions from hologram to hologram; this would cause the strain values determined from these holograms to vary markedly in these regions (non-linear) while little change would be observed from the gage readings because of their relatively poor sensitivity.

An additional source of error, and probably more serious, is that which results from measurement inaccuracies in determining fringe positions. Since these data are used to compute the second derivative of fringe spacing, the error in the in-plane strain calculation is a strong function of the rate of change of the fringe spacing or strain level being measured. For example, if a one percent error is made in data acquisition at the 100 με level, then an error of approximately 5% would be made in the strain calculation. However, if this same percent error is made at the 10 με level, then an error of 50% would be made in the strain calculation. This latter source of error is the probable cause for the erratic behavior of the data below 50 με. (This source of error is not a peculiarity of this technique, but is an inherent error associated with determining the second derivative and as such will always be present when determining in-plane strain data from out-of-plane displacement data.)

In an effort to limit the error due to measurement inaccuracies as much as possible, a data smoothing procedure was adopted. The procedure entailed plotting the fringe spacing between several fringes located symmetrically about the point

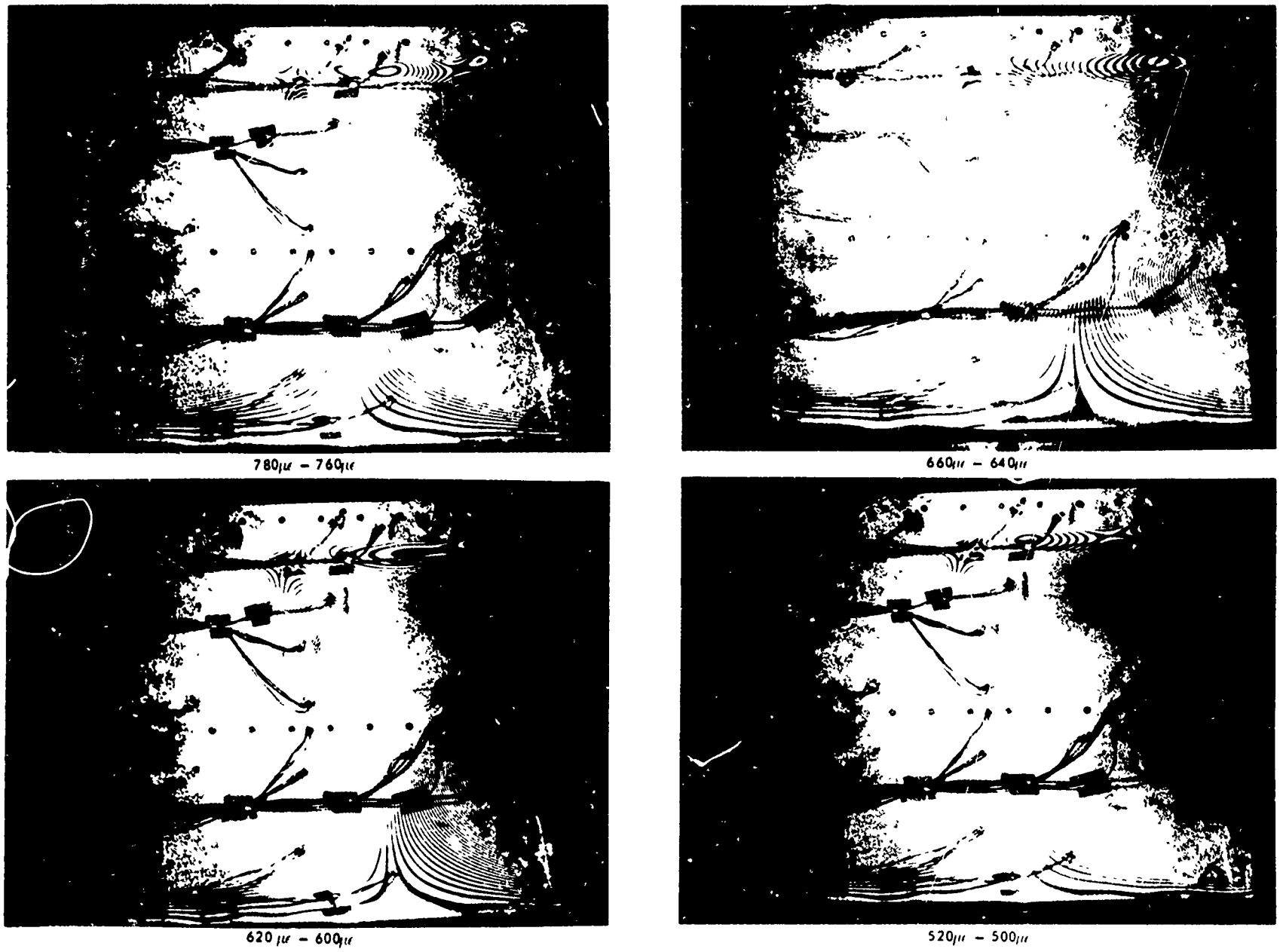

FIGURE 33. MAXIMUM STRAIN AND STRAIN PATTERNS

of interest. A best fit curve was then applied and the data used in the final calculations taken from the curve.

The principal strain direction was found according to the procedure outlined in the section on Conversion of Holographic Data to In-Plane Strain Data. Results presented in Table I show good correlation between the gage and holographic values even down at the low micro strain levels.

In conclusion, the strain data obtained from a double-exposure hologram made of the test panel was in fair agreement with the data obtained from strain gages. Determination of the principal strain axis was also in good agreement. The experimental test did bring to light that if the holographic data is only taken over a small increment of the total strain of interest, then assurances have to be made that the smaller increment is an accurate representation of the larger. This can be accomplished by making several holograms over the total increment to determine the strain linearity. It should be noted that many of the problems encountered with these experimental tests were related to attempts at making a comparison between strain gage and holographic data and would not be a consideration otherwise. Indeed, this reinforces the potential advantages of developing a holographic strain visualization system.

Cylinder

In an effort to determine the effect that object curvature has upon the holographic determination of in-plane strain, a thin-walled steel cylindrical shell was experimentally evaluated. The cylinder, 40 cm high by 30 cm in diameter, had a wall thickness of 0.1 cm and was closed off at each end by thin steel panels. The cylindrical object was chosen because it approximates the structure of some typical aircraft components; the wall thickness of the cylinder could be chosen so that the ratio of in-plane to out-of-plane displacement is such that it is possible to better match the sensitivity of strain gages to that of holographic interferometry; and it allows testing of the more general theory for obtaining in-plane strain from holographic data with a minimum of complication added to the data reduction procedures.

In order to introduce high local strains in this cylindrical structure, various shapes were cut out of its surface; squares, circles, and slits cut at various angles to the axis of the cylinder. The introduction of non-uniformities in the strain field made it possible to compare the relative values between the various gages to the values obtained holographically. Preliminary double-exposure holograms were made of the cylinder before and after it was loaded uniformly with a force of 100 Kgf along the symmetry axis. From the resulting reconstructions, suitable locations for nine rectangular rosette strain gages were determined.

It was found, however, after the strain gages were cemented in place, that forces in excess of 400 Kgf applied along the symmetry axis of the cylinder were required before any of the strain gage readings were sufficiently large to be considered reproducible. In order to increase the surface strain (for reproducible gage readings), an eccentric load parallel to the symmetry axis was applied in place of the axial load first tried.

For the purpose of obtaining strain gage readings, a force of 60 Kgf over half of the cylinder end wall was applied; and for the holographic interferograms, 25% full load was applied for the first exposure and zero load for the other. The strain field was thus sampled in the same manner as the strain field in the simulated airframe test panel. In the case of the panel, however, a much smaller increment, 2% of full load, was sampled.

A photograph of the resulting interferogram from a typical test is presented in Fig. 34. Also shown are the positions of the nine strain gages which are both near and distant from the surface cutouts. Using measured values for the angle between the surface normal and the line of sight, α, and the values for the fringe spacing obtained from this holographic interferogram, the principal strain, ε_H (Eq. 10) was calculated. Also, the principal strain direction, ϕ_H, was found from this interferogram. The data obtained from the gage rosettes were reduced to find the principal strain, ε_G, and principal strain angle, ϕ_G. As in the case of the simulated airframe panel the two sets of data were then adjusted so that the mean value of the ratios between gage and holographic data was unity. The relative strain values along with the angle α (angle describing surface curvature effects), are presented in Table II and are listed in descending strain magnitude as determined by the gage readings. In addition, the ratios between the holographic and gage values are presented on the far right of the table.

As can be seen in Table II, the holographic strain values were calculated at angular positions (α) from 5° up to 50°. The resulting values are in good agreement with those obtained from the gages even at the lower strain levels and at angles slightly greater than 45° (the maximum viewing angle established by theoretical considerations). The mean value of the ratio data is of course 1, and the standard deviation is .49. (This is approximately the same standard deviation found for the simulated aircraft panel.) Comparing this with reduced data that were obtained without accounting for surface curvature change, the standard deviation was .56. Thus, the corrected data shows an improvement over the data which is obtained without regard to viewing direction and surface curvature.

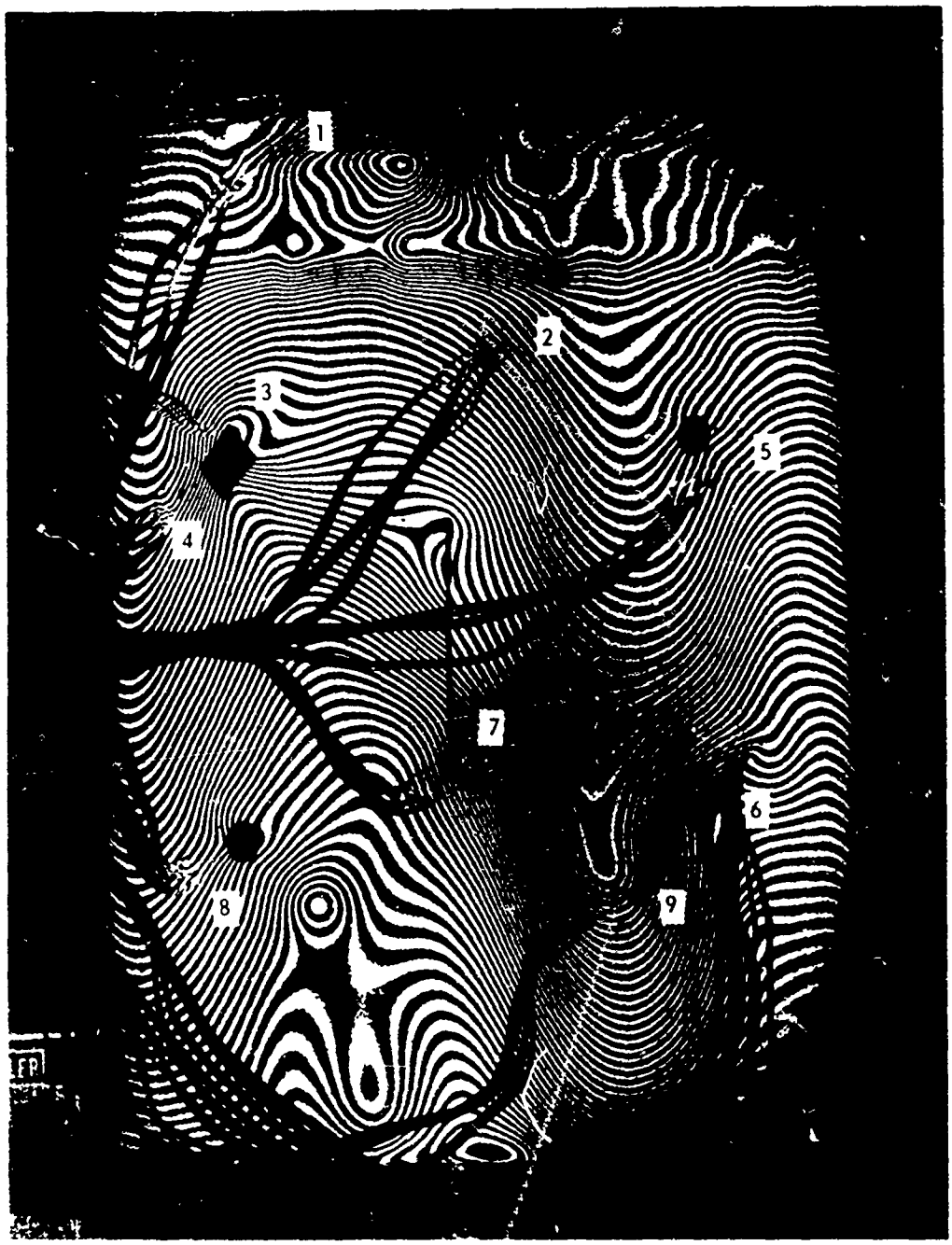

FIGURE 34. HOLOGRAPHIC STRAIN ANALYSIS OF ASYMMETRICALLY LOAD CYLINDER

TABLE II

Comparison of Strain Gage and Holographic Interferometry Measurements (Cylinder)

Gage Position	Strain Gage Measurements		Holographic-Interferometry Measurements			Ratio $\varepsilon_G/\varepsilon_H$
	Principal Strain $\lvert\varepsilon_G\rvert$ ($\mu\varepsilon$)	Principal Strain Angle ϕ_G(°)	Surface Angle α(°)	Principal Strain $\lvert\varepsilon_H\rvert$ ($\mu\varepsilon$)	Principal Strain Angle ϕ_H(°)	
4	46.0	91.4	48	54.6	0	1.19
1	35.4	83.6	34	38.0	120	1.07
7	27.0	77.0	5	27.1	40	1.01
5	22.6	115.1	45	9.6	110	.43
8	22.1	93.6	43	21.0	40	.95
2	21.5	77.1	10	3.9	80	.18
6	19.2	107.1	50	18.7	60	.97
3	16.0	45.0	38	19.7	170	1.23
9	9.2	99.2	25	17.8	40	1.93

The correlation between the principal strain angle determined from the holographic interferogram and the value obtained from the strain gages is not in very good agreement. The points of large disagreement occur in both the high and low strained areas.

Thus, it has been demonstrated that in-plane strain can be determined for curved surfaces, provided that consideration of the angle between the viewing direction and surface normal are taken into account. Although an absolute one-to-one correlation is not obtained in these experiments (nor were they for the experiments involving the simulated aircraft panel), the general trend of the in-plane strain values is established.

It should further be noted that in experiments involving both the cylinder and simulated aircraft panel, the stress loads were applied so that relatively large components of the force were tangential to the surface. This was purposely done to evaluate the effect of such forces on holographically obtained strain data. The results indicate that the application of such forces do not seem to significantly affect the relative values obtained from the holograms.

SECTION VI

SPECIFIC PROBLEM INVESTIGATIONS
NDT OF COMPOSITE COMPRESSOR BLADES

INTRODUCTION

One of the major areas of study under the Contract is a laboratory investigation of various holographic nondestructive testing (HNDT) procedures as applied to composite compressor blades, cooling passage alignment and weak adhesive interface bonds. In accordance with the program schedule, as presented previously (Fig. 2), the first year's work in this area was concerned with composite compressor blades. Laboratory feasibility studies were conducted to evaluate the applicability of holography for the inspection of boron-polyimide, graphite-polyimide, and Borsic(R)/aluminum fan blades. The use of such composite materials has been under intensive investigation over the past few years with the ever increasing need for high strength, lightweight materials for both engine and airframe components in advanced aircraft.

One specific application being considered for composites is in the compressor stages of gas turbine engines where relatively large airfoils are utilized. One example is Borsic(R)/aluminum fan blades which solve some vibrational problems encountered with homogeneous metal airfoils because the high modulus provides reinforcement allowing elimination of partspan shrouds. Thus efficiency increases on the order of one percent (Ref. 19) are possible, a significant step at this stage in compressor development. Of additional significance is the 40% weight saving over titanium blades. However, in this type of application the airfoil undergoes tremendous stress loads; and if manufacturing defects are present, complete failure of a compressor blade is possible. It is therefore essential that an effective nondestructive testing procedure be developed for the inspection of these composite airfoils. Because of their complex nature, HNDT would seem to be particularly applicable to this type of structure.

In general, these structures are usually fabricated entirely of fiber reinforced resin material (boron or graphite-polyimide) or metal bonded fibers (Borsic(R)-aluminum) and only contain a slight amount of noncomposite material (usually some metal is present at the base of the foil); typical examples are presented in Fig. 35 showing both a boron-polyimide airfoil and a Borsic(R)-aluminum fan blade. Except for the composite material used, the construction of the foils is similar; vertical unilateral fibers forming a core with 45° fiber cross plies bonded to this to form the outer shell. The root material is then usually added to the foil after fabrication. The particular types of flaws

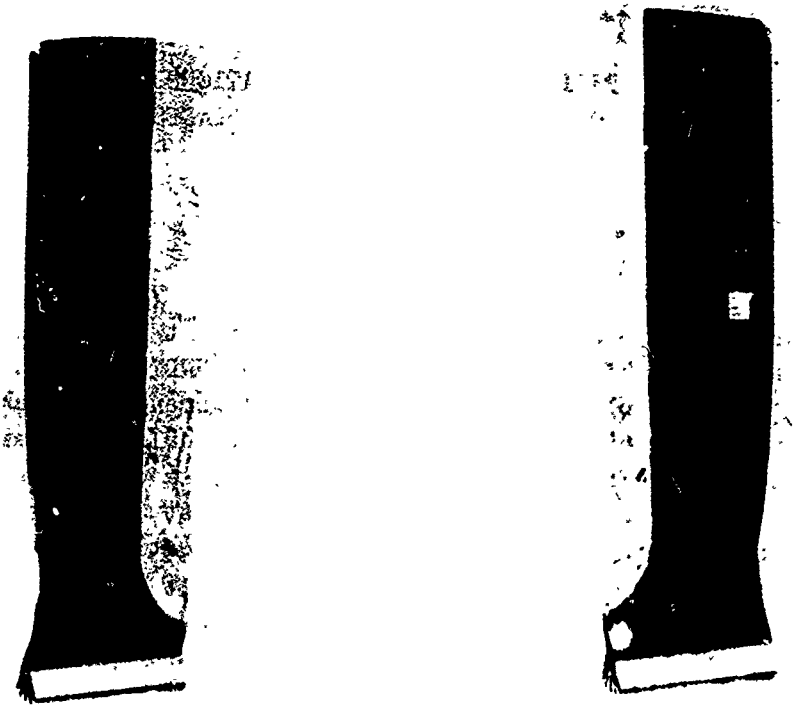

PRESSURE SIDE SUCTION SIDE

BORON POLYIMIDE

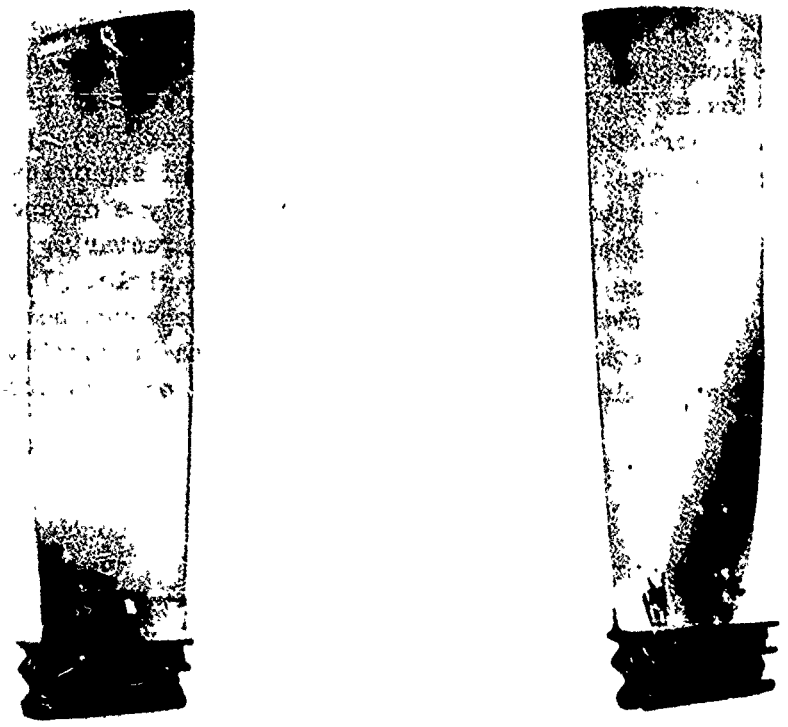

PRESSURE SIDE SUCTION SIDE

BORSIC ALUMINUM

FIGURE 35. COMPOSITE AIRFOILS

encountered in manufacturing are disbonds between successive cross-plies, between the core and the 45° plies, between the foreign object damage (FOD) shield and the composite, and between the fibers and the root material, the latter being the most difficult to detect because of the thickness and complexity of the fir tree type of root.

EXPERIMENTAL PROCEDURE

In the present investigations, time-average interferometric holography was employed to record the surface of the test object as it was physically deformed by excitation with ultrasonic standing waves. In this manner, it is possible to detect any defect or disbond within the object which manifests itself as an anomaly, or disturbance, in an otherwise regular interferometric fringe pattern characteristic of the surface deformation to be expected from the applied ultrasonic excitation. Application of ultrasonic stressing systems for the inspection of composite compressor blades can be accomplished by electrically driving a piezoelectric transducer which has been bonded to the surface of the test piece. The electrically induced transducer deformation causes flexural displacements due to the restraining force of the bond and in this way, a resonant plate mode can be established in the sample with a proper choice of driving frequency. Additional transducers can be used as sensors to aid in establishing plate resonances. This method of excitation has the advantage of having a nearly unlimited range of frequencies; from a few 100 Hz to several 100 KHz.

Another approach, and one which greatly facilitates the experimental procedure by eliminating the bonding process, is to mechanically couple a transducer to the test piece through a solid exponential horn (acoustic transformer). The horn consists of an aluminum exponential cylinder (radius of the cylinder decreases exponentially from end to end) with a piezoelectric transducer mounted on the larger diameter end. The smaller diameter end is pressed against the test piece and the transducer driven at resonance to couple a large amount of acoustic energy into the sample. A complete assembly, designed for operation at 50 KHz, in an operating configuration is shown in Fig. 36. In addition to being easier to use, thereby making it a practical method for implementation of HNDT, this type of drive can provide much larger amplitude vibrations; peak displacements of approximately 10 microns have been obtained at the horn output.

Several airfoils, fabricated by the Pratt & Whitney Aircraft Division, have been examined, using ultrasonic excitation with the exponential horn drive and time-average holography, for flaws in both the as-manufactured condition and after fatigue cycling. For proper interpretation of the holographic reconstructions, it is necessary to holographically record both sides of the blade simultaneously. This assures that the ultrasonic driving frequency and amplitude is identical for both holograms, and in addition, facilitates the experimental procedure by shortening the test time. This is done by employing two holographic plates, one for viewing each side of the blade, as shown in the experimental arrangement of Fig. 36.

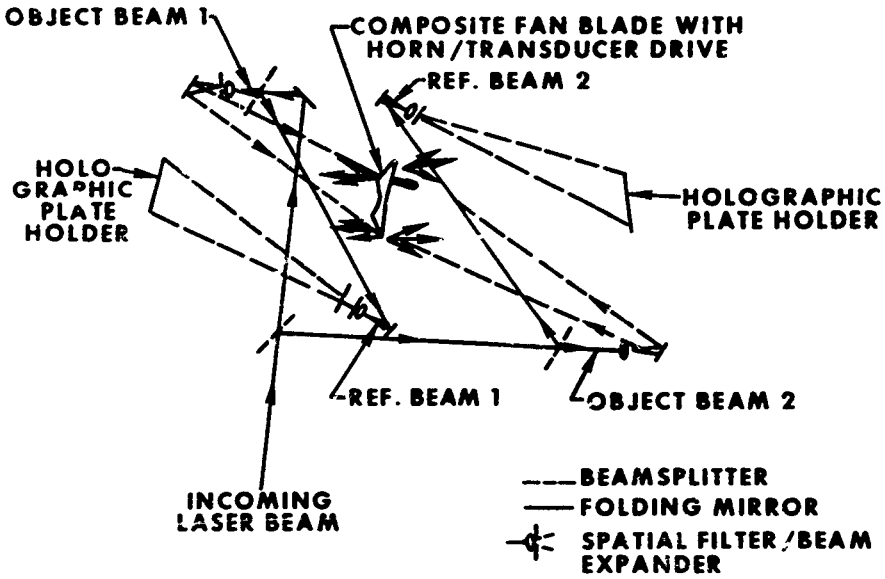

SCHEMATIC

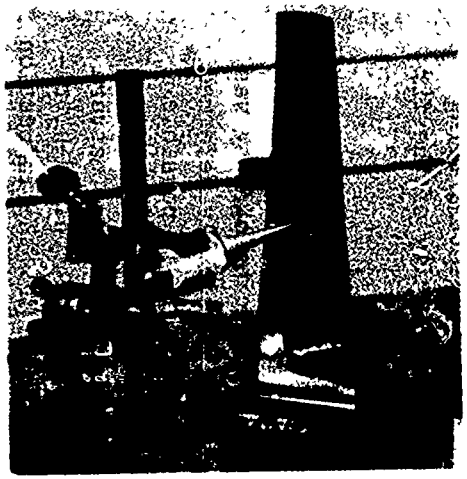

BLADE WITH HORN DRIVE

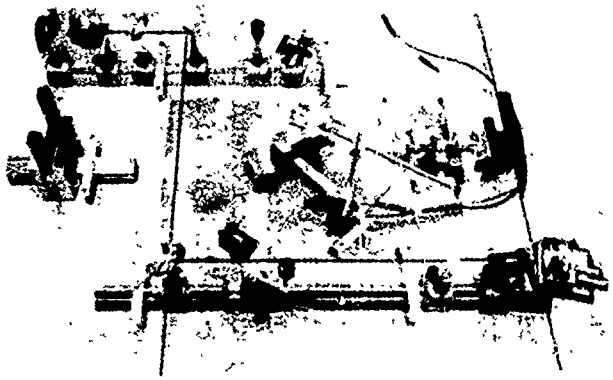

EXPERIMENTAL SET-UP

FIGURE 36. COMPOSITE FAN BLADE INSPECTION

The reasonably compact size (4' x 4') and symmetrical nature are apparent in the figure. An incoming laser beam is first split into two beams (one for each hologram), each of which is subsequently split again into a reference and object beam as shown in the schematic diagram. In general, more than one view was recorded of each side to assure complete coverage of the airfoil surface. When this procedure was used, the lower reconstruction covered all or almost all of the blade surface. In addition, a close-up of the tip area, which is sometimes obscured by the transducer in the lower picture, was recorded. While the driving frequency, and thus resonant plate mode pattern, may be slightly different for each pair of reconstructions, the important consideration is that both sides in each pair are recorded simultaneously, permitting the comparison which allows pattern differences, and thus flaws, to be detected.

The major portion of the work to be described in the following section was performed with cw He-Ne laser systems. However, the most recent studies, concluding this phase of the investigation, were conducted with pulsed laser systems in order to demonstrate their applicability to time-average holography which is necessary for effecting this type of NDT.

EXPERIMENTAL RESULTS

Boron and Graphite Polyimide Airfoils

When using the experimental procedure described in the previous section, two vibrational characteristics, as recorded holographically, indicate lamination defects in this type of structure.

First, a clearly smaller well defined mode size, with a larger amplitude, identifies a definitely more compliant region, and thus indicates an unbonded area. Further, the nonexistence of this mode on the other side of the blade shows that the unbonded area is closer to the surface on which the mode is visible. An example of this type of flaw is visible in the reconstruction shown in Fig. 37. This blade was studied before instituting the double holographic plate procedure and thus only one side, exhibiting disbonding between the FOD shield and the airfoil surface, is reproduced here. The flawed area indicated below the FOD shield was probably caused by the removal of an earlier, and longer, protective strip. This blade, as well as those to be described subsequently, was also examined with more conventional ultrasonic NDT procedures, and the results are presented in Fig. 38. The test consisted of manually probing the blade and noting the areas of signal loss on a schematic diagram. Further consideration of the differences and/or similarities between the holographic and ultrasonic results are discussed in a later section entitled Correlation Studies.

The second type of vibrational characteristic indicating a structural anomaly is seen in the reconstructions of Fig. 39. In this instance, the defect exists

FOD SHIELD DISBONDING

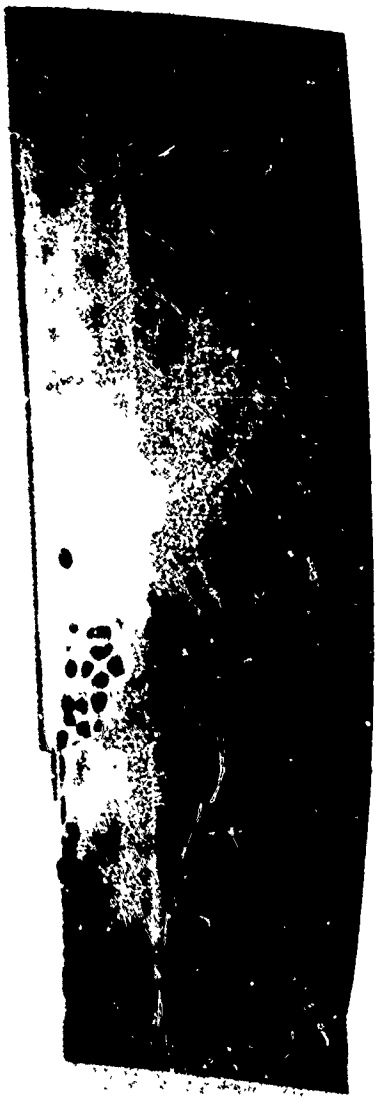

HOLOGRAPHIC RECONSTRUCTION

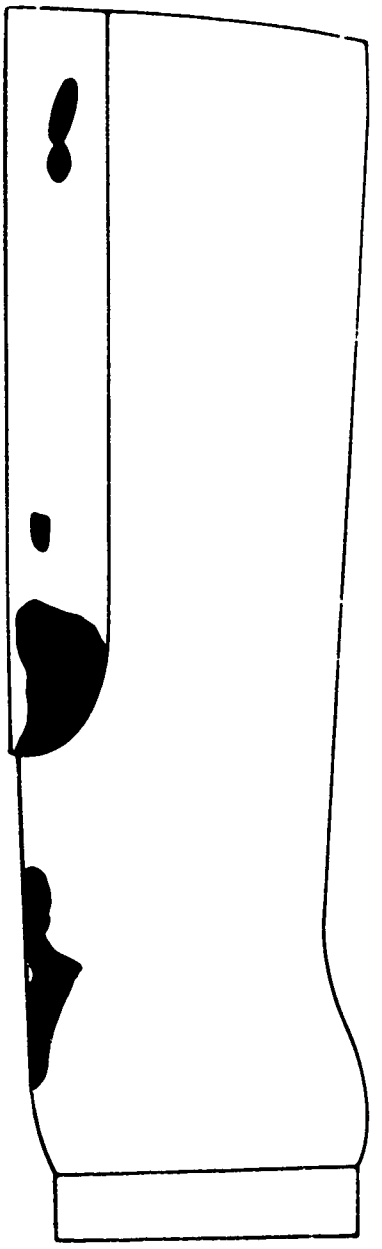

SCHEMATIC

FIGURE 37. HOLOGRAPHIC INDICATIONS ON BORON POLYMIDE BLADE – B1

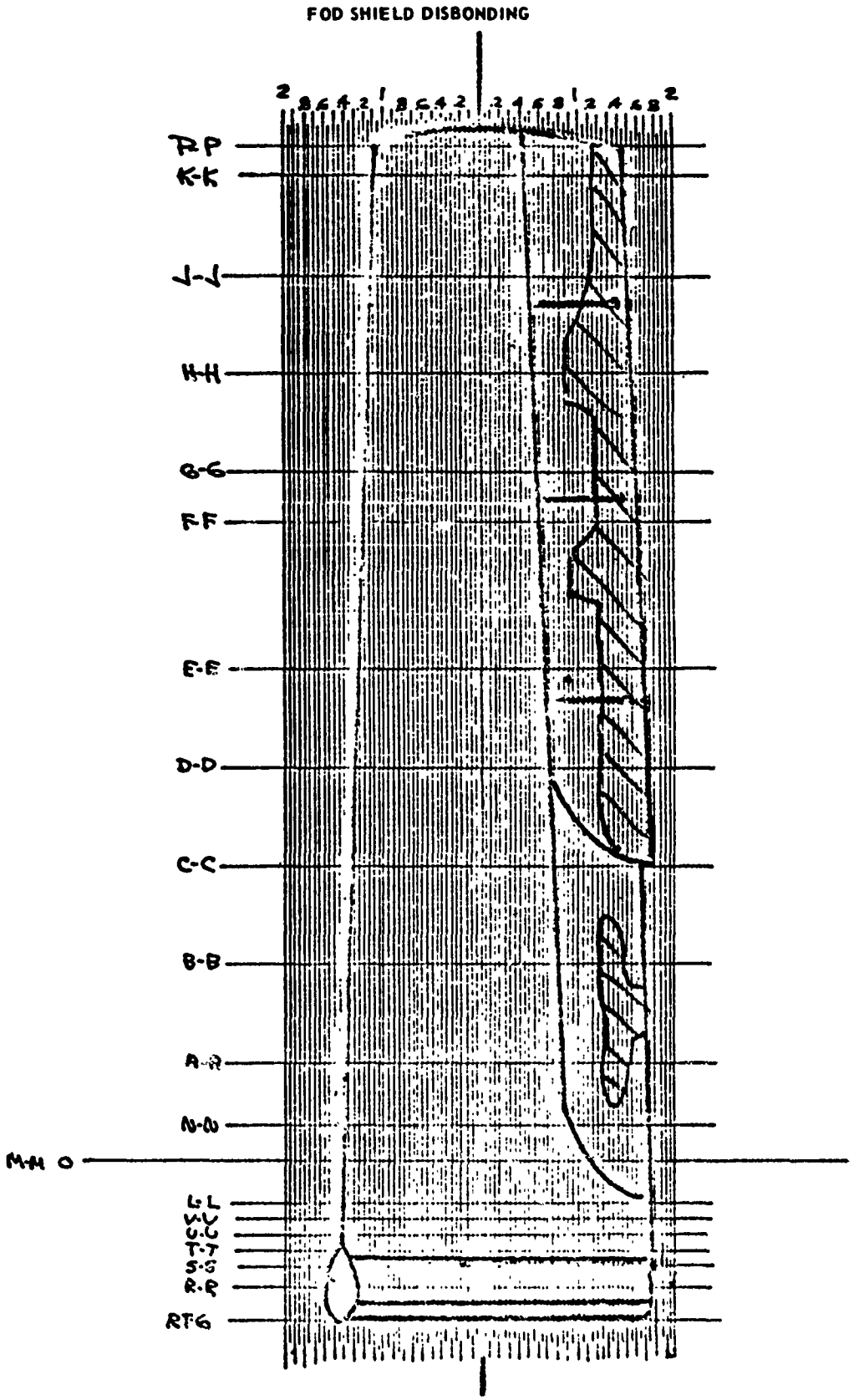

FIGURE 38. ULTRASONIC INDICATIONS ON BORON POLYMIDE BLADE – B1

Reproduced from best available copy.

GENERAL DELAMINATIONS

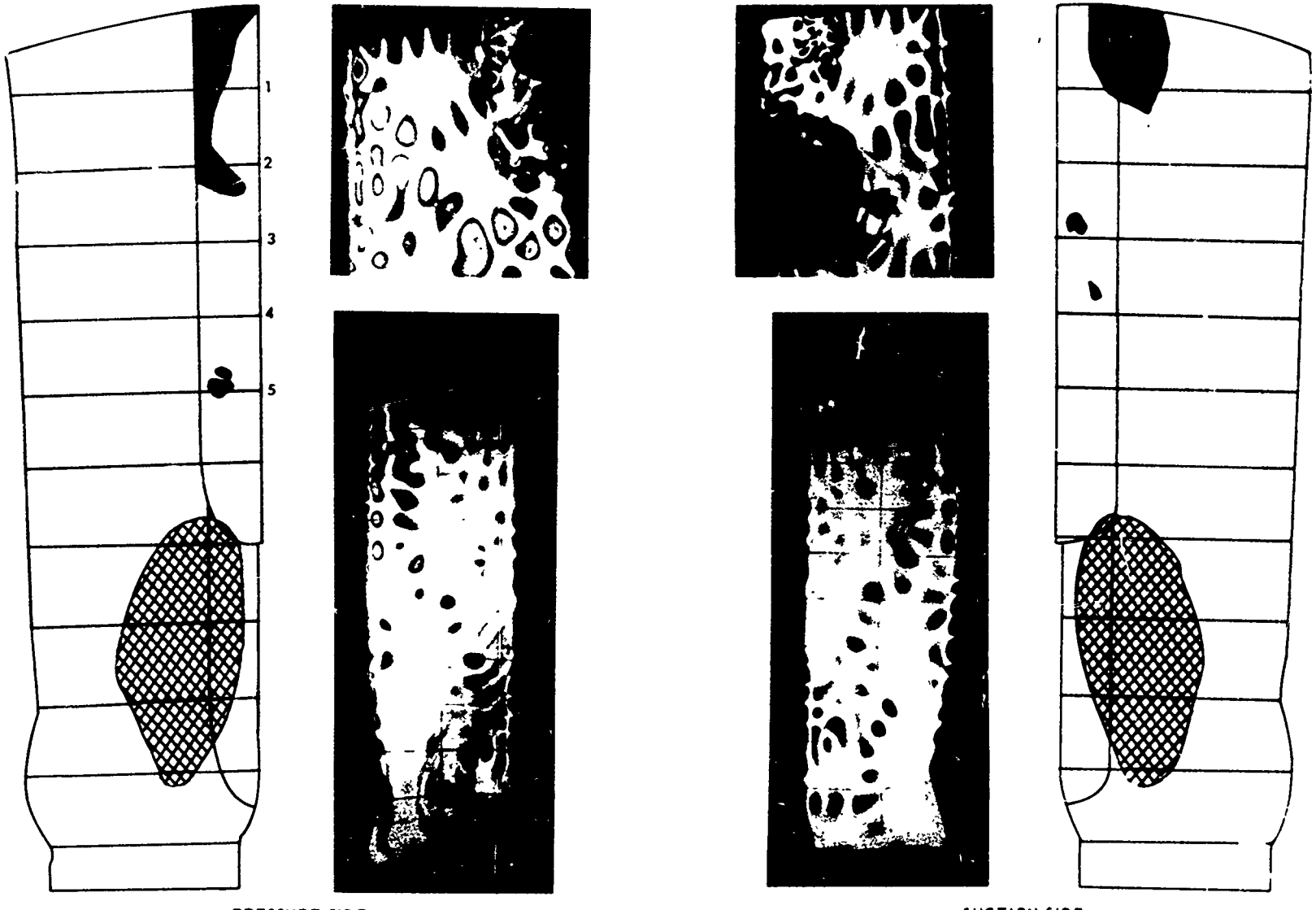

PRESSURE SIDE

SUCTION SIDE

FIGURE 39. HOLOGRAPHIC INDICATIONS ON BORON POLYIMIDE BLADE – B2

in the area denoted by the lighter cross hatched area in the accompanying schematics. The vibrational characteristic of interest lies in the fact that the overall mode pattern itself, not the size and amplitude of individual adjacent modes, is different for the two sides of the blade. This indicates a probable deterioration of the adhesive within the blade, without a complete disbond. Also seen in Fig. 39 are several flaws detected by the first type of vibrational characteristic; these are indicated by the blackened areas on the schematic. They are particularly apparent near the tip of the blade, both under and overlapping the FOD shield. In this particular instance, the delaminations observed were apparently the result of ice ball impact damage during blade testing conducted after fatigue cycling. Results of the ultrasonic examination of this blade are presented in Fig. 40.

A second example of FOD shield disbonding is presented in Fig. 41; again, the bad areas are indicated on the accompanying schematic. A third, less obvious type of vibrational characteristic which might suggest a possible bonding defect within the blade or a weakening of the bond under the FOD shield is also exhibited in this figure. This particular anomaly, while much more subtle than either the well defined higher amplitude mode patterns (indicated in black on the schematic of Fig. 39) or the different mode patterns for the two sides of the blade (presented in Fig. 39), manifests itself as a distinct difference in vibrational amplitude between the two sides of the blade. The area exhibiting this phenomenon is indicated by the shaded area in the schematic. Though not observed during the holographic testing, the reconstructions of Fig. 41 were re-examined following ultrasonic examination which indicated regions of signal loss in this area. During the re-examination the differences in amplitude between the two sides, as can be seen in Fig. 41, were clearly evident. The results of the ultrasonic examination of this blade are presented schematically in Fig. 42. Of further interst in Fig. 41 is the excellent correspondence in the mode patterns, both position and amplitude, for the two sides of the blade, indicating good bond quality, over the remaining surface.

In Fig. 43 the holographic reconstructions from a good blade are presented. The striking feature in this case is the exact one-to-one correspondence of the mode patterns over the entire surface for both sides of the blade, verifying that it is vibrating as a structural entity, and that apparently no flaws are present. As with the preceding blade, the ultrasonic examination, shown in Fig. 44, indicated one area of signal loss not immediately obvious in the holographic tests; some discussion of this point is presented in the section on Correlation Studies.

Borsic(R)-Aluminum Fan Blades

Three examples of flaws, as detected in Borsic(R)-aluminum fan blades, using ultrasonic stressing are presented in Fig. 45. In one of the blades (holographic reconstruction in Fig. 45a) a very distinct vibrational point (the dark circular

GENERAL DELAMINATIONS

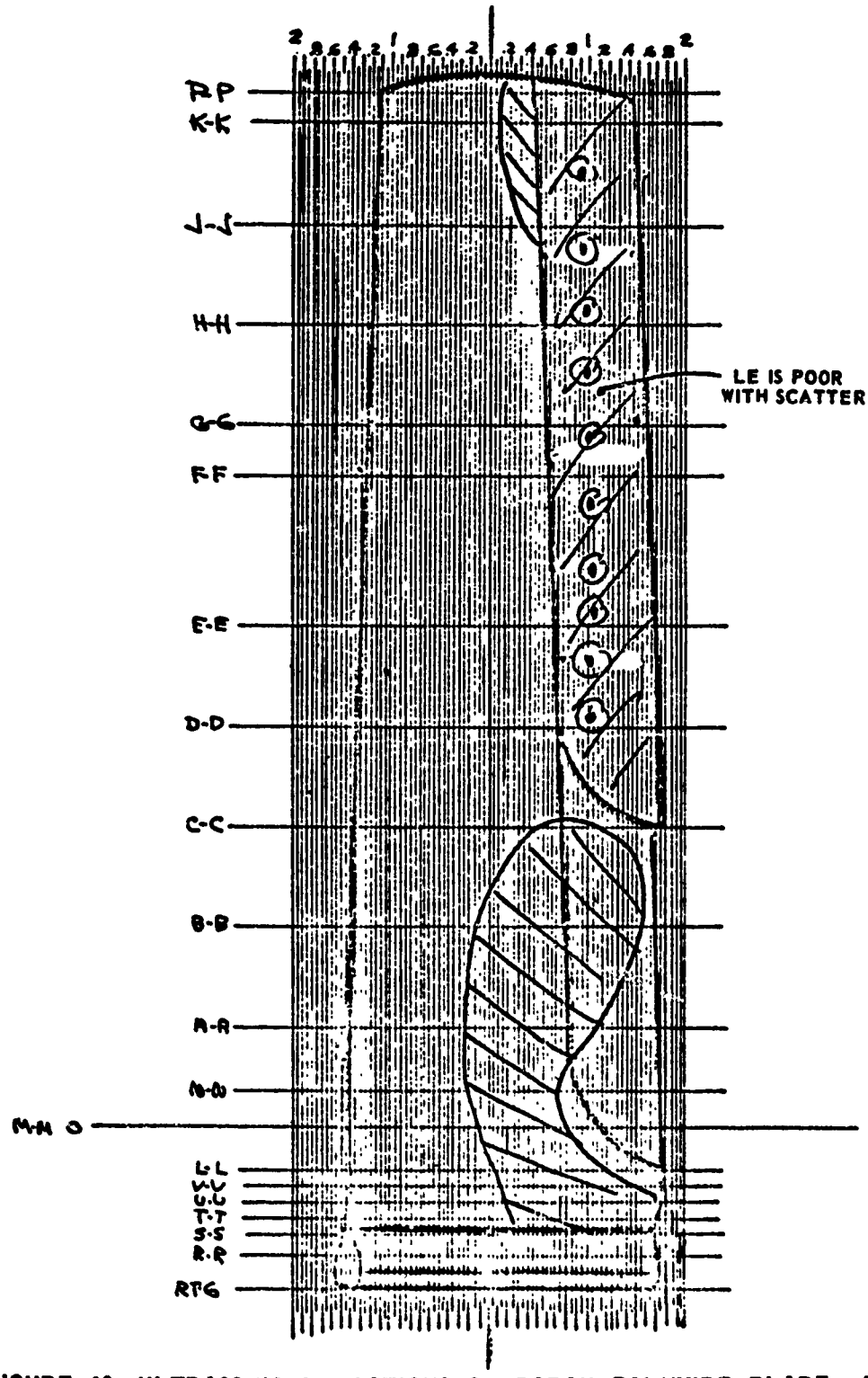

FIGURE 40. ULTRASONIC INDICATIONS ON BORON POLYMIDE BLADE – B2

FOD SHIELD DISBONDING

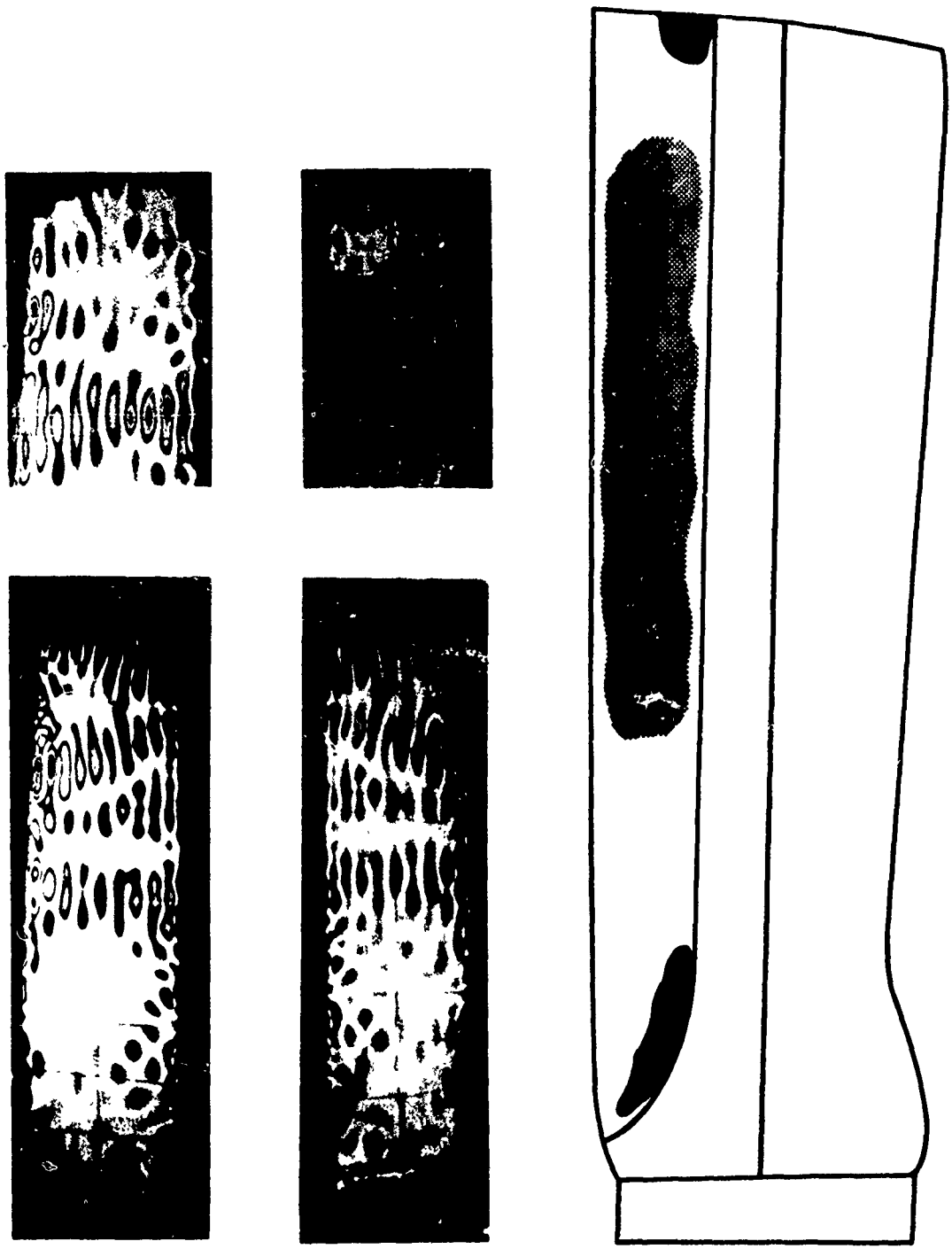

PRESSURE SIDE SUCTION SIDE SUCTION SIDE

FIGURE 41. HOLOGRAPHIC INDICATIONS ON GRAPHITE POLYMIDE BLADE – G1

FOD SHIELD DISBONDING

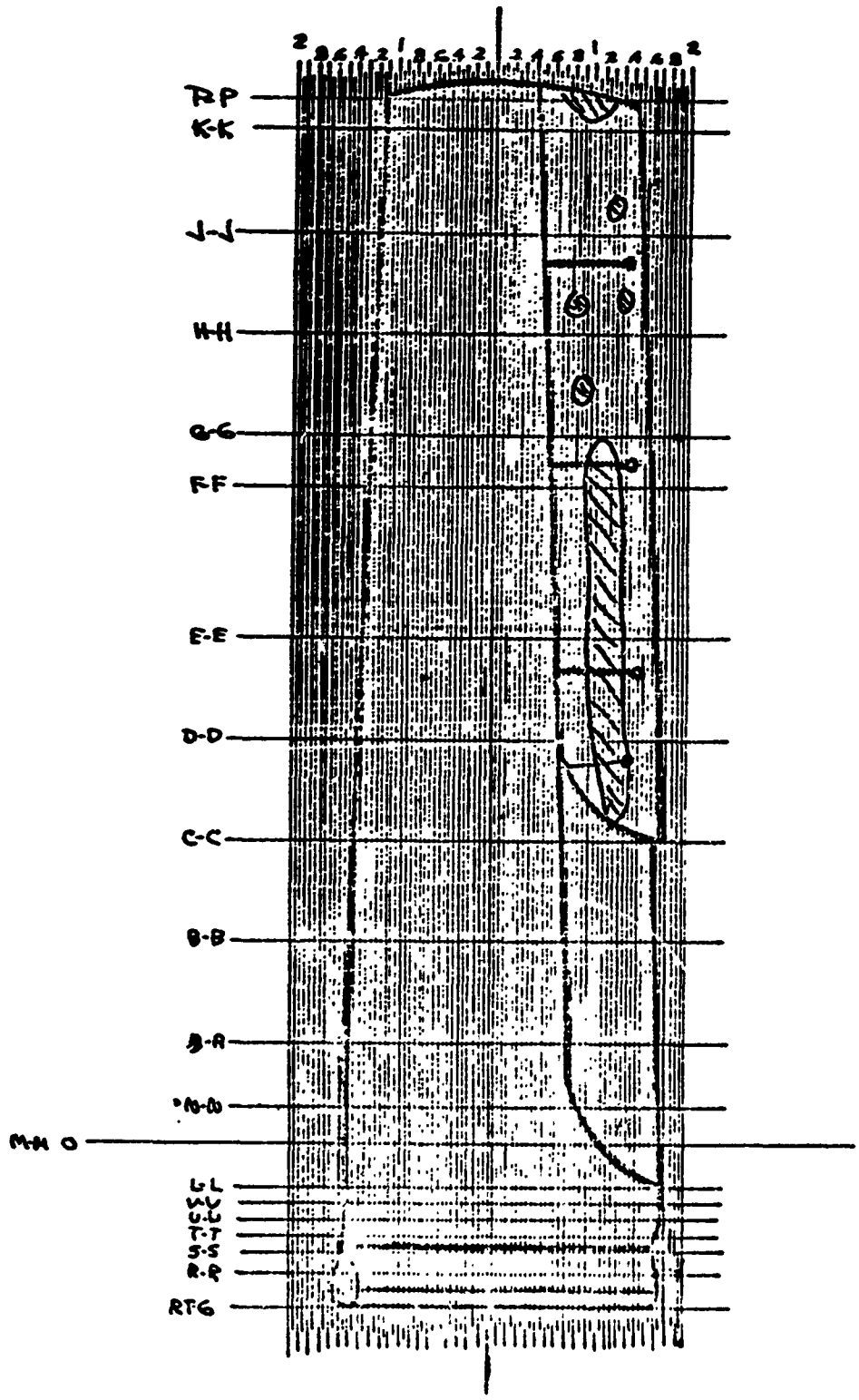

FIGURE 42. ULTRASONIC INDICATIONS ON GRAPHITE POLYMIDE BLADE – G1

NO SIGNIFICANT DETECTABLE FLAWS

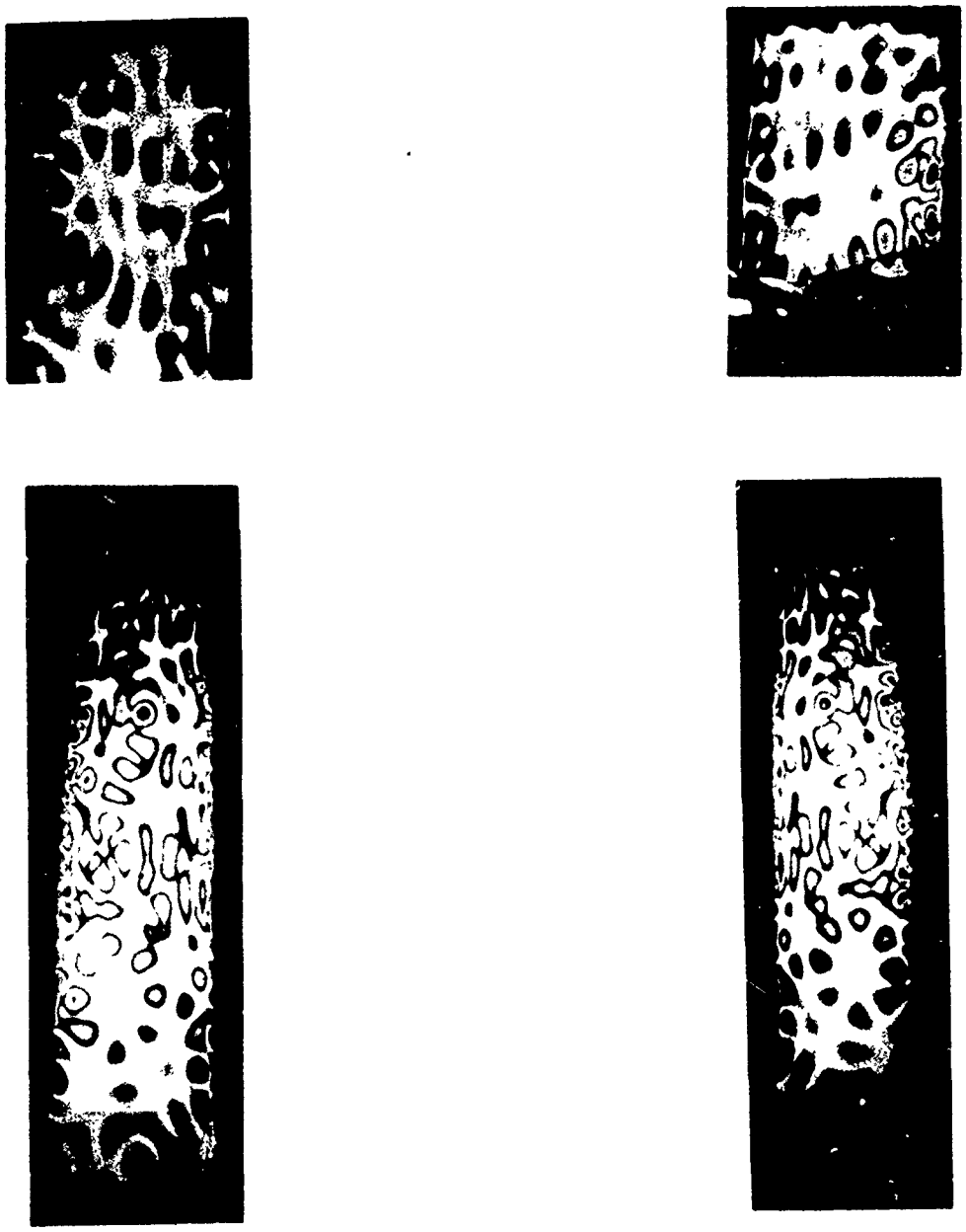

PRESSURE SIDE

SUCTION SIDE

FIGURE 43. HOLOGRAPHIC INDICATIONS ON BORON POLYMIDE BLADE – B3

NO SIGNIFICANT DETECTABLE FLAWS

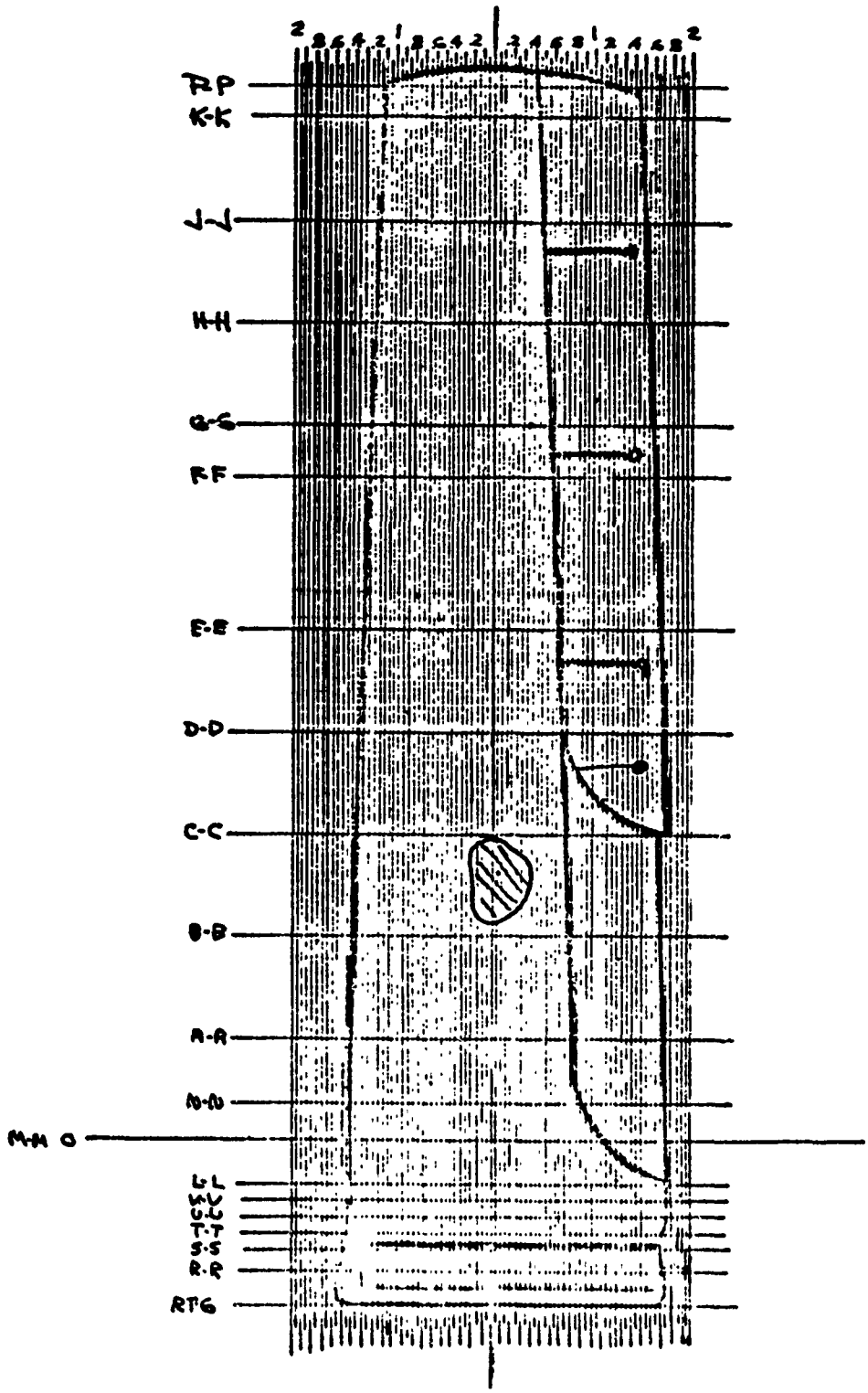

FIGURE 44. ULTRASONIC INDICATIONS ON BORON POLYMIDE BLADE – B3

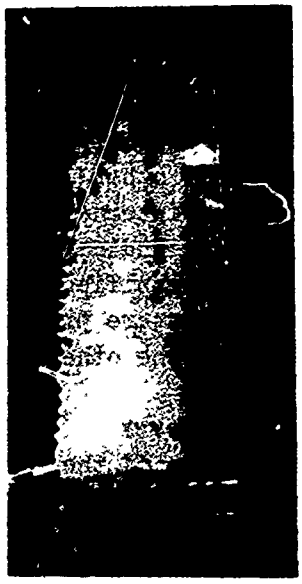

(a) 273 KHz

(b) 89.6 KHz

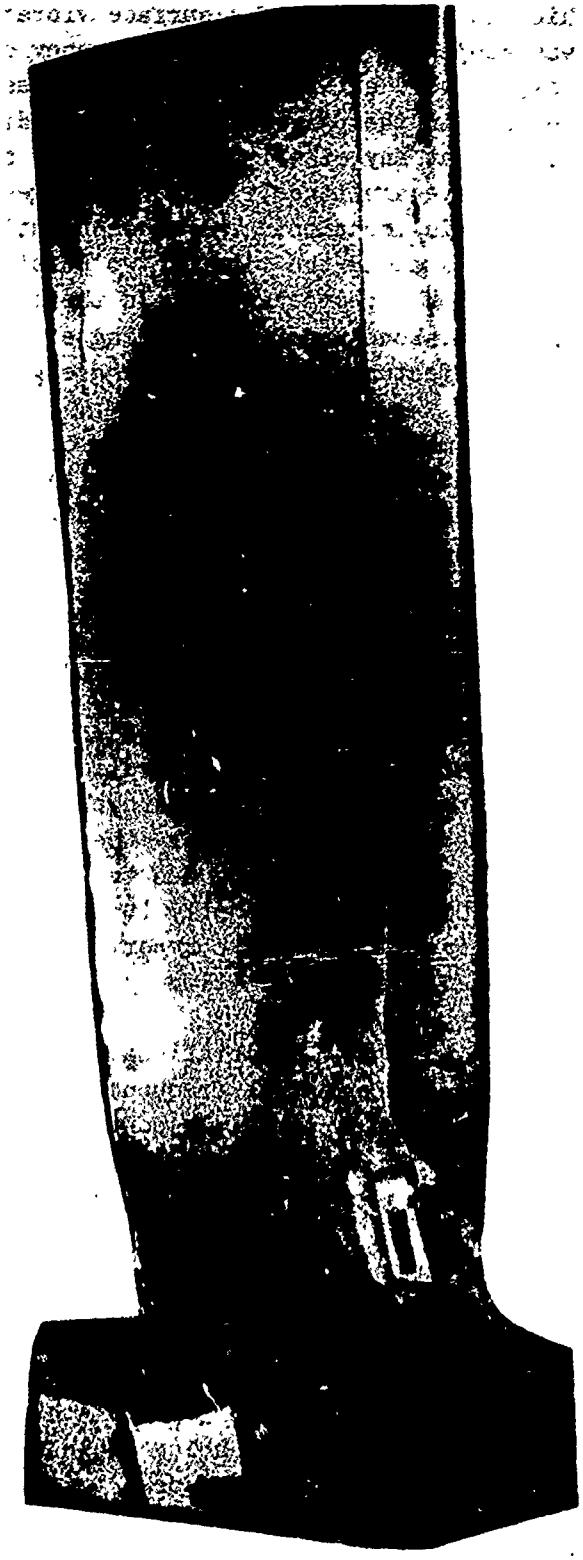

(c) 225 KHz

FIGURE 45. BORSIC (R) – ALUMINUM BLADES

spot), which is indicative of a surface vibratory motion, was observed on the root when it was subjected to a driving frequency of 273 KHz. (These Borsic(R)-aluminum blades were excited with bonded transducers, rather than the exponential horn drive used in the polyimide airfoil studies.) This particular anomaly was not in evidence at any other point on either side of the root at any other frequency or drive amplitude. Thus, it suggests the presence of an internal flaw or disbond at this location. The reconstructions in Figs. 45b and c indicate similar anomalies along the tips of two Borsic(R)-aluminum blades identified at 89.6 KHz and 225 KHz respectively. In the latter case, two anomalies are present; one denoting a disbond under the leading edge protective strip, and the other identifying a defect nearer the trailing edge.

One of the more significant results obtained during this portion of the first year's contract effort concerned with HNDT of composite compressor blades is presented in Fig. 46. The pictures shown were reconstructed from pulsed laser holographic recordings of a Borsic(R)-aluminum fan blade being vibrationally excited at approximately 50 and 100 KHz. The results clearly demonstrate the applicability of pulsed laser methods to time-average holographic study of vibrating systems, a technique which has just been shown to offer considerable promise in the nondestructive inspection of composite structures. As briefly described earlier in the present report, open lasing (non Q-switched) of a pulsed laser provides an effective pulse duration on the order of several milliseconds, sufficiently long to record time-average holograms of an object excited in the Kilohertz frequency range. However, the pulse is short enough to effectively isolate objects which are moving due to environmental vibrations whose frequencies are less than 100 Hz. Consequently it is possible to perform the HNDT work as described in this section of the report without the degree of sophistication required in the vibration isolation systems associated with cw holography.

As seen in Fig. 46 the vibrational mode patterns for both sides of the blade appear identical at excitation frequencies of 51 KHz and 96 KHz. The results suggest, therefore, that the blade contains no internal defects or delaminations. The work was included to illustrate the adaptability of pulsed laser holography to the time-average process, which is necessary for this type of HNDT.

Correlation Studies

For the cases (polyimide blades) where correlation studies of the above results have been made with ultrasonic NDT procedures, good agreement has, in general, been observed. In the 3rd and 4th examples (Figs. 41, 42, and 43, 44), however, re-examination of the holographic reconstructions was required to obtain complete agreement with the ultrasonic tests. In another case (1st example, Figs. 37 and 38) the holographic data did not indicate the FOD shield disbonding to be as extensive as the ultrasonic evaluation did, and in the second example (Figs. 39 and 40), as well as the 3rd, the holographic data indicated small additional areas not observed ultrasonically.

PRESSURE SIDE

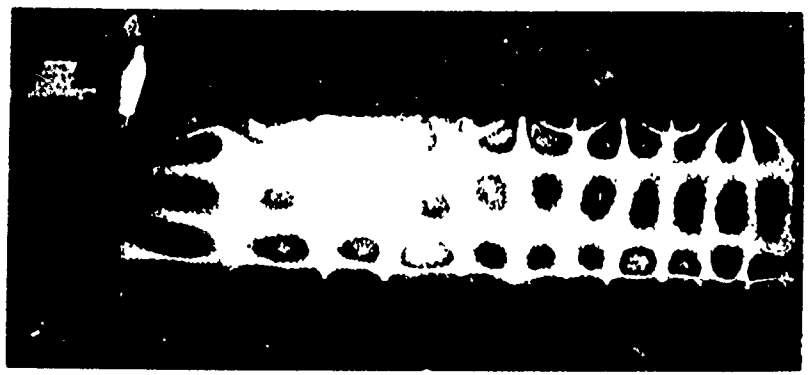

PRESSURE SIDE

SUCTION SIDE

(b) 96 KHz

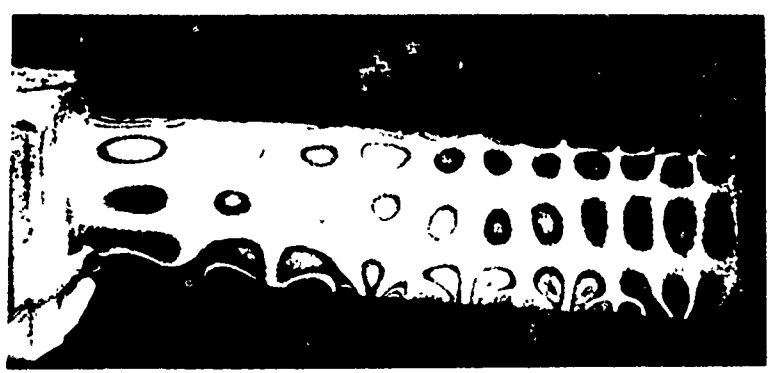

SUCTION SIDE

(a) 51 KHz

FIGURE 46. BORSIC(R) – ALUMINUM FAN BLADE

Of the two cases requiring re-examination, one (Figs. 41 and 42) was discussed previously. It should be added, however, that the ultrasonic evaluation did not suggest any difference in the type of defects identified at the tip and further down the FOD shield. Indeed, it was not established whether structural differences did exist within the blade which might account for the distinct difference in holographic response. However, the HNDT results certainly suggest two different phenomena; a distinct vibrational mode pattern difference between the two sides (blackened areas) suggesting total delamination, and a slight difference in vibrational amplitude between the two sides (shaded areas) suggesting a much lesser degree of internal defects.

In the second case (Figs. 43 and 44) requiring re-examination of the holographic reconstructions to realize complete correlation with the ultrasonic evaluation, the difference between the mode patterns for the two sides was quite subtle. In the same area identified in one type of ultrasonic test (passing the blade between two wheels) as a region of signal loss, a slight difference is observable in the holographic results; it is manifested as a separation, on the pressure side, of the "loop" from the three "looped" antinode seen on the suction side. In another type of ultrasonic test (introducing the source energy through a wedge shaped coupler) this area was not identified as a flawed region. In substance, therefore, the ultrasonic and holographic tests appear to provide the same conclusion; if indeed a defect is present, it is probably one of relatively little significance.

SECTION VII

CONCLUSIONS AND RECOMMENDATIONS

Based on the theoretical and experimental investigations discussed in the four major preceding sections of the present report, the following conclusions can be drawn.

PHYSICAL ENVIRONMENT EFFECTS

1. Study of the deleterious effects of extraneous lighting demonstrated that good quality interferometric holograms can be constructed in areas which contain high levels of ambient illumination, without filtering, provided that the exposure time can be controlled. For example, the tests conducted with 200 foot-candles measured at the photographic plate indicate this to be the limit for a 75 millisec exposure. However, extrapolation suggests that holographic exposures can be constructed with the object in direct sunlight (average subject produces 600 foot-candles on reflection) by reducing the exposure time to approximately 25 milliseconds. This exposure time is possible with the present shutter assembly by reducing the size of the curtain opening. The results further indicate that there is considerable latitude in the construction parameters within which the quality of the reconstructed objects does not degrade. For example, it is desirable to maintain the reference-to-object beam intensity ratio greater than unity, but the results appear comparable for ratios which range from 30:1 to 2:1. In addition, it is evident that in constructing double-pulse interferometric holograms, it is not necessary that the two pulse amplitudes be precisely matched to optimize the reconstructed fringe contrast.

2. The results obtained in the Fatigue Test Laboratory demonstrated that holograms could be constructed in areas of high vibrational fields with pulse separations as long as 100 microseconds. For this case, the displacements which occur at 1 KHz were not large enough to cause image degradation. The displacements at 1 KHz would have to approach approximately 0.04 microns before subsidiary fringes related to optical component shift would be detected.

3. Preliminary investigations carried out to examine the effects of small ($<1\mu$) particles upon holographic image quality showed that smoke concentrations far in excess of the Industrial Hygienist's threshold limit value for oil vapors, did not preclude the construction of holograms, although there was a noticeable loss in both resolution and contrast.

SURFACE FINISH EFFECTS

From the various surface sizes (up to 16 sq ft) and finishes (4 μ in to 2000 μ in) which were examined in these studies, the following results can be stated:

1. Interferometric holograms of surfaces with a roughness of less than 4 μ in (a very high polish) have been easily recorded.

2. The intensity of the radiation scattered from a surface is highly peaked in the specular direction. This will tend to limit the area coverage on smooth surfaces. The present tests have demonstrated the capability of recording a 4 foot square object, with a surface roughness of 8 μ in with an 8 foot separation between object and hologram.

3. Specular reflections are enhanced perpendicular to the surface finish direction. Thus, interferometric fringe information may be lost or degraded (a slight narrowing of the fringes) in areas of very intense specular reflection (usually a single narrow line).

4. Interferometric fringe contrast decreases as the recorded intensity decreases.

5. Holographic interferometric quality is independent of the laser beam expansion element (simple lens system or diffuser plate), except in cases where the raw laser beam has an uneven intensity distribution; in this event diffuser plates are preferred.

6. To obtain the maximum recorded area in a holographic interferogram, the specular point should be centered about the surface area of interest and in the case of no ambient illumination, the reference beam adjusted to yield a hologram with a N.D. of approximately 0.6

7. The degree of surface roughness up to 1000 μ in does not significantly affect interferometric fringe location.

8. Retro-reflective surface preparations may afford an enormous increase in allowable area coverage for a given laser system. On the basis of this preliminary finding it is recommended that the effect of such retro-reflective coatings on the rolling direction line effect be studied; and that other properties of the material be explored for applicability to aircraft hardware.

MAXIMUM STRAIN & STRAIN PATTERNS

The thecretical work, supported by experimental measurement, established that

holographic interferometry is a viable technique for visualizing strain patterns and areas of maximum strain concentrations on large structures. The results showed that both:

1. Good correlation exists between the principal strain fields on thin structures as sampled by conventional strain gages, and as determined by holography.

2. The effects of surface geometry and rigid body motion on the interferometric fringe data reduction procedures will not adversely influence the determination of high strain areas or relative strain magnitude.

Further, the experience gained in performing these studies has led to the following recommendations applicable to on-site measurement of strain by holographic interferometry:

1. The object-illumination source should be placed next to the holographic plate.

2. The hologram-to-object distance should be greater than 1 meter.

3. The angle between the surface normal and the viewing direction should be less than $\pm 45°$.

4. Preliminary double-exposure holograms of the object in the unstressed state should be taken to determine the effect that environmental influences will have on the strain field.

5. For comparative purposes, two or three holograms should be taken at small equal increments of strain in order to check linearity of the flexure field with respect to strain.

6. Surface curvature effects should be taken into account for surfaces where the normal varies over $\pm 20°$ with respect to the viewing direction.

NDT-COMPOSITE COMPRESSOR BLADES

Considering the relatively recent emergence of holography, as compared with ultrasonic techniques, for the performance of nondestructive testing, it can be concluded that the method will offer a viable technique for the inspection of various components. Certainly, when considering a specific part, further work is necessary to build up a backlog of experimental evidence which will aid in the interpretation of holographic data and recognition of specific defects. However, with regard to composite fan blades, it has been shown that:

1. The use of interferometric holographic techniques in combination with ultrasonic excitation may offer one of the most inclusive test methods for the detection and characterization of bond defects.

2. It appears that this approach can define the area of delamination, determine which surface it is nearer to, has the potential to determine the degree of disbonding, and is applicable to complex surface geometries as illustrated by the blade root studies described.

3. The use of a nonbonded exponential horn transducer drive configuration for introducing acoustic energy into a test object and the use of pulsed laser techniques for recording the data illustrate one potential method for implementing HNDT in a production or maintenance type of environment.

4. The relatively low frequency range (up to a few hundred kilohertz) that this combination of ultrasonics and holography affords as opposed to the megahertz operating frequency range of more conventional ultrasonic inspection procedures both contributes to its demonstrated effectiveness and offers the following important advantages: a) the effects of grain scattering, acoustic attenuation and surface roughness on resolution capability are much less severe; b) the inspection of much larger areas at one time is possible, thereby easing the material handling problem; and c) the techniques of transducer coupling are generally less elaborate, which should increase system reliability.

REFERENCES

1. Gabor, D.: "A New Microscopic Principle", Nat., Vol. 161, 1948, p. 777.

2. Leith, E. and J. Upatnieks: "Wavefront Reconstruction with Diffused Illumination and Three-Dimensional Optics", J. Opt. Soc. Am., Vol. 54, 1964, p. 1295.

3. Stetson, K. and R. Powell: "Hologram Interferometry", J. Opt. Soc. Am., Vol. 56, 1966, p. 1161.

4. Hamasaki, J.: "Signal-to-Noise Ratios for Hologram Images of Subjects in Strong Incoherent Light", Appl. Opt., Vol. 7, 1968, p. 1613.

5. Friesem, A. A. and J. S. Zelenka: "Effects of Film Nonlinearities in Holography", Appl. Opt., Vol. 6, 1967, p. 1755.

6. Wyant, J. C. and M. P. Givens: "Undesired Light in a Reconstructed Hologram Image Caused by the Nonlinearity of the Photographic Process", Appl. Opt., Vol. 9, 1970, p. 810.

7. Haines, K. A., and B. P. Hildebrand: "Surface Deformation Measurement Using the Wavefront Reconstruction Technique", Appl. Opt., Vol. 5, 1966, p. 595.

8. Sollid, J. E.: "Holographic Interferometry Applied to Measurements of Small Static Displacements of Diffusely Reflecting Surfaces", Appl. Opt., Vol. 8, 1969, p. 1587.

9. Shibayama, K. and H. Uchiyama: "Measurement of Three-Dimensional Displacements by Hologram Interferometry", Appl. Opt., Vol. 10, 1971, p. 2150.

10. Aleksandrov, E. B. and A. M. Bonch-Bruevich: "Investigation of Surface Strains by the Hologram Technique", Sov. Phys. - Tech. Phys., Vol. 12, 1967, p. 258.

11. Ennos, A.: "Measurements of In-Plane Surface Strain by Hologram Interferometry", J. Sci. Instrum., Series 2, Vol. 1, 1968, p. 731.

12. Leendertz, J.: "Interferometric Displacement Measurements of Scattering Surfaces Utilizing Speckle Effect", Journ. of Phys. E: Sci. Instr., Vol. 3, 1970, p. 214.

13. Butters, J. N. and J. A. Leendertz: "Application of Video Techniques and Speckle Pattern Interferometry to Engineering Measurement", Proceedings of the Symposium on Engineering Applications of Holography, February, 1972, p. 361.

14. Perry, C. C. and H. R. Lissner: The Strain Gage Primer, McGraw-Hill Book Company, New York, 1962, p. 122.

15. Mansfield, E. H.: The Bending and Stretching of Plates, MacMillan Company, New York, 1964, p. 4.

16. Waters, J. P., H. Aas and R. K. Erf: "Investigation of Applying Interferometric Holography to Turbine Blade Stress Analysis". Contract N00019-69-C-0271, UARL-J990798-13, February, 1970, AD 702 402.

17. Timoshenko, S. P., and J. N. Goodier: The Theory of Elasticity, McGraw-Hill Book Company, New York, 1970, p. 43.

18. Stetson, K. A.: "Moiré Method for Determining Bending Moments from Hologram Interferometry", Optics Technology, Vol. 2, 1970, p. 80.

19. Schulz, W. J., J. A. Mangiapane and H. Stargardter: "Development of Borsic(R)-Aluminum Composite Fan Blades for Supersonic Turbofan Engines", ASME Publication 71-GT-90, March, 1971.

APPENDIX A

ABSTRACT - STRAIN ANALYSIS OF LARGE AIRFRAME STRUCTURES

A paper on the above topic was presented to the Spring Meeting of the Optical Society of America in New York City on 13 April, 1972. The following abstract appeared in the Journal of the Optical Society of America, Vol. 62, 1972, p. 738.

ThC13. Strain Analysis of Large Airframe Structures*
F. Michael and J. P. Waters

A study has been made to anticipate and resolve the problems expected in performing pulse-laser holographic strain analysis on large aircraft structures in realistic environments. Toward this end, holographic and strain-gauge measurements were simultaneously recorded on structures simulating airframe surfaces. The static-strain fields were generated in a stressing frame by applying stress from a variety of directions. The values of strain obtained from the gauges were then compared with the holographic-interferometry data. In addition, the paper will consider holographic-interferometric theory as applied to large three-dimensional structures and a study of the relevant parameters, including holographic-layout geometry, plus object orientation and curvature for recording holograms of such structures. Also considered are a study of simple translational and rotational motion for various object geometries that may produce spurious strain data; procedures for obtaining data under adverse conditions, and a procedure for data reduction and computation of spatially resolved maximum-strain fields.

* Supported in part by Air Force Materials Laboratory, Wright-Patterson AFB, Ohio 45433.

APPENDIX B

OBJECT MOTION COMPENSATION BY SPECKLE REFERENCE BEAM HOLOGRAPHY

A new technique which considerably lessens the stringent vibration isolation requirements associated with conventional cw holography has been developed and recently reported in Applied Optics. Referred to as speckle reference beam holography, the method was conceived and demonstrated as part of United Aircraft Research Laboratories Corporate sponsored research program. Nevertheless, it is most apropos to the present contract work since it offers a viable technique for applying the cw holographic process in a practical environment, away from the massive stable tables of an Optics Laboratory and, as such, serves to complement the use of pulsed laser holographic techniques in these situations.

The method involves focusing a portion of the laser illuminating beam to a spot on the object, which then serves as the reference beam for recording a hologram of the object. Thus, object motion affects both reference and object beams similarly, and therefore does not, per se, preclude a successful recording. The technique has all the characteristics of conventional cw holography, though in its present state of development, it is somewhat restricted in area coverage thereby limiting the allowable size object which can be recorded. However, in addition to the reduction of vibration isolation requirements, speckle reference beam holography offers the following features: (a) several holograms of the same scene, with different viewing directions, can be recorded simultaneously; (b) vibration requirements on the holographic plate are similar to conventional photography; (c) relative phase between two points on a vibrating surface can be determined; and (d) it can be used to eliminate residual fringes between recordings of pulsed holographic interferograms.

A portable speckle reference beam holographic camera has been fabricated, and its use demonstrated in the Materials Laboratory of UARL by recording interferometric holograms of an aluminum tensile specimen being stressed in a Tenius Olsen Universal Testing Machine. A typical result from these studies is presented in Fig. B1 along with a photograph of the experimental test configuration. (The latter figure depicts the tripod-mounted holocamera resting on both a desk and the testing machine itself.) The laser beam was directed toward the upper portion of the tensile test specimen and a static double-exposure (one at each of two different states of stress) interferometric hologram, requiring several seconds of exposure, was recorded. The reconstruction indicates a much stronger vertical fringe system then would normally be expected for such a test, together with some shifting of the fringe pattern toward the stress concentration points. The former effect (vertical fringes) was subsequently found to be caused by a slight twisting of the specimen as a result of the clamping jaw arrangement. The results,

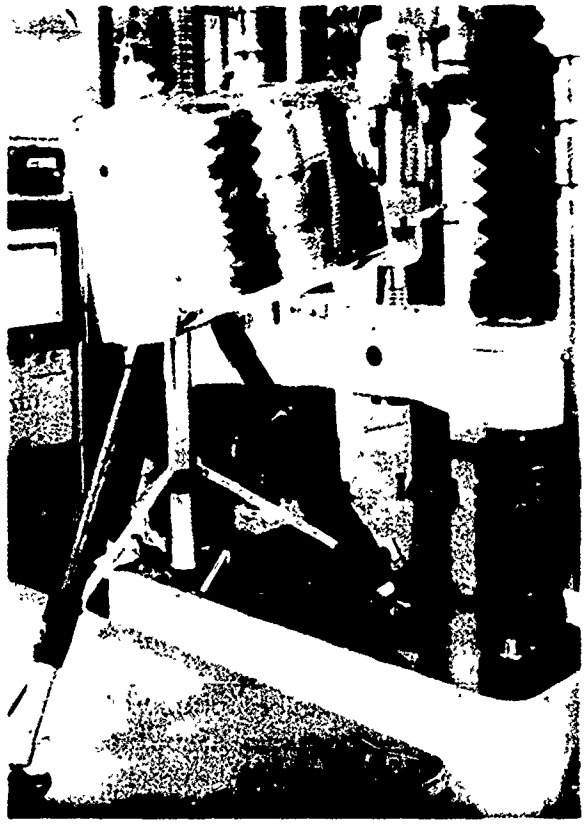

TEST CONFIGURATION

HOLOGRAPHIC RECONSTRUCTION

FIGURE B1. PORTABLE CW HOLOGRAPHY IN A MATERIALS TESTING LABORATORY

however, clearly demonstrate the capabilities of the technique for long exposure cw holography without the need for vibration isolated mounting systems.

Because of the significant relevance of speckle reference beam holography to one of the prime objectives - "determine the feasibility of using holographic interferometry in manufacturing or maintenance environments" - of the current contract, a description of the method and its applications are presented below. The work originally appeared in Applied Optics, Vol. 11, 1972, p. 630.

1. INTRODUCTION

Since the advent of cw holography[1,2], vibration isolation requirements have essentially limited its use to a laboratory type environment; this has promoted skepticism on the part of potential users as to its eventual role in a practical environment. Although the introduction of pulsed holography[3] has done much to eliminate these objections, the additional technology required and the expense associated with it have detracted from its widespread acceptance.

The method described in this paper is primarily intended for lessening the stringent vibration isolation requirements associated with conventional cw holography. The method does not require an electronic feedback servo system[4,5], scanning reference beam[6], attachment of mirrors[7], or optical processing of the reference beam before striking the hologram[8] and has all the advantages of conventional cw holography in that double-exposure, time-average, and real-time holograms can be obtained of three-dimensional diffusely reflecting objects.

Following a description of speckle reference beam holography and its application for lessening the stringent vibration isolation requirements of cw holography, two additional applications will be described. These are the determination of relative phase on the surface of vibrating objects and the elimination of residual fringes associated with double-pulse holographic interferometry.

2. SPECKLE REFERENCE BEAM HOLOGRAPHY

A speckle reference beam hologram is formed in a conventional manner; that is, a coherent light source is divided into two beams, one being used to illuminate an object and the other being used as a reference beam. The light from the diffusely reflected object interferes with the light from the reference beam on a photographic plate to form the hologram. The difference arises in the type of reference beam used in the construction of the hologram. Conventionally, the

reference is formed by directly illuminating the hologram with a portion of the coherent light via mirrors and appropriate expanding optics. In making a speckle reference beam hologram, a portion of the coherent light source is focused to a point on any diffuse surface (e.g., wood, paper, unpolished metal, etc.), and the diffusely reflected radiation from the surface is used as the reference beam. Presented in Fig. B2a is a schematic diagram showing a typical component arrangement for making a speckle reference beam hologram.

In general, radiation reflected from a diffuse surface forms a speckle pattern (randomly oriented spots of light) which is characteristic of the surface microstructure. As the scattering area is reduced by focusing, the randomly oriented spots increase in size. Finally, if the focused spot can be made smaller than the surface discontinuities, the speckle pattern disappears and the surface behaves in a specular manner. Under these conditions, a conventional hologram could be recorded using the light reflected from the focused spot as the reference beam. However, a point source smaller than the discontinuities on a diffuse surface is generally not obtainable due to the diffraction limits associated with the optics. This would seem to rule out the use of a reference beam reflected from a diffuse surface, because the phase characteristics of the reference beam used in the construction process cannot be matched identically by the reconstructing beam, and image resolution should therefore be degraded.

However, recent experiments at UARL have demonstrated that a focused spot with a diameter of approximately 0.2 mm (a 2-mm laser beam brought to a focus with a lens having a focal length of 25 cm) on a diffuse surface is sufficient to approximate a specular point source when constructing a hologram. The hologram can then be reconstructed using a readily available specular point source. The attendant loss in resolution, as a result of using two unidentical point sources in this manner, has been found to be minimal. Figure B2b is a photograph of a holographic plate obtained using the diffusely reflected radiation from a focused spot, 0.2 mm in diameter, on an unpolished metal surface. The characteristic speckle pattern of the surface is clearly visible in the figure. Presented in Fig. B2c is the photograph of the reconstructed image (Nat. Bur. Stand. resolution chart) obtained from the hologram pictured in Fig. B2b. An angular resolution better than 6.5×10^{-4} rad (determined from the smallest divisions on the resolution chart) was obtained. (Even higher resolutions can be expected using a smaller focused spot.) In the experiments to date, it has been found that this resolution (6.5×10^{-4} rad) is more than adequate for general applications of holography such as nondestructive inspection, vibration analysis, and strain analysis. The method is also applicable to all conventional forms of cw holography (double-exposure, real-time, and time-average).

The speckle illumination which serves as the holographic reference beam has a feature that a conventional reference beam does not have; the diffusely reflected radiation subtends a solid angle of approximately 180°. This feature makes it possible to record many holograms simultaneously from different viewing

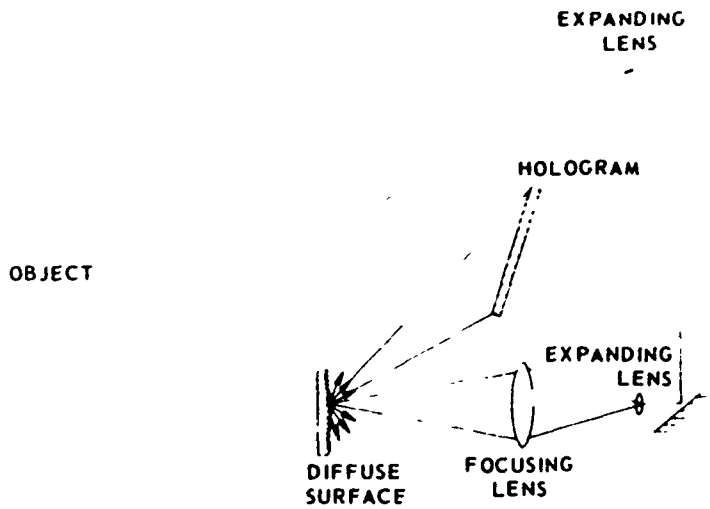

(a) TYPICAL EXPERIMENTAL SETUP

(b) SPECKLE REFERENCE BEAM HOLOGRAM

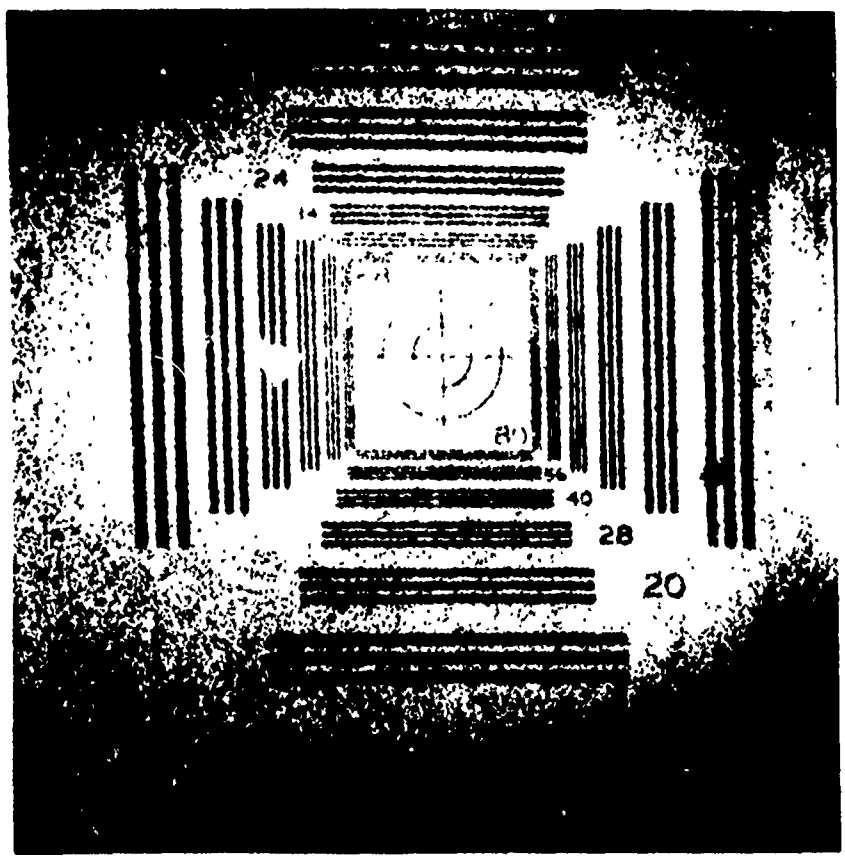

(c) RECONSTRUCTION OF HOLOGRAM DEPICTED IN (b)

FIGURE B2. SPECKLE REFERENCE BEAM HOLOGRAPHY

directions without additional optics to provide the required reference beams. Compensation for different irradiance ratios between reference and object illumination beams is not required since both have the same angular scattering properties and the irradiance of both decreases with distance in the same way. This feature is particularly helpful in strain analysis where more than one viewing direction is sometimes required to obtain the three displacement vectors of the surface.

3. ELIMINATION OF STRINGENT VIBRATION ISOLATION REQUIREMENTS OF CW HOLOGRAPHY

The primary application of speckle reference beam holography is in the elimination of the stringent vibration isolation requirements associated with conventional cw holography. This is accomplished by focusing a portion of the laser illumination beam to a spot on the object, which then serves as the reference beam for recording the object. Motion of the object will now be compensated for by a change in the path-length of the reference beam. This is similar to the technique of Corcoran et al[7], where a mirror is attached to the object so that the reference beam can be reflected from it. In this case, however, mirrors are not required. This difference makes it possible to illuminate easily the hologram with the reference beam without having to locate the expanding optics near the object or attach mirrors that could influence the motion of the object in holographic interferometry applications.

In making a hologram of this type (reference point on the object) the reconstruction will contain two virtual images (orthoscopic and pseudoscopic) centered symmetrically about the reference point. Therefore, care must be taken to position the reference point to one side of the object illumination field, or the two reconstructed images will overlap and degrade the image.

In practice, holograms of reasonable quality can be obtained of objects over a limited illuminated area without special precautions as to illumination beam divergence or angular acceptance of the holographic plate. Shown in Fig. B3 are two photographs of the reconstruction obtained from a hologram constructed with the illumination optics, reference beam optics, and photographic film holder, all located on a vibration isolation table, while the object (Nat. Bur. Stand. resolution chart) was attached to a tripod resting on the laboratory floor. (Prior to these experiments, holograms were not obtainable in this laboratory without vibration isolation of the object.) As seen in the figure, one photograph shows both the real image and the twin image, while the other is a closeup of just the real image. These photographs show the extent in area over which the reference beam is automatically compensating for the object movement due to random environmental vibrations. Direct measurements using heterodyning techniques showed that the maximum amplitude of the object motion was $\pm 4\lambda$, while the frequency varied between 5 Hz and 30 Hz.

(a) PSEUDOSCOPIC (LEFT) AND ORTHOSCOPIC (RIGHT) IMAGES

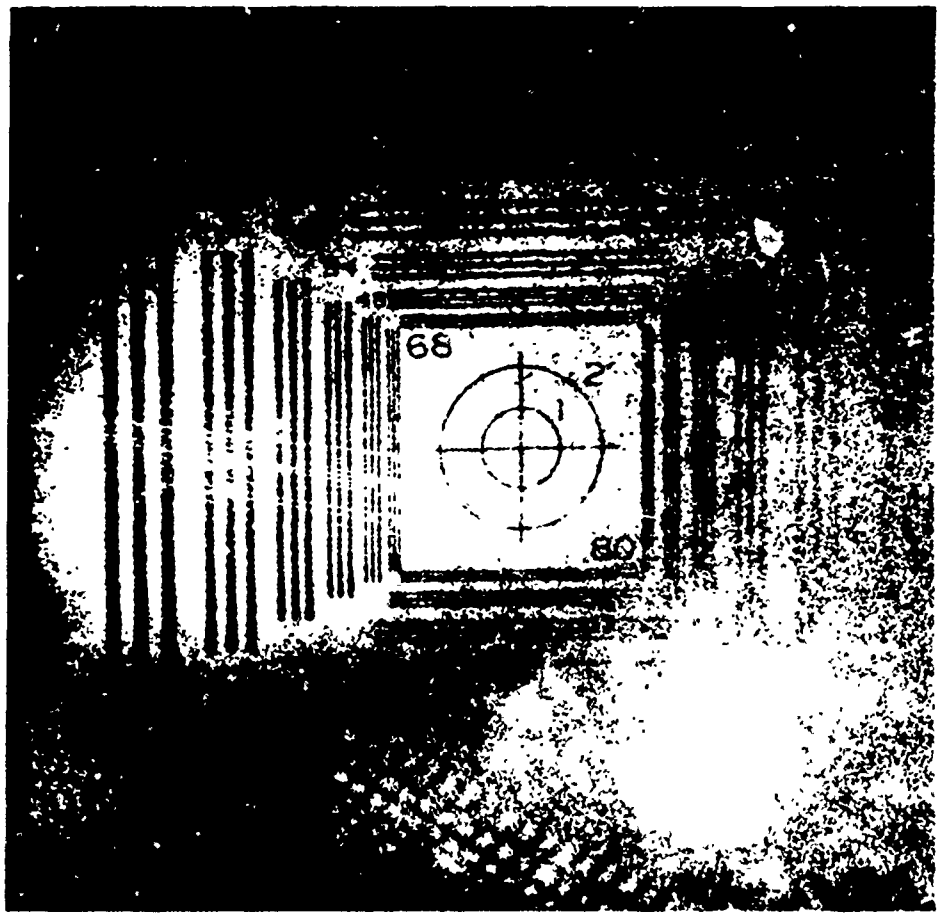

(b) MAGNIFIED VIEW–ORTHOSCOPIC IMAGE

FIGURE B3. RECONSTRUCTED IMAGES

To improve the quality of the reconstructed image and increase the area of the object that can be recorded, special precautions are necessary. Referring to Fig. B4, the required precautions can be determined by noting that the phase change, $\Delta\delta_o$, introduced by random object motion at the focused reference spot, is

$$\Delta\delta_o = \frac{2\pi\Delta Z}{\lambda} (\cos \beta_o - \tan \alpha_o \sin \beta_o + \sec \alpha_o), \qquad (1)$$

where λ is the wavelength of illuminating light, α_o is the angle between the z axis and the central ray of the incident reference beam, and β_o is the angle between the z axis and the direction to a point, H, on the hologram. This distance between the object and hologram is considered to be much larger than the random surface displacement. The phase change, $\Delta\delta_n$, at a point on the illuminated portion of the object, is

$$\Delta\delta_n = \frac{2\pi}{\lambda} [\Delta Z (\cos \alpha_n + \cos \beta_n) - \Delta X (\sin \alpha_n - \sin \beta_n)], \qquad (2)$$

where α_n is the angle between the z axis and the incident illumination beam, and β_n is the angle between the z axis and the direction to the point, $\bar{n}$, on the hologram. In this equation, the distance from the illumination point source, S, is also considered to be much larger than the random displacement of the surface. (A similar equation can be generated for the y,z plane.) Since the phase change on the illuminated object is dependent on the interference between identical displaced points while the phase change of the reference beam is due only to a displacement of the focused spot, Eq. (1) and (2) are not of the same form. As can be seen, Eq. (1) is completely independent of ΔX, and therefore compensation for a change in the ΔX direction cannot be effected with this technique. When the two Z components of Eqs. (1) and (2) are equal, maximum object motion compensation in this direction is achieved. One set of conditions for which the two components are equal is when $\alpha_o = \alpha_n = 0$ and $\beta_n = \beta_o$.

The first condition ($\alpha_o = \alpha_n = 0$) can be achieved by collimating the object illumination beam and keeping the central ray of the focused reference beam parallel to it. The second requirement ($\beta_o = \beta_n$) is achieved by either recording the object in the far field (lensless Fourier transform holography[9]), or at the focal plane of a lens positioned between the object and the hologram. In this manner, the rays that form the interference pattern at the position of the hologram are essentially parallel when leaving the object, thus $\beta_o = \beta_n$. Figure B5 is a schematic illustration of a holographic system that meets the above requirements. The reconstructed image (orthoscopic) from a hologram made in a manner similar to this is presented in Fig. B6a. The increase in image quality over that found in Fig. B3 is apparent. This particular hologram was recorded approximately 50 cm from the object, a distance found to be sufficient for reasonable quality holograms.

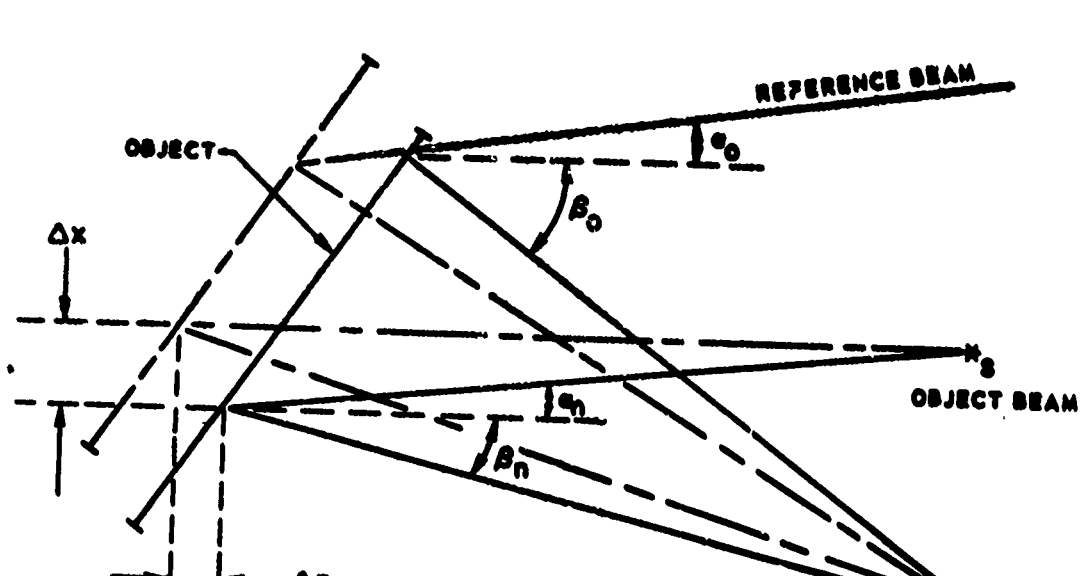

FIGURE B4. PHASE CHANGE PARAMETERS

SCHEMATIC OF CONSTRUCTION SYSTEM

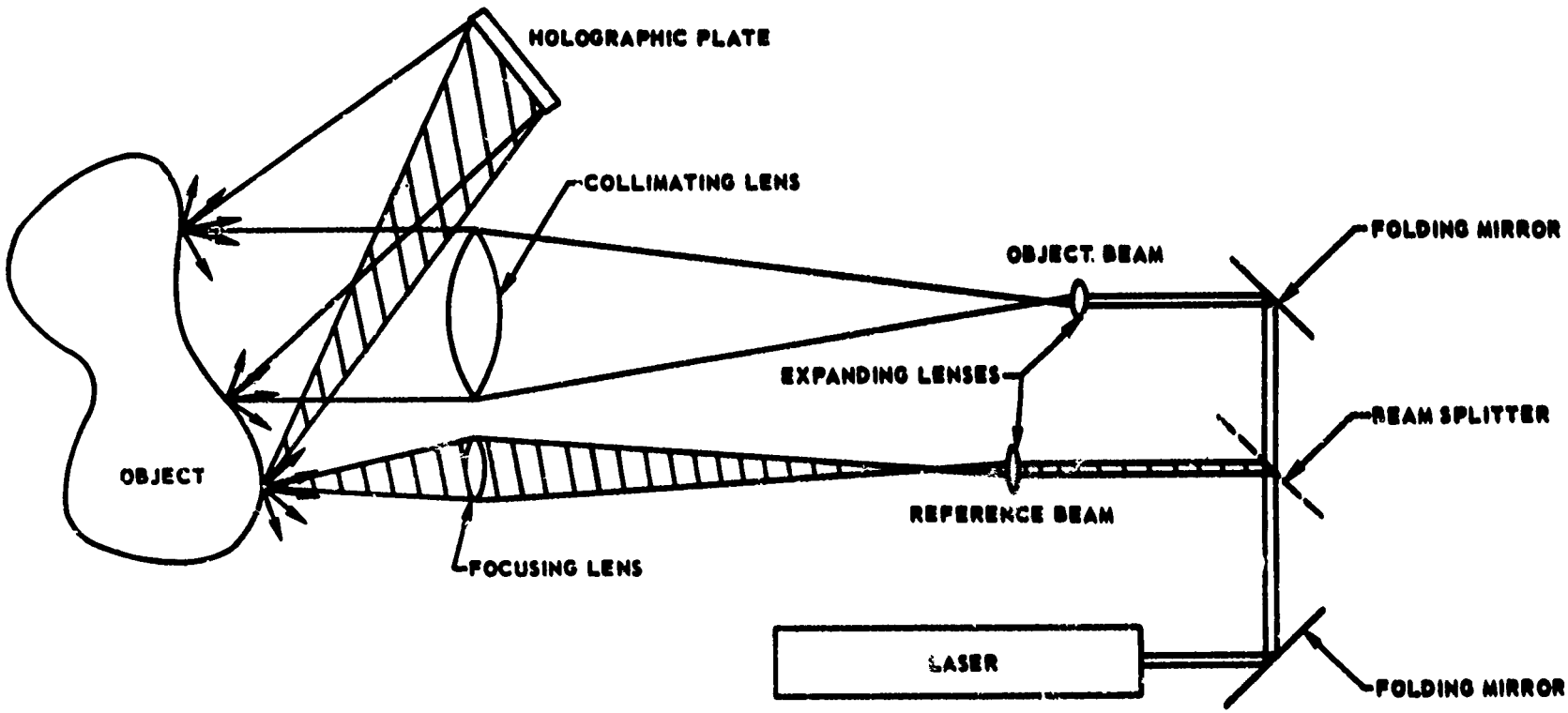

FIGURE B5. SPECKLE REFERENCE BEAM HOLOGRAPHY

(a) TWO-DIMENSIONAL OBJECT

(b) THREE-DIMENSIONAL OBJECT

FIGURE B6. RECONSTRUCTIONS OF SPECKLE REFERENCE BEAM HOLOGRAMS

Reproduced from best available copy

These conditions, which produce equal phase change, are theoretically applicable for flat objects only and will not be as effective when the normal to the surface varies considerably, as in the case of objects having a complicated geometry. However, our experiments have shown that considerable variation of the surface normal can be tolerated with little degradation to the image. An example of a reconstruction showing a complicated surface is presented in Fig. B6b. The unisolated object was a model of the lunar landing craft and illustrates the wide variety of angular surface orientation that can be automatically corrected for by the speckle reference beam technique. The somewhat low quality of this reconstructed image was found to be partially a result of slow thermal expansion, which occurs if the focused reference spot dwells on a painted surface. This effect was eliminated in future reconstructions by allowing the painted surface at the focused reference spot to obtain equilibrium before making the hologram. (A reconstruction of a hologram made in this fashion is presented in Fig. B9.)

As shown in Eq. (1), the random surface movement in a lateral direction (perpendicular to the surface normal) cannot be compensated for with this technique or any of the other techniques mentioned previously[3-8]. However, if the object illumination is approximately normal to the surface and the recording angle (β_n) is kept small, in general, the holographic quality is not degraded as severely by this type of displacement (lateral) as it is by longitudinal motion. From Eq. (2), the phase change due to a random displacement in the X direction of magnitude λ where $\beta_n \approx 10°$ is 0.02 rad while the phase change produced by a comparable movement in the Z direction is 0.11 rad. For this particular system, there is a factor of 5 difference in the phase change between a movement perpendicular to the surface and one parallel to the surface. This type of motion becomes even less significant as the recording angle is decreased.

An additional type of random motion that is not compensated for by the focused reference spot, and which will degrade or completely obliterate the reconstructed holographic image, is a change in the longitudinal displacement across the surface of the object (e.g., rotation about an axis parallel to the surface). Experimentally, this type of random displacement has been found to be small over a large portion of the object and can usually be minimized by a judicious choice in the initial orientation of the object.

Vibration restrictions on the photographic plate during the holographic exposure are no greater than those associated with conventional photography since the hologram is recorded either in a lensless Fourier transform configuration[9] or in a conventional Fourier transform configuration. Limitations on the remainder of the system, namely, the optics used for handling the two beams prior to illumination of the object, can be minimized by rigidly mounting the optical elements in relation to each other. (This is not particularly difficult since these elements can be made fairly compact.)

To demonstrate the applicability of speckle reference beam holography in an unisolated vibration environment, the holographic camera shown in Fig. B7 was constructed. The camera consisted of a 5-mW, 6328 Å laser, collimation optics to produce an illumination beam 10 cm in diameter, and f/40 optics for focusing the reference beam to a point on the object. The various optical components were mounted on a 2.5-cm thick piece of aluminum as shown in Fig. B7a. A thin aluminum cover was then placed over the optics to prevent air currents from affecting the system, and the entire system was mounted on a conventional photographic tripod as shown in Fig. B7b. Representative photographs of the reconstructions from holograms made with the camera are shown in Fig. B8. Figure B8a is a reconstructed image of an Nat. Bur. Stand. resolution chart which was mounted on the laboratory wall. (Little difference between this reconstructed image and the one presented in Fig. B6, made with the optics on the isolation table, can be noted.) A photograph of a reconstructed three-dimensional image, ordinary laboratory clamp resting on a table, is presented in Fig. B8b, and a time-average reconstruction of a vibrating speaker cone is presented in Fig. B8c, the latter demonstrating the capability of the system to record time-average holographic interferograms of unisolated objects.

4. DETERMINING PHASE OF VIBRATING OBJECTS

Using a modulated reference beam and time-average holographic interferometry (real-time holographic interferometry is equally applicable) Neumann et al.[10] have shown that phase differences between different points on a vibrating object can be determined. This is effectively done by modulating the reference beam using a vibrating mirror while recording the hologram. The reconstructed image will then exhibit a shift in the irradiance of the various reconstructed interferometric fringes. With a stationary reference beam, the irradiance characteristically has its maximum value on those portions of the object that have no motion, while the succeeding maxima exhibit a lower irradiance value as the vibratory amplitude increases. By modulating the reference beam, those points on the object that have the same vibratory amplitude and phase as the reference beam will now be of maximum intensity, and in this manner, a phase determination can be made.

This same type of information can be obtained using speckle reference beam holography. This is accomplished by positioning the focused reference spot on that portion of the vibrating object where the phase, in relation to the remainder of the object, is to be determined. Upon making a time-average interferometric hologram of the vibrating object, the brightest areas (nodal regions in conventional time-average holographic interferometry) on the reconstructed image surface are those that have the same phase and amplitude as that portion of the object upon which the reference spot is focused. An example of this type

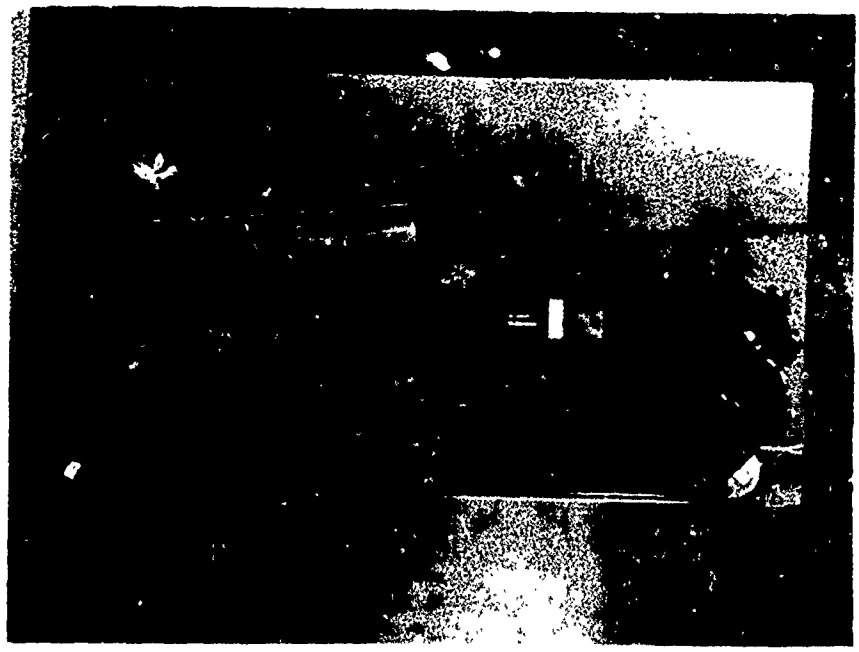

(a) COMPONENT ARRANGEMENT

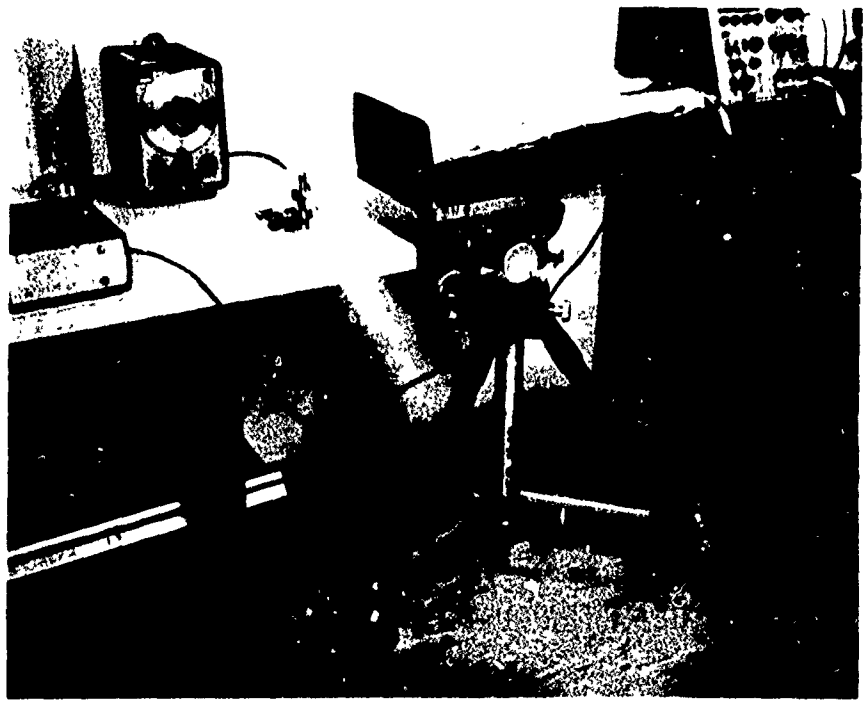

(b) TRIPOD-MOUNTED CAMERA

FIGURE B-7. SPECKLE REFERENCE BEAM HOLOCAMERA

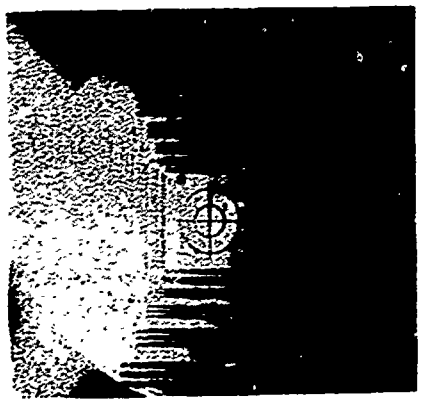

(a)

(b)

(c)

FIGURE B8. RECONSTRUCTIONS OF HOLOGRAMS RECORDED WITH THE SPECKLE REFERENCE BEAM TRIPOD-MOUNTED HOLOGRAPHIC CAMERA

of application is presented in Fig. B9, showing three photographs from holographic reconstructions made of a speaker cone vibrating with a frequency of 2680 Hz. In the photograph of Fig. B9a, the focused reference spot was positioned on the frame of the speaker cone. Thus, the maximum intensity areas are nodal points. This hologram served to locate the position of the reference spot for the succeeding two holograms which were reconstructed and are presented in Figs. B9b and c. For the reconstruction shown in b, the reference spot was focused on a node located near the rim of the cone, and for the one in c, the reference spot was focused on an adjacent antinode. By recording the holograms in this manner, the reference spot was located at a different point in the vibratory cycle for each, but the same approximate area of the cone was recorded for easy comparison. Since the reference spot was located within the area illuminated by the object beam in the latter two recordings, a small portion of the object near the point source had to be occluded to prevent the twin image from degrading the reconstruction. In comparing Figs. B9b and c, it can be seen that the maximum intensity areas have shifted from points of no motion on the speaker cone to points that had formally been areas where motion had occurred. This is particularly noticeable near the rim of the cone. (The driving voltage applied to the speaker cone was identical for both of these holographic exposures.) The advantage of this method for determining phase is that it does not require expensive piezoelectric mirror drives or the control electronics associated with them. A disadvantage is that the entire image cannot be viewed at one time when relative phase is being evaluated. If the entire image were reconstructed, the twin image would overlap and degrade the reconstruction.

5. ELIMINATION OF RESIDUAL FRINGES IN PULSED INTERFEROGRAMS

In many applications of pulsed holographic interferometry, a relatively long period may elapse between the two holographic exposures that make up the pulsed interferogram. As a result of environmental vibration, movement of the entire object can occur between the exposures, and residual fringes having no relationship to the motion of interest appear in the holographic reconstruction. Elimination of these fringes can be accomplished using speckle reference beam holography by positioning the focused spot on the object. Any movement between exposures will now be automatically compensated for by the reference beam in a manner similar to that described previously for the cw case. However, care must be taken in this type of application to keep the reference beam power low enough to prevent air breakdown or the evaporation of surface material at the focused spot, which will result in a loss of coherence between the reference beam and object illumination beam.

(a) REFERENCE BEAM ON FRAME

(b) REFERENCE BEAM ON NODE

(c) REFERENCE BEAM ON ANTINODE

FIGURE B9. VIBRATORY PHASE DETERMINATION

Reproduced from best available copy.

6. REFERENCES

1. D. Gabor, J. Appl. Phys. 19, 1191 (1948).

2. E. N. Leith and J. Upatnieks, J. Opt. Soc. Am. 53, 1377 (1963).

3. R. E. Brooks, L. O. Heflinger, and R. F. Wuerker, IEEE Trans. Quantum Electron. QE-2, 275 (1966).

4. D. B. Neumann and H. W. Rose, Appl. Opt. 6, 1097 (1967).

5. H. W. Rose and H. D. Pruett, Appl. Opt. 7 87 (1968).

6. J. C. Palais, Appl. Opt. 9, 709 (1970).

7. V. J. Corccran, R. W. Herron, Jr., and J. G. Jaramillo, Appl. Opt. 5, 668 (1966).

8. W. T. Cathey, Jr., U.S. Patent 3,415,587, 10 December, 1968.

9. G. W. Stroke, A. Funkhouser, C. Leonard, G. Indebetouw, and R. G. Zech, J. Opt. Soc. Am. 57, 110 (1967).

10. D. B. Neumann, C. F. Jacobson and G. M. Brown, Appl. Opt. 9, 1357 (1970).